

Juzsakova Tatjana_205_24



University of Pannonia

DSc DISSERTATION

**MODIFICATION AND CHARACTERIZATION OF
ADVANCED MATERIALS FOR ENVIRONMENTAL
APPLICATIONS**

WRITTEN BY

Tatjana Juzsakova

**Veszprém, Hungary
2024**

Abstract

The dissertation deals with novel adsorbent materials, namely with functionalized multiwalled carbon nanotubes (MWCNTs) and nanometal oxide-based ones for hydrocarbons and methylene blue removal from water. The synthesis methods, the ways of MWCNTs modification including the functionalization with microemulsion and metal oxides (V_2O_5 , CeO_2 and $V_2O_5:CeO_2$) addition are discussed. Raw MWCNTs, microemulsified MWCNTs and metal oxide nanoparticle-doped MWCNTs were characterized using different analytical techniques like XRD, TEM, SEM, EDX, AFM, Raman, TG/DTA and BET to determine the structure as well as the chemical and morphological properties of these newly prepared adsorbents.

The experimental results revealed that the microemulsion technique as a type of surface functionalization proved to have a beneficial effect on MWCNTs' hydrophobic properties without the need for additional functionalization and substitution steps to attach hydrocarbon side chains. The undecane and kerosene removal efficiency from water was 94% and 96% respectively, while over raw MWCNTs the removal efficiency was 57% and 35% only. The kinetic studies demonstrated that the toluene adsorption process over μ EMWCNTs could be well described by the pseudo-second order model with a high correlation coefficient.

The aim of the development of nanometal oxide-based MWCNTs was to improve the adsorption properties towards organic pollutants. MWCNTs, Ce/MWCNTs, V/MWCNTs and V:Ce/MWCNTs were applied for the removal of MB from an aqueous model solution. UV-Vis analysis indicated that high MB removal efficiency (63.8%) and adsorption capacity (56.7 mg/g) were obtained after 35 min of treatment over V:Ce/MWCNTs in comparison with raw MWCNTs, MWCNTs oxidized, Ce/MWCNTs and V/MWCNTs. The studied MWCNTs-based materials are promising adsorbents for pollutant removal from surface waters. These composites are also compatible with green materials hence these are considered as environmentally friendly adsorbents.

Bauxite residue, known as red mud, is a highly alkaline waste sludge that is generated in the industrial production of alumina. The red mud contains several valuable metals including iron oxide (33-40%), titania (4-6%), vanadia (0.2-0.4%), rare earth elements (REEs) (1500-2500 ppm), etc. Therefore, it can be considered as a

potential secondary metals resource of valuable REEs. One of the main problems of scandium recovery from red mud is its selective separation from other elements of similar physico-chemical properties. This study aims at the investigation of the impact of crown ethers (15-C-5, 12-C-4, DC18-C-6), cryptand (C2.2.2) as novel extractants for scandium extraction systems. The macrocyclic compounds are known to recognize fairly strictly the size of the guest cation accommodating in their cavity. The complexation reaction between Sc^{3+} and macrocyclic compounds in model solutions was confirmed by ICP-OES technique. The results showed that 15-C-5, 12-C-4 and C2.2.2 have high selectivity for Sc^{3+} ion which could be of potential value in the separation and purification of Sc^{3+} in REEs processing industry. Moreover, this study demonstrated a significant effect of solution pH and the concentration of macrocyclic compounds on the extraction efficiency. The main results showed that the high extraction efficiency (95-99%) has been achieved by 15-C-5, 12-C-4, and C2.2.2 compounds above pH 3. In case of using DC18-C-6 the maximum efficiency has reached 26%. Moreover, the complexed metal ions can be efficiently recovered/stripped out from the complex by HCl and HNO_3 .

Keywords: metal oxide-doped MWCNTs; microemulsified MWCNTs; hydrocarbons and methylene blue removal from water; macrocyclic compounds; Sc recovery

Kivonat

A kutatómunka célja funkcionális többszárú szén nanocső (MWCNT) és nanofém-oxid alapú szén nanocső adszorbensek előállításának és vizsgálatának szénhidrogének és festékanyagok vízből történő eltávolítására. A szén nanocső felületmódosítása mikroemulziós funkcionálással és fémoxidok hozzáadásával (V_2O_5 , CeO_2 és $V_2O_5:CeO_2$) történt. A friss MWCNT, a mikroemulzifikált MWCNT és a fém-oxid nanorészecskékkel adalékolt MWCNT kémiai, morfológiai és felületi tulajdonságainak vizsgálatára számos nagyteljesítményű analitikai módszert (XRD, TEM, SEM, EDX, AFM, Raman, TG/DTA and BET) alkalmaztam.

A kísérleti eredmények azt mutatták, hogy a mikroemulziós technika, mint a felületi funkcionálás egy fajtája, jótékony hatással van az MWCNT hidrofób tulajdonságaira anélkül, hogy további funkcionálási és átalakulási lépésekre lenne szükség a szénhidrogén láncok rögzítéséhez. A mikroemulzifikált (μ EMWCNT) minták undékán és a kerozin eltávolítási hatékonysága 94%, illetve 96% volt, míg a friss MWCNT esetén csak 57% és 35% volt elérhető. A kinetikai vizsgálatok kimutatták, hogy a toluol adszorpció folyamata μ EMWCNT adszorbensen jól leírható a magas korrelációs együtthatójú pszeudo-másodrendű modellel.

A nanofém-oxid alapú MWCNT fejlesztésének célja a szerves szennyező anyagokkal szembeni adszorpciós tulajdonságok javítása volt. MWCNT-t, Ce/MWCNT-t, V/MWCNT-t és V:Ce/MWCNT-t alkalmaztam metilénkék (MB) vizes modelloldatból való eltávolítására. Az UV-Vis kísérletek eredménye azt mutatta, hogy összehasonlítva a nyers MWCNT-vel, oxidált MWCNT-vel, Ce/MWCNT-vel és V/MWCNT-vel a V:Ce/MWCNT esetében magasabb MB eltávolítási hatékonyság (63,8%) és adszorpciós kapacitás (56,7 mg/g) érhető el. A vizsgált MWCNT-alapú anyagok ígéretes adszorbenseknek tekinthetők a felszíni vizek szennyezőanyagainak eltávolítására. Ezek a kompozitok zöld anyagokkal is kompatibilisek, ezáltal környezetbarát adszorbenseknek számítanak.

A vörösiszap bauxitércék feldolgozásából származó, erősen lúgos kémhatású ipari szilárd alapú hulladék, amely számos értékes fémeket tartalmaz: Fe_2O_3 (33-40%), TiO_2 (4-6%), V_2O_5 (0,2-0,4%), ritkaföldfémek (2000-2500 ppm), Sc (50-100 ppm), stb. Ezért a vörösiszap potenciális másodlagos fémforrásnak tekinthető. A szkandium

vörösiszappból történő kinyerésének egyik fő nehézsége a hasonló fizikai-kémiai tulajdonságokkal rendelkező többi elemtől való szelektív elválasztása.

A kutatómunka másik célja a koronaéterek (15-C-5, 12-C-4, DC18-C-6) és a kriptand (C2.2.2), mint új extrakciós szerek hatásának vizsgálata szkandium ion kinyerési rendszerekben. A makrociklusos vegyületekről ismert, hogy méretük alapján felismerik az üregükben elhelyezkedő "vendég" kationokat. Az Sc^{3+} és a makrociklusos molekulák közötti komplexképző reakciót modell oldatos ICP-OES technikával igazoltam. Az eredmények azt mutatták, hogy a 15-C-5, 12-C-4 és C2.2.2 vegyületek nagy szelektivitással rendelkeznek Sc^{3+} ionra, ami jelentőséggel bírhat a Sc^{3+} elválasztásában és tisztításában a RFF feldolgozóiparban. Ezen túlmenően ez a vizsgálat kimutatta az oldat pH-jának és a makrociklusos vegyületek koncentrációjának jelentős hatását az extrakció hatékonyságára. A fő eredmények azt mutatták, hogy a Sc^{3+} maximális extrakciós hatékonyságot (> 95%) a 15-C-5, a 12-C-4 és a C2.2.2 vegyületek érték el az oldat pH értékétől függően. A DC18-C-6 alkalmazása esetén a maximális hatásfok csupán 26% volt. Ezt követően a komplexált fémionok hatékonyan kinyerhetők/eltávolíthatók a makrociklusos szerves fázisból HCl és HNO_3 segítségével.

Kulcsszavak: fémoxyddal adalékolt MWCNT; mikroemulzifikált MWCNT; szénhidrogének és metilénkéék eltávolítása a vízből; makrociklusos vegyületek; Sc kinyerés

Table of contents

Introduction	1
1. Objectives and goals	13
2. Experimental	15
2.1. Materials	15
2.2. Microemulsification preparation of MWCNTs	16
2.3. Preparation of metal-oxides nanoparticles	16
2.3.1. Preparation of vanadium pentoxides nanoparticles	16
2.3.2. Preparation of cerium dioxides nanoparticles	16
2.3.3. Preparation of mixed V ₂ O ₅ :CeO ₂ nanocomposite	17
2.3.4. Functionalization of MWCNTs with metal oxide nanocomposites	17
2.4. Characterization methods	18
2.5. Adsorption tests	19
2.5.1. Hydrocarbon solution preparation and adsorption tests	19
2.5.2. Protocol for samples analysis via gas chromatography	20
2.5.3. Analysis of toluene by UV-Visible spectroscopy	21
2.5.4. Methylene blue adsorption study by UV-Visible spectroscopy	21
2.6. REEs extraction by macrocyclic compounds and stripping procedure	23
3. Results and discussion	25
3.1. Functionalized carbon nanotubes for hydrocarbon removal from water	25
3.1.1. Results of SEM analysis	25
3.1.2. Results of the morphological analysis	26
3.1.3. Results of the XRD investigations	29
3.1.4. Results of thermoanalytical investigations	30
3.1.5. Results of Raman spectroscopic measurements	32
3.1.6. UV-Vis spectrophotometric results on toluene sorption test	33
3.1.7. GC results of the sorption test	34
3.1.8. Kinetic studies over μ EMWCNTs	35
3.1.9. Microemulsification mechanism of MWCNTs	41
3.1.10. Mechanism of hydrocarbon adsorption over MWCNTs	42
3.2. V₂O₅, CeO₂ and their MWCNTs nanocomposites modified for the removal of methylene blue dye from water	43
3.2.1. Results of the X-ray diffraction study	43
3.2.2. Electron spectroscopy and energy dispersive X-ray spectroscopy results	45
3.2.3. Atomic force microscopy results	46
3.2.4. Raman spectroscopy results	47
3.2.5. Thermogravimetric analysis results	50
3.2.6. Low-temperature nitrogen adsorption results	52
3.2.7. Results of methylene blue adsorption over metal oxide-doped MWCNTs	55
3.2.8. Mechanism of MB adsorption over metal oxide-doped MWCNTs	58
3.3. Macrocyclic compounds for selective recovery of rare earth scandium element from aqueous media	60
3.3.1. Results of extraction with varying concentrations of macrocyclic compounds	60
3.3.2. Extraction of Sc ions as a function of pH	61
3.3.3. Stripping of Sc with inorganic acids	63
3.3.4. Results of extraction of REEs from multielement model solution	63

3.3.5. Extraction and stripping mechanism _____	65
3.3.6. Flowchart for scandium recovery from red mud _____	66
Conclusions _____	70
NEW SCIENTIFIC FINDINGS, DSC THESIS _____	72
Publications forming the bases of the theses _____	78
References _____	83
Supplementary part _____	94
Table S1. Effect of varying concentrations, mg/L, of macrocyclic compounds on Sc extraction efficiency, E%. _____	94
Table S2. Effects of pH of macrocyclic extractant solution on Sc ³⁺ extraction. _____	94
Table S3. Spectral analysis data from the deconvolution of D- and G-bands and the calculated ratios. _____	95
Table S4. Mass loss data from the termoanalytical measurements _____	96
Acknowledgement _____	97
Fundings _____	97

INTRODUCTION

Global contamination of water bodies by *organic* and *inorganic* pollutants from different industrial effluents poses threats to aquatic flora and fauna and public health (Inamuddin, 2019). The organic pollutants mainly include phenols, nonylphenols, chlorinated phenols, azo dyes, phthalic esters, petroleum hydrocarbons, pesticides, persistent organic pollutants (POPs), etc. (Bharagava et al., 2020). The inorganic water pollutants are usually trace elements, mineral acids, metals, metals compounds, inorganic salts, metals with organic compounds as complexes, sulfates, and cyanides (Wasewar et al., 2020). Water pollution is a threatening issue since it affects hundreds of millions of people within a short period of time.

The main part of this research focuses on the development of novel carbon nanotubes (CNTs)-based adsorbent for the removal of hydrocarbons and dyes from decontaminated water. The oil contamination generated by oil-spill is floating on the surface causing serious damage to the aquatic life (Khandelia and Patel, 2022). Numerous research studies have extensively assessed VOC pollutants in industrial untreated wastewaters and have found that petroleum hydrocarbons, benzene, toluene and p-xylene (BTX) toxicity levels have exceeded the limit values set by international standards (Anjum et al., 2019a). The oil concentration limit value in natural and treated water should not exceed 10–15 mg/L (Sajid et al., 2022).

In case of dyes improper treatment of wastewater also has negative health effects on humans and wildlife (Hassan et al., 2021). Methylene blue (MB) with an aromatic molecular structure is among the most widely used cationic dyes on an industrial scale in disinfectants, colouring agents, varnishes, pesticides and pharmaceuticals as well as in the printing and rubber industries. It has been extensively applied in the dyestuff industry (Jawad et al., 2016). Due to the presence of dyes in water, the penetration of sunlight is reduced. This results in inhibition of photosynthesis in aquatic plants causing irreparable damage in aquatic environments (Ihsanullah et al., 2020). In addition, changes in the taste and colour of water is commonly observed. Waters polluted with dyes can cause multiple health problems for human beings, including breathing difficulties, nausea, skin irritation, allergic contact dermatitis, vomiting and mental confusion, moreover, can even lead to cancer (Siddiqui et al., 2018).

Hence, it is necessary to make urgent and concerted efforts to develop modern methods for the remediation of the organic matter- or hydrocarbon-polluted waters. There are several traditional depollution methods used in different applications. These include physical, biological and chemical techniques such as adsorption, filtration, bioremediation, chemical precipitation, oxidation, ion-exchange, photocatalysis and others (Hassan et al., 2021; Ihsanullah et al., 2020; Inamuddin, 2019; M. Li et al., 2019). Of these techniques, the adsorption-type remediation with numerous types of adsorbents has been regarded as the most pronounced, feasible, environmental-friendly and cost-effective technique showing good efficiency for clean-up of oil spillages or removal of others pollutants (Hassan et al., 2021; Valcárcel et al., 2008).

Since the last decade, nanotechnology has greatly revolutionized the methods for environmental remediation because nanoparticles hold manifold merits such as large surface area, more active adsorption sites, high reactivity and small size (Hoang et al., 2022; Sajid et al., 2022). Nanomaterials differ from bulk materials in many features, having at least one dimension in the range of <100 nm (Sohail et al., 2019).

Carbon-, metal/metal oxides-, ceramic-based, polymeric nanomaterials are applied in different technological and scientific fields because of their unique physico-chemical features compared with bulk ones (Sajid, 2022). Carbon based adsorbent such as activated carbon (AC), graphene oxide (GO), CNTs are widely used materials for the removal of water pollutants. Activated carbon as a common adsorbent has higher specific surface area (up to 2100 m²/g) than CNTs do (120-1300 m²/g). At the same time, CNTs - due to their tubular morphology - show selectivity towards certain types of pollutants after proper functionalization (Sajid et al., 2022).

The *carbon nanotubes (CNTs)* can simply be defined as a group of carbon nanomaterials which have tubular structure and have an arrangement of hexagonal carbon atoms bonded covalently. They have internal diameters in the range of nanometers and lengths in the range of micrometers (Sajid et al., 2022). The tubular nanostructure of graphitic carbon was discovered by Sumio Iijima in 1991 (Kharlamova and Eder, 2020). Likewise, in the most recent times, CNTs are considered as potential adsorbents finding a variety of remediation applications in almost all environmental fields including removal of organic pollutants and heavy metals from aqueous media (H. Li et al., 2019; M. Li et al., 2019). This attention is attributed to a number of characteristic features such as low density/weight, electrical

conductivity, large specific surface area and porosity, higher adsorption capacity, high tensile strength, good hydrophobicity, and ease of chemical activation (Sajid, 2022; Sajid et al., 2022). Moreover, these materials exhibit good thermal stability and strong affinity for organic materials and ionic pollutants (Sengupta et al., 2017). The methods for the CNTs preparation are usually selected on the basis of the required properties and the field of application.

CNTs have been mainly categorized based on the number of graphene sheets. There are three categories of CNTs reported in the literature such as single-walled SWCNTs, double-walled DWCNTs, and multiwalled MWCNTs (Ren et al., 2011). The surface properties of the CNTs can be modified via surface functionalization and in this way the hydrophobic and hydrophilic surfaces can be generated by modifications. In this way their surfaces become highly selective (Ren et al., 2011). Hence, for applications like removal of organic pollutants and heavy metals from water bodies, the MWCNTs are preferred (Pourzamani et al., 2015; Ren et al., 2011).

To date, numerous models have been tried to describe the adsorption of organic molecules over CNTs in aqueous phase, such as Freundlich, Langmuir isotherms and others. The rate of organic chemical adsorption over MWCNTs is equivalent to or even higher than that on activated carbon. Thus, the surface area may not be a direct factor to forecast organic chemical–MWCNTs interactions. Su et al. attributed the higher organic material adsorption over CNTs to larger average pore diameter and volume, morphology and functional groups (Su et al., 2010).

It is worth to mention that the adsorption over CNTs is of paramount importance due to the existence of high-energy adsorption sites such as CNTs and functional groups and interstitial and groove regions between the CNTs bundles (Pan and Xing, 2008). These adsorption sites mainly exist over grown CNTs. Thus, adsorption seems to be a general feature. The second is the condensation phenomenon, in which the pores and capillaries of CNTs become filled with liquid condensed from the vapour phase. While the organic chemicals adsorb on the CNTs surfaces, multilayer adsorption might happen. In this process, the first couple of layers collaborate with the surface, while the molecules further to the first two layers interact with each other. This process is known as surface condensation (Pan and Xing, 2008).

The sorption performance can also be enhanced through functionalization of the MWCNTs surface or by producing MWCNTs-based composites which show high

selectivity for adsorption, too. Functionalization of CNTs through physico-chemical methods can be classified into covalent and non-covalent categories as shown in Fig. 1 (Jun et al., 2018).

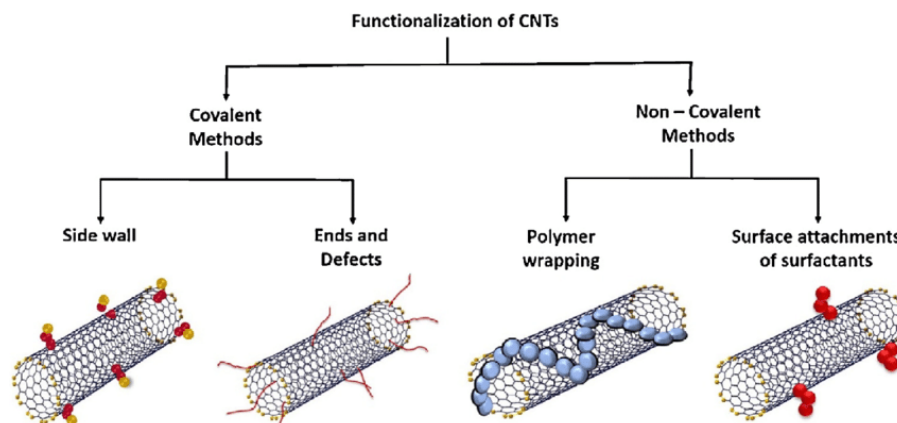


Fig. 1. Various modes of functionalization of MWCNTs (Jun et al., 2018).

After non-covalent functionalization the original CNT structure is preserved, but covalent functionalization changes the sp^2 hybridization to sp^3 one, leading to partial conjugation losses (Sajid et al., 2022).

Fig. 2. illustrates some of the main covalent and non-covalent functionalizations of CNTs. Functionality imparts useful properties which are lacking in the original MWCNTs. The surface modification of the CNTs with non-covalent modifications such as Van der Waals force, hydrophobic and π - π staking interactions is preferable as it enhances the interfacial properties of the CNTs by avoiding the destruction of CNTs structure (Jeon et al., 2011). Aromatic compounds, surfactants, and polymers are used for the non-covalent functionalization of CNTs (Jeon et al., 2011). It was shown that the surfactant-modified adsorbent treatment was successfully applied also for natural compounds such as coconut bagasse, sugarcane bagasse, bentonite, and diatomite in the removal of microplastics from wastewater (A. Oliveira et al., 2023).

Usually surfactant treatments are applied to lower the surface tension of CNTs and hence prevent aggregation of CNTs (Jeon et al., 2011). During CNTs aggregation bundles are formed where individual nanotubes stack together because of Van der Waals interactions (Pan and Xing, 2008).

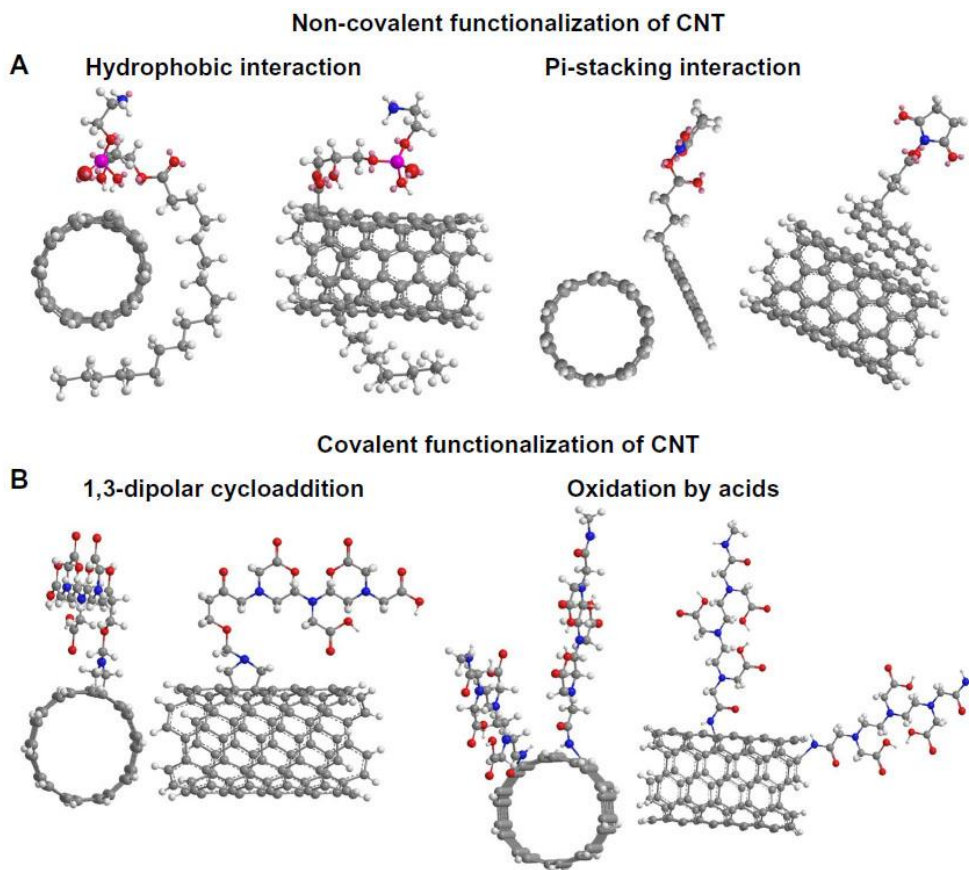


Fig. 2. Modes of CNTs functionalization (Kotagiri and Kim, 2014).

The physical adsorption of surfactants on the surface of CNTs tends to overcome the Van der Waals attraction by electrostatic/steric repulsive forces (Jeon et al., 2011). Furthermore, the dispersion of CNTs aggregates by surfactant's presence significantly increases. In this case the CNTs are well dispersed and more adsorption sites are available (Pan and Xing, 2008). Nanotubes in the presence of anionic, cationic and non-ionic surface active molecules such as sodium dodecylsulfate, benzylalkonium chloride, Triton X-100 were used in water purification steps (Alosime, 2023). Generally, the hydrophobic part of surfactants is oriented towards the surface of CNTs, whereas the polar moiety interacts with solvent molecules in the outer region (Dubey et al., 2021). It is believed that the nanotubes are in the hydrophobic interiors of the corresponding micelles, which results in stable dispersions (Hirsch, 2002).

Non-covalent functionalization with surfactants of the nanotubes can be performed by microemulsification procedure. Microemulsion-modified diatomite and

activated carbon were studied for the removal of organic (having aromatic nature) and inorganic (heavy metals) pollutants (Al-Ghouti and Al-Degs, 2011). In this case the anionic surfactant $\text{CH}_3(\text{CH}_2)_{10}\text{COO}^-\text{Na}^+$ was loaded on the solid surface. The effective removal of both types of pollutants was noted and was possible mainly due to adsorption by (I) an electrostatic force of the anionic head group of the surfactant and the positive charge of the organic molecules or the cation metal, and by (II) tail groups of the surfactant and the hydrophobic character of the organic molecules (Al-Ghouti and Al-Degs, 2011).

Covalent defect functionalizations are commonly achieved via oxidation by strong inorganic acids (Sezer and Koç, 2019) with oxidants such as KMnO_4 , ozone, or reactive plasma (Jeon et al., 2011). There are trials “to go green”, replacing the conventional oxidizing agents with residual biomass extracts such as vitamins, sugars, biodegradable polymers (M. Oliveira et al., 2023). Those oxidation treatments increases the hydrophilicity and can introduce carboxylate groups onto the MWCNTs surface (Anjum et al., 2019b). Similarly, further addition of any functionality to the surface of nanotubes can be carried out after the first step (Chiang et al., 2011). The adsorption ability and the hydrophilic nature is enhanced by oxygen-containing functional groups leading to increased dispersion in water and a better adsorption of polar molecules (Jung et al., 2015; Sajid et al., 2022). Moreover, strong acidic treatment of CNTs might wash out to a high extent the catalytic impurities such as Fe, Co, and Ni incorporated during the synthesis of carbon nanotubes by arc-discharge or chemical vapor deposition (Kotagiri and Kim, 2014). Hence, environmental and human risks associated with heavy metals contamination in waters are diminished (Afzaal et al., 2022).

Another method including cycloadditions (e.g. addition of carbenes, nitrenes), fluorination, hydrogenation, epoxidation have also been successfully employed (Hauke and Hirsch, 2010; Kotagiri and Kim, 2014; Syrgiannis et al., 2021). During covalent functionalization polar and/or non-polar functional groups are formed on CNTs surface. These groups can promote the CNTs dispersion in a wide variety of organic solvents (Jeon et al., 2011).

Hydrophobic CNTs surface can physically sorb organic molecules through π - π , Van der Waals, or hydrophobic interactions (Khandelia and Patel, 2022). Due to the sp^2 -hybridized carbon atoms, π - π interactions may occur between π electrons of

carbon atoms in CNTs and organic pollutant molecules with carbon-carbon double bonds or phenyl/benzene rings. With functionalized CNTs, π - π interactions may occur between delocalized π electrons of the phenyl ring and carbonyl groups (Sajid, 2022). Other mechanisms can involve hydrogen bonds and electrostatic interactions (because of the charged CNTs surface).

Recently, researchers have utilized numerous *metal-oxide nanoparticles* for the treatment of wastewaters such as zinc oxide (ZnO), iron oxide (Fe₂O₃), titanium dioxide (TiO₂), manganese oxide (MnO₂), cerium oxide (CeO₂), aluminium oxides (Al₂O₃), silver nanoparticles (N. Ghosh et al., 2022). Since these nanoparticles can be dispersed in water, their use in wastewater treatment can be justified. In addition, they are good adsorbents and show catalytic, antifungal and antibacterial activities (Kumari et al., 2019).

In order to overcome the poor stability and mechanical strength of metal-oxide nanomaterials, nanocomposites are increasingly used for purification of wastewater by removing unwanted species (Kumari et al., 2019). Different metal oxides-based CNTs were designed for removal of various dangerous pollutants from aqueous solutions: CeO₂-CNTs for arsenate removal (Peng et al., 2005), ZrO₂/MWCNTs for defluoridation (Ramamurthy et al., 2011), Ag-MWCNTs for removal of Cu(II) and Cd(II) (Venkata Ramana et al., 2013), mixed Pd/Fe nanonapaticles-MWCNTs for 2,4-dichlorophenol removal (Xu et al., 2012) and etc. The oxidative functionalization of CNTs is easy, followed by the precipitation of metal oxides in alkali media (Sarkar et al., 2018).

The use of semiconductor metal oxide-based CNTs as photocatalysts is also promising, especially for wastewater treatment. V₂O₅/CeO₂, V₂O₅/TiO₂, V₂O₅/ZnO nanocomposites can be applied as photocatalysts for the degradation of the organic pollutants, methylene blue (Zelege and Kuo, 2019). Combining the narrow band gap V₂O₅ (2.2 eV, $\lambda=564$) semiconductor photocatalyst with large band gap photocatalysts such TiO₂ (3.2 eV, $\lambda < 390$ nm) the visible light adsorption and hence the photocatalytic activity of the composites can be improved (Rakkesh et al., 2015; Saravanan et al., 2014; Yang et al., 2016). V₂O₅ compound showed significant photocatalytic activity (64%) toward various organic pollutants.

It was reported that the titania-modified carbon nanotube composite exhibited enhanced adsorption of organic pollutants such as methyl orange for the purpose of

their removal in comparison to pure TiO₂ nanoparticles (Duan et al., 2016). The improved catalytic activity of titania-modified MWCNTs may be due to the dominant contribution of nanotubes in MWCNTs/TiO₂ composites. The CNT was responsible to a decrease in the recombination rate of photogenerated electron-hole pairs. CNTs also provide a large surface area support for metal oxide particles (Saleh, 2022). The photocatalytic material V₂O₅-TiO₂ chemically deposited on the nanosheets was used for the total decomposition of acridine orange (2.5×10^{-5} M) dye in an aqueous medium under sun-light irradiation (Rakkesh et al., 2015). Methylene blue at concentrations of 50-250 mg/L was removed by anionic sulfonate group-functionalized CNTs, having maximum capacity of 236 mg/g (Lei et al., 2021). The reusable and easily removable magnetic Fe₃O₄-based MWCNTs adsorbent was designed for 20 mg/L of MB. It showed a maximum adsorption capacity of 204 mg/g. Removal efficiencies of MB from distilled and lake water were 99.5% and 89.9%, respectively (Song et al., 2021).

The rare earth elements (REEs) such as scandium (Sc), yttrium (Y), lanthanum (La) and lanthanides (Ln) play an important role as strategic materials for high technology, and there is a growing demand for these due to the wide-scale applications such as in fluorescent powders, light emitting diodes, permanent magnets, superconductors, electronic communications and magnetic materials (Haxel, et al., 2002). The metallurgical, chemical, and electrical industries can all benefit from the utilization of the REEs. Scandium is primarily used in energy saving lamps and glasses, as well as in the production of high strength aluminum-scandium alloys for domestic and military applications (Gambogi, 2021) in 0.1-2.0% concentration (SCY, 2023).

Scandium, yttrium and other rare earth elements can be investigated together because of their similar chemical properties. In fact, scandium is different from yttrium and other REEs in many aspects. Scandium does not have its own deposits (Neikov et al., 2019). The most important thing is that the scandium content in many rare earth element-rich minerals is very low, around 25 ppm. There are very few independent scandium minerals (Zhang et al., 2016). The only known ones are thortveitite and lolbeckite ores having Sc₂O₃ content up to 45% (Botelho et al., 2021).

Scandium is considered as a critical element by the EU, USA and Brazil due to its high economic importance (3800 US \$/kg). It is available in limited mining regions, practically irreplaceable in green technology applications and has a low

recycling rate (Botelho et al., 2021). This highlights the need of finding efficient recycling technologies. Recently many researchers have been working on the recovery of rare earth elements – including scandium - from secondary resources, such as nickel laterite (Chassé et al., 2019), ashes from power plants (Valentim et al., 2019), used electronic products (Kohl and Gomes, 2018), phosphogypsum waste (Cánovas et al., 2018) and bauxite residue (Cusack et al., 2019; Juzsakova et al., 2018; Salman et al., 2021). Scandium could be extracted from industrial wastes and deposits, for example, bauxite/red mud residues, accompanied by an enormous number of other elements such as iron and aluminum, which have genuinely comparative physical and chemical properties (Nawab et al., 2022). The red mud is the main solid residue of bauxite processing, which is rich in many important metal elements. Studies have shown that red mud contains about 100 to 390 ppm scandium, which is high in percentage as compared to other sources (A. Ghosh et al., 2022). Therefore, it is of great significance to study the extraction of scandium from red mud (Narayanan et al., 2018). The real challenge in this study is to increase selectivity towards Sc, since the red mud leachate contains some 30 other metals.

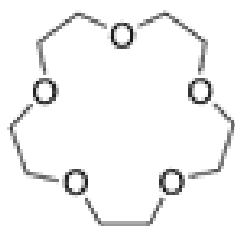
In the past decade, comprehensive investigations and significant efforts have been made on the recovery and separation of scandium. Different processes are employed for metal separation from ores or from waste solutions. These are used alone or in combination with the following methods: solvent extraction (aqueous-organic extraction) (Hu et al., 2020; Zou et al., 2022), liquid membrane separation (Hedwig et al., 2022), ion exchange (Molchanova et al., 2019) and co-precipitation (Nawab et al., 2022). Another group of processes is referred to as solid-phase extraction which involves macro ligands immobilized on a solid phase (Zhang et al., 2019).

Among these processes, ion exchange (Mikeli et al., 2022), solvent extraction (Zou et al., 2022) and solid-phase extraction (Ramasamy et al., 2018) have been increasingly employed for the selective separation of metals. The choice of organic extractants and aqueous solutions is influenced by several factors including technical performance, environmental impacts and cost considerations. The main problem of Sc_2O_3 production comes from high cost of the cationic resins, organic solvents and inorganic acids - used for leaching of Sc from raw/waste sources (Narayanan et al., 2018). Development and application of efficient and selective target metal recovery processes can potentially contribute to cost reductions of Sc recovery from any

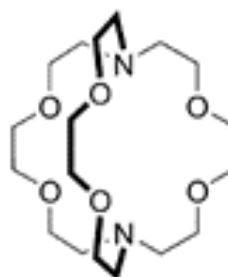
prospective industrial waste such as red mud. Organic ligands as metal extractants are used either alone or in mixtures in different media in diverse hydrometallurgical processes to achieve efficient separation of the desired metals. Commonly used organophosphorus commercial extractants include di-2-ethylhexylphosphoric acid (D2EHPA), 2-ethylhexylphosphonic acid mono-2-ethylhexyl ester (HEHEHP), bis(2,2,4-trimethyl pentyl) phosphinic acid (Cyanex® 272) and tributyl phosphate (TBP) (Yudaev et al., 2021; Botelho et al., 2021; Lakshmanan and Vijayan, 2018).

The several known macrocyclic and oxygen-containing compounds have also been used extensively in extraction, because of the excellent matching between the crown-ring sizes and the ionic radii of metals (Kostikova et al., 2018). The pioneering work on crown ethers and cryptands was made by Charles Pedersen in 1967 (Hamilton, 1984) and Jean-Marie Lehn in 1973 (Jong and Reinhoudt, 1980; Marcus, 2004). As to the notation „x-crown-y”, x means the number of atoms in the ring and y is the number of oxygens building up the repeated ethylenoxy unit (OCH₂CH₂) (Gierczyk, 2013). Cryptands have one or more coordination bridges across the macrocycle forming a pre-organized polycyclic cavity. They have CH₂CH₂X building units where X is the donor atom (O, N, S, P) (Gierczyk, 2013).

In case of cryptand 2.2.2, the numbers indicate the number of ether oxygen atoms in each of the three bridges connecting the two nitrogen heteroatoms (Redd et al., 2003). Examples of crown ethers and cryptand compounds are shown in Fig.3.



15-crown-5:
1,4,7,10,13-
Pentaoxacyclopentadecane,
(C₁₀H₂₀O₅)



cryptand 2.2.2:
4,7,13,16,21,24-hexaoxa-
1,10diazabicyclo[8.8.8]hexacosane,
(C₁₈H₃₆N₂O₆)

Fig. 3. Examples of a crown ether and a cryptand.

The binding energy for the crown-ether complexes with hard Lewis acid cations is probably due to cation-dipole interactions (Jong and Reinhoudt, 1980). Cations like Sc^{3+} and La^{3+} are non-polarizable (Haas and Franz, 2009). Bis- or tris-macrocyclic cryptands with bound cations can strongly attract ionic agents into the organic phase with higher efficiencies than simple macrocycles. Using chemically diverse and highly coordinating ligands, the range of sequestered ions can be extended to lanthanides and transition metal ions (Zaleski, 2022). The stability of macrocycle complexes depends on three main factors: (a) *steric effects*, these include cavity size of the ligand, extracted metal cation radii; (b) *electronic effects*, these include electron density at the binding sites of organic ring, the number and type of the donor heteroatoms (e.g. O, N), presence of additional binding sites; (c) *solvent effects*, rises from the type of the solvent used (Jong and Reinhoudt, 1980; Leite et al., 2007).

One of their most remarkable properties is the capability to complex metal cations based on their cavity size. The stability of the complexes is increased when the cation-to-cavity ratio is approaching unity (Jong and Reinhoudt, 1980). The binding capacity is decreasing with imperfect fit and when the size of the metal is bigger than that of the cavity, an „on-top” arrangement occurs (Zaleski, 2022).

Macrocyclic compounds are soluble in different types of organic compounds, protic (H_2O , methanol) and polar aprotic solvents (dimethyl sulfoxide, dimethylformamide, propylene carbonate), and can also be used in extraction of salts by crown ethers from water into an organic solvent with a low dielectric constant (trichloromethane, dichloroethylene, benzene) (Petrenko et al., 1988).

As to the cation complexation stability, the electron density around the crown ether oxygen atoms has a significant effect (Hamilton, 1984). When a CHCH unit is replaced by a benzo- or dicyclohexyl group in the 18-crown-6 compound, the electron density is reduced at two oxygen binding sites (Jong and Reinhoudt, 1980). Crown ethers with rings have stronger organophilic character. The ones with cyclohexyl groups are more soluble in water, alcohols and aromatic hydrocarbons (CE, 2003).

Depending on the number of oxygen and nitrogen donor atoms being in the macro-cyclic ring, it has the size of selectively matching metal ions. The complexation of highly polarizable ions can be enhanced with softer nitrogen and sulphur heteroatoms replacing the donor oxygens. The lone pair of the less-electronegative nitrogen atom makes the aza-microcycles more favourable to bind transition metal ions

(Zaleski, 2022). The cyclic crown ether structure with multidentate O and N atoms offers a feasible approach for the complexation of lanthanide(III) ions (Huang, 2010). The stability and selectivity of complex formation of macrocyclic compounds with cations are influenced by the interaction of the cation with the solvent as well as with the crown ether, cryptand (Rounaghi et al., 2011). Thus, if the solvent medium is or its properties (e.g. polarity, hydrogen bond donor/acceptor ability, polarizability, acidity/basicity, hydrophobicity/hydrophilicity) are changed, a significant effect on the metal binding constant is observed.

Macrocyclic compounds of various sizes and substituents have been used in the extraction of REEs (Lakshmanan and Vijayan, 2018). A great variety of crown ethers was used to extract REEs from picrate- and nitrobenzene- containing aqueous solutions (Lakshmanan and Vijayan, 2018). It was found that Tb^{3+} , Eu^{3+} , Gd^{3+} , Nd^{3+} and Yb^{3+} can be more easily extracted using 15-crown-5 than Ce^{4+} , Sm^{3+} , Dy^{3+} and Lu^{3+} . A quantitative removal of Ce^{4+} (3.57 mol/L) by 18-crown-6 (0.07 mol/L) from 4 mol/L HNO_3 solution containing other lanthanides into kerosene was reported (El-Hefny et al., 2011). The separation of light REEs (like La, Ce, Pr, Nd, Sm or Eu) from heavy elements (Tb, Tm, Lu) by the use of 18-crown-6 and trichloroacetate was also reported (Samy et al., 1988). Using a similar system, 18-crown-6 in dichloroethane, extraction of La^{3+} and Eu^{3+} in the form of trichloroacetate complexes can be achieved (Lakshmanan and Vijayan, 2018).

1. OBJECTIVES AND GOALS

Development in the field of nanomaterials has opened new avenues in their environmental applications. The application of adsorbents for environmental pollution control has attracted the attention of the scientific community. This can be due to the potential of nanotechnology to successfully cope with long-term environmental problems including the pollution of surface waters with hydrocarbon derivatives. However, further development of novel adsorbent materials with customized and tailored properties including but not limited to the topics of hydrophobicity and oleophilicity is necessary.

This research is aimed at the development of advanced oil adsorbents for the removal of hydrocarbons from surface waters via functionalization and chemical modifications of multiwalled carbon nanotubes (MWCNTs). The development of the multiwalled carbon nanotubes included the microemulsification of MWCNTs with the goal to enhance the dispersion and adsorption properties of MWCNTs. The functionalization with microemulsion method was implemented to modify the surface structure of MWCNTs by attaching a hydrocarbon tail of anionic surfactant on its surface while the hydrophilic head of the surfactant faces to solvents. In addition, it is proposed that direct modification of MWCNTs by the microemulsion technique tends to improve the hydrophobicity of the nanotubes surface, hence improve adsorption ability towards hydrocarbon pollutants (alkanes, aromatic compounds).

In addition, another modification method was applied via oxidation of MWCNTs followed by doping the MWCNTs with nanometal oxides (V_2O_5 , CeO_2 and $V_2O_5:CeO_2$) to enhance removal efficiency towards methylene blue dye from model contaminated water solution. In this work, the structural and surface chemistry properties of the prepared adsorbent materials are studied by different surface analytical techniques and their methylene blue removal efficiency from a model aqueous solution is correlated.

Also, this research deals with the study of the ways of metal ion capture in liquid–liquid extractions. The research is focused on the most important variables (extractants concentrations, pH of solution) affecting the process of extracting Sc^{3+} from the aqueous matrices by 12-crown-4 (12-C-4), 15-crown-5 (15-C-5), DC18-crown-6 (DC18-C-6) and cryptand 2.2.2 (C2.2.2). The identification of the structure

of the complexes between these macrocyclic compounds and Sc^{3+} is an important task to elaborate efficient extraction systems based on molecular recognition methodology. It is assumed that the experimental results can contribute to the successful and complex utilization of red mud.

2. EXPERIMENTAL

2.1. Materials

Raw (commercial) and modified MWCNTs were used for the experiments. Commercial grade MWCNTs were purchased from Timesnano Ltd. (TNNF-6 type, China) made by chemical vapour deposition technique (CVD) and were used for this research. From now on, commercial MWCNTs are referred to as untreated, fresh or raw multiwalled carbon nanotubes. The purchased MWCNTs had a length of 5-20 μm and 10-20 nm outer average diameter with a purity of $> 95\%$ and a specific surface area of $120 \text{ m}^2/\text{g}$.

The following chemicals were used: undecane ($\text{C}_{11}\text{H}_{24}$, 99%), toluene (C_7H_8 , 99.5%), isoamyl alcohol ($\text{C}_5\text{H}_{12}\text{O}$, 99%), and coconut fat purchased from Sigma Aldrich, cyclohexane (C_6H_{12} , 99.99%, Reanal Ltd.), kerosene (EU number: 649-423-00-8) obtained from MOL Company, ammonium metavanadate (NH_4VO_3 , 99.99%), nitric acid (HNO_3 , 99%), cetrimonium bromide (CTAB, $\text{C}_{19}\text{H}_{42}\text{BrN}$, 99%), ethanol ($\text{CH}_3\text{CH}_2\text{OH}$, 99.8%), cerium(IV) sulfate tetrahydrate ($\text{Ce}(\text{SO}_4)_2 \cdot 4\text{H}_2\text{O}$, 99.0%), urea (NH_2CONH_2 , 99%), methylthioninium chloride or methylene blue (MB) ($\text{C}_{16}\text{H}_{18}\text{N}_3\text{S}$), oxalic acid ($\text{C}_2\text{H}_2\text{O}_4$, 98%) purchased from Merck Kft., Budapest, Hungary as well as hydrochloric acid (HCl , 99.7%), sodium hydroxide (NaOH , 99.0%) and sulfuric acid (H_2SO_4 , 99.7%) were purchased from VWR International Kft., Debrecen, Hungary. All chemicals used for the REEs extraction with macrocyclic compounds were of analytical grade:

- 1,4,7,10-tetraoxacyclododecane (12-crown-4, 12-C-4, $\text{C}_8\text{H}_{16}\text{O}_4$, 98%),
- 1,4,7,10,13-pentaoxacyclopentadecane (15-crown-5, 15-C-5, $\text{C}_{10}\text{H}_{20}\text{O}_5$, 98%),
- 4,7,13,16,21,24-hexaoxa-1,10diazabicyclo[8.8.8]hexacosane (cryptand 2.2.2 or kryptofix 2.2.2, C2.2.2, $\text{C}_{18}\text{H}_{36}\text{N}_2\text{O}_6$, 98%),
- di-cyclohexano-18-crown-6 (DC18-crown-6, DC18-C-6, $\text{C}_{20}\text{H}_{36}\text{O}_6$, 98%) as well as
- 1,2-dichloroethane ($\text{C}_2\text{H}_4\text{Cl}_2$, 99.8 %) solvent.

Sc, Y, La, Ce (1000 mg/L) in 2% HNO_3 were used as standards for analytical and model solution measurements. All aqueous solutions were prepared with distilled water.

2.2. Microemulsification preparation of MWCNTs

Raw MWCNTs were treated by microemulsion according to the procedure described (Al-Ghouti and Al-Degs, 2011; De Castro Dantas et al., 2001). In this method, saponified coconut oil (mostly lauric acid, $\text{CH}_3(\text{CH}_2)_{10}\text{COOH}$) was used as surfactant. Coconut oil was saponified in alkali solution to form $\text{CH}_3(\text{CH}_2)_{10}\text{COOK}$. After saponification a mixture of the surfactant (10 m/m%), deionized water (25 m/m%), the co-surfactant isoamyl-alcohol (40 m/m%) and the hydrocarbon phase (n-octane) (25 m/m%) was made. To prepare microemulsified adsorbents, 10 g of MWCNTs and 20 mL of microemulsion were mixed for 4 h and then dried at 65°C for 48 h. Hereinafter the microemulsified multiwalled carbon nanotubes are referred to as “ $\mu\text{EMWCNTs}$ ”.

2.3. Preparation of metal-oxides nanoparticles

2.3.1. Preparation of vanadium pentoxides nanoparticles

Vanadium pentoxide (V_2O_5) was prepared by surfactant-mediated method (Asim et al., 2009) using cetyltrimethylammonium bromide (CTAB) a cationic surfactant. The CTAB is applied for synthesis of nanomaterials (Yu et al., 2004). At first 0.1 g of NH_4VO_3 and 0.1 g of CTAB were dissolved in a mixture of distilled water-ethanol (100 mL) in the ratio of 7:3. This was followed by adding HNO_3 slowly under continuous stirring until the pH became 2.5 in order to get clear solution and formation of H_3VO_4 (Bouzbib et al., 2023). The mixture was stirred for 6 h. The precipitate was washed 10 times with distilled water and it was followed by washing with ethanol. Then it was dried at 90°C in an oven for 60 min to obtain the vanadia nanoparticles, named “as prepared sample”, and the sample was annealed at 500°C . (V_2O_5 is thermally stable until the measured temperature of 600°C).

2.3.2. Preparation of cerium dioxides nanoparticles

Cerium dioxide was prepared by hydrothermal method using an autoclave. The conventional hydrothermal method is successfully used for preparation of the nanosized material (Lin et al., 2012) as well as for high-purity, homogeneous, and ultrafine powders (Wu et al., 2002). The resulting high crystallinity is the main advantage of this technique (Alhalili, 2023; Yin and Hasegawa, 2023). Ceric sulfate tetrahydrate, urea and cetyl-trimethylammonium bromide were used for the

preparation. CTAB was applied as surfactant for the prevention of nanoparticles coagulation (Lin et al., 2012). At first, 2.34 g of $\text{Ce}(\text{SO}_4)_2 \cdot 4\text{H}_2\text{O}$, 1.39 g of urea and 2.1 g of CTAB were dissolved in 50 mL distilled water and then mixed for 30 min. The materials were put into the autoclave and were kept at 200 °C for 12 h. The cerium hydroxide obtained was washed with distilled water several times and was centrifuged. Following this, it was washed with ethanol, dried at 90 °C for 60 min, and annealed at 500 °C.

2.3.3. Preparation of mixed $\text{V}_2\text{O}_5:\text{CeO}_2$ nanocomposite

Combination the narrow band gap V_2O_5 semiconductor (2.2-2.8 eV) photoactive material with large band gap CeO_2 (3.23 eV) photoactive material makes the application of the $\text{V}_2\text{O}_5:\text{CeO}_2$ composite suitable not only for removing of hazardous MB but also for the degradation its nontoxic by-products (Saravanan et al., 2013; Zeleke and Kuo, 2019). The $\text{V}_2\text{O}_5:\text{CeO}_2$ composite was prepared by mixing V_2O_5 and CeO_2 in a molar ratio of 3:1. The oxides were mixed in a beaker with ethanol for 6 h on a magnetic stirrer, then the mixture was placed into a furnace and annealed for 2 h at 500 °C.

2.3.4. Functionalization of MWCNTs with metal oxide nanocomposites

Firstly, MWCNTs were treated using strong acids H_2SO_4 and HNO_3 with ratio of 3:1. The process of modification was carried out using strong oxidizing agents to introduce chemically active oxidative defects sites to connect the carboxyl ($-\text{COOH}$), carbonyl ($-\text{CO}$) and hydroxyl ($-\text{OH}$) groups onto the MWCNTs surface (Sezer and Koç, 2019). The oxygen containing groups can act as anchoring sites for the metal oxide phases during the functionalization of MWCNTs (Chiang et al., 2011). MWCNTs and the concentrated acid mixture were added to a beaker and ultrasonicated for 30 min. Following this, the mixture was transferred to a round bottom flask for reflux for 8 h at 180 °C before being diluted several times with distilled water, filtered by a membrane filter and washed until the pH became 7.

The addition of functionality to the surface of nanotubes was carried out with metal oxides and their composite nanoparticles applying the hydrothermal method. The prepared individual metal oxides (CeO_2 and V_2O_5) as well as their mixed nanocomposites were added to MWCNTs in 70 mL of ethanol in an amount of 5 m/m%. The solution was stirred at 40 °C for 4 h using a magnetic stirrer and

ultrasonicated for 30 min before being heated under reflux for 4 h at 90 °C. The solution was transferred to an autoclave reactor and kept at 200 °C for 4 h. Finally, the samples were dried by evaporating the ethanol at 85 °C. Hereinafter the metal oxide-doped MWCNTs are referred to as “Ce/MWCNTs”, “V/MWCNTs”, and “V:Ce/MWCNTs”.

2.4. Characterization methods

The specific surface area, pore volume and pore-size distribution of the samples within the micropore (1.7–2 nm), mesopore (2–50 nm) and macropore (50–100 nm) regions were determined by nitrogen adsorption/desorption isotherms at -196 °C using an analyzer ASAP 2000 manufactured by Micromeritics, USA. The specific surface areas of the samples were determined by the BET (Brunauer–Emmett–Teller) method from the corresponding nitrogen adsorption isotherms. The pore-size distribution and pore volumes were calculated from the nitrogen desorption isotherms using the BJH (Barret–Joyner–Halenda) model.

Identification of the solid crystalline phases in the samples was made by X-ray diffraction analysis (XRD) using a Philips PW3710 X-ray diffractometer equipped with Cu-K α radiation ($\lambda=0.1541$ nm) and recorded at room temperature over the 4–70° 2 θ angular range with a scanning acquisition speed of 0.02 °/sec.

The morphology of the surface of the nanocomposites was studied using transmission electron microscopy (TEM) and scanning electron microscopy (SEM) techniques. The nanocomposites for TEM were prepared by depositing a drop of nanocomposites suspended in ethanol on copper grids covered by an amorphous lacey carbon support film. SEM and TEM analyses were performed using a Thermo Fisher Scientific Apreo S LoVac SEM in the Czech Republic operated at 2.0 kV for backscattered electron imaging and at 30.0 kV for transmission electron imaging, equipped with an energy-dispersive X-ray spectrometer (EDX), (AMETEK’s Octane Elect Plus, USA).

Atomic Force Microscopy (AFM) analyses were carried out using a SPM-AA 3000 type instrument. AFM was used to probe the sample surface in nanometer scale in order to investigate the surface roughness and surface particle-size distribution. The samples were dispersed in ethanol and transferred onto a glass plate of 0.5 x 0.5 mm size for analysis.

Raman spectra were recorded using a Bruker RFS 100/S FT-Raman spectrometer with a Nd:YAG laser source (1064 nm, 30mW) and a liquid N₂ cooled Ge detector. Signal-to-noise ratio was improved by the coaddition of 2048 spectra with a resolution of 4 cm⁻¹. Spectral deconvolution of the baseline-corrected Raman spectra was achieved by a mixture of Gaussian and Lorentzian line shapes with the PeakFit software (v4.12, Seasolve).

Thermoanalytical measurements (TG/DTG) were carried out using a Netzsch TG-209 type thermobalance. Samples were measured in ceramic crucibles. The TG/DTG curves were registered while heating the samples to 1000 °C (10 °C/min heating rate) in dynamic argon flow (99.998%).

Elemental analyses were performed using inductively coupled plasma optical emission spectroscopy by means of an Avio 550 Max ICP-OES type instrument (Perkin Elmer Inc., USA) in the 0-50 mg/L. The analytical wavelengths (in nanometers)-were as follows: Sc 361.383, Y 360.073, La 408.672, Ce 418.660.

The pH of the aqueous solutions was measured by a Metter Toledo, Seven Multi type pH meter (Germany) within the 0 to 7 pH range.

2.5. Adsorption tests

The adsorption tests over MWCNTs, functionalized MWCNTs as well as nanometal oxides particles were carried out with selected pure hydrocarbons, kerosene-cut and methylene blue to study the efficiencies of their removal from water. The adsorption capacities were evaluated using two methods such as gas chromatography (GC) and ultraviolet-visible spectroscopy (UV-Vis). Selection of the suitable analytical technique depends on the type of the model hydrocarbon (undecane: n-C₁₁H₂₄, toluene: C₆H₅-CH₃ and kerosene).

2.5.1. Hydrocarbon solution preparation and adsorption tests

Typical hydrocarbons present in produced/spilled oil-contaminated water include aliphatic, naphthene-types and aromatic compounds. Accordingly, several hydrocarbon model compounds were used for studying the adsorbents.

The commercially available kerosene (EU number: 649-423-00-8, MOL Co.) was further purified. The obtained kerosene cut contained only alkanes from C₁₀ to C₁₆, and it was used for the preparation of kerosene-water mixtures. The kerosene cut had a boiling point range of 174–287 °C with a density of 0.800 g/mL. The solutions

were prepared in a glass flask by adding 156 μL kerosene to 250 mL distilled water, resulting in a kerosene solution concentration of 500 mg/L. The model solutions were mixed for 10 min using a magnetic stirrer followed by adding the adsorbent in an amount of 10 mg. Then the solutions were kept under continuous mixing for an additional 30 min at room temperature. The adsorbent was separated from the solution with S1 porous glass filter having a pore size of 100–160 μm . The filtered solution was taken for the extraction step for the determination of the hydrocarbon content by gas chromatographic (GC) method according to Hungarian Standard MSZ 1484-7 (MSZ, 2009). The kerosene-water solution was extracted two times, with 15 mL hexane. The collected hexane fraction was dried with Na_2SO_4 powder. The blank solution was prepared by the same method without adding adsorbent. Kerosene standard was prepared by dissolving 156 μL kerosene in 25 mL hexane to prepare the reference solution.

UV-Vis analysis was carried out for studying toluene removal by MWCNTs and $\mu\text{EMWCNTs}$, as well as by activated carbon from water samples. The solutions were prepared in a glass flask by adding 145 μL toluene (0.8669 mg/ μL) to 100 mL distilled water, resulting in a toluene solution with a carbon concentration of 500 mg/L. The model solutions (250 mL) were mixed for 10 min using magnetic stirrer followed by adding the adsorbent in an amount of 10 mg. After 30 min of running the adsorption test, the adsorbent was separated by filtration, and the organic phase (aromatic hydrocarbon) was extracted from the filtrate by cyclohexane. The extract was dried over sodium sulfate.

2.5.2. Protocol for samples analysis via gas chromatography

The liquid samples were analyzed by an Agilent, GC 7890A type gas chromatograph using a J&W HP-5 type capillary column (30 m x 0.320 mm, 0.25 μm film thickness) and a flame-ionization detector (FID). The determination of the hydrocarbon contents was carried out according to the Hungarian Standard MSZ 1484-7 (MSZ, 2009). Before the extraction with hexane, 1-chloro-octadecane standard was added to the samples to determine the recovery efficiency of the hydrocarbons by GC techniques. The kerosene-water solution (250 mL) was extracted two times, with 15 mL hexane. The collected hexane fraction was dried with Na_2SO_4 powder. The blank solution was prepared in the same method without adding adsorbent. Kerosene

standard was prepared by dissolving 175 μL kerosene in 25 mL hexane to determine the manipulation efficiency of the kerosene–water sample. An internal/injection standard was added to the 25 mL hexane solution, and an aliquot of 2 μL was injected into the gas chromatograph. An injection standard, 1,4-dichlorobenzene, was used for control of the GC analysis. The adsorption capacity of the $\mu\text{EMWCNTs}$ was compared with those of commercially available activated carbon sorbents as reference materials. Chemiviron Carbon F300 and Norit GAC 1240EN with a surface area of about 1100 m^2/g were used as benchmark sorbents.

2.5.3. Analysis of toluene by UV-Visible spectroscopy

Toluene was selected as a model hydrocarbon for the ultraviolet-visible (UV-Vis) spectroscopic studies. UV-Vis spectrophotometry with a deuterium lamp can be used for the determination of the aromatic hydrocarbon content of water samples. A Nicolet Evolution 500–UV-Vis double beam spectrometer (Thermo Electron Co.) with 1 cm quartz cuvette and a single photomultiplier detector was used in the 230–400 nm wavelength range to detect the aromatic hydrocarbon content of the water samples. The preparation of the model toluene-water mixture was the same as given earlier. After 30 min of running the adsorption test, the adsorbent was separated by filtration, and the organic phase (aromatic hydrocarbon) was extracted from the filtrate by cyclohexane and the extract was dried over sodium sulfate.

2.5.4. Methylene blue adsorption study by UV-Visible spectroscopy

Metal oxide-based MWCNTs were used for the removal of MB by adsorption from water. Two different methylene blue resonance cation structures are presented in Fig. 4a. (Saad et al., 2015). The maximum absorbance of a MB solution in water (MB concentration: 20 mg/L) was monitored by a NANOCOLOR UV-Vis spectrophotometer (MACHEREY-NAGEL, Germany) within the range of 400 to 700 nm. The maximum absorbance of the MB monomer form was observed at $\lambda_{\text{max}} = 665$ nm as shown in Fig. 4b as reported (Wani et al., 2023). A stock solution was used to prepare the calibration curve at different MB concentrations (4, 8, 12, 16, 18 and 20 mg/L). The absorbance vs. concentration plot is shown in Fig. 4c.

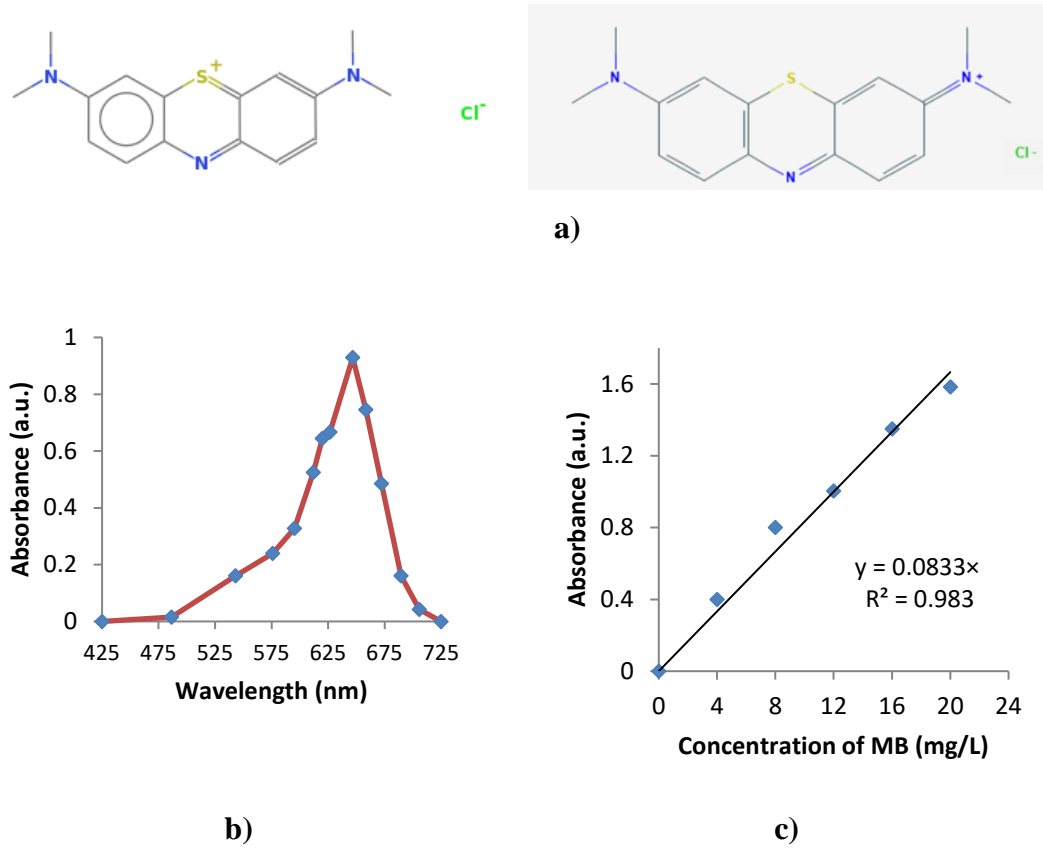


Fig. 4. Methylene blue cation forms (a), UV-Vis absorption spectrum of the MB solution (b), and standard calibration curve of MB solutions at 665 nm (c).

MB stock solutions were diluted with distilled water. The pH of the dye solution was set at the desired pH of 7 using 0.1 M NaOH or 0.1 M HCl. For each experiment, 20 mL of MB solution (20 mg/L) was extracted and 20 mg of metal oxide was added to the solution. The removal efficiency of MB was studied as a function of contact time, adsorbent dosage and temperature in order to determine the optimum conditions for the process. Once the reaction had finished, the samples were stockpiled and taken for separation. The dye concentration in the supernatant was checked using the UV-Vis spectrometer at 665 nm. The efficiency of pollutant removal (RE, %) and the quantity of organic molecules adsorbed (q_t) were calculated by Eqs. (1) and (2), respectively (Hameed et al., 2007; Song et al., 2021):

$$RE = \left(\frac{C_0 - C_t}{C_0} \right) \cdot 100 \% \quad (1)$$

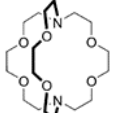
$$q_t = \frac{(C_0 - C_t)}{m} \times V \quad (2)$$

where C_0 denotes the initial pollutant concentration (mg/L); C_t stands for the final pollutant concentration at time t (mg/L); q_t represents the adsorption capacity at time t (mg/g); V refers to the volume of model solution (L); and m is the weight of adsorbent (g).

2.6. REEs extraction by macrocyclic compounds and stripping procedure

Extraction studies were carried out at room temperature with two types of macrocyclic compounds: crown ethers and cryptand. Their structures and size characteristics are illustrated in Table 1.

Table 1. Structure of the macrocompounds used (Agarwal et al., 2023; Buschmann, 1988; Faridbod et al., 2008).

Compound	Cavity radii, r (Å)	Abbreviation	Molecule dimension	Structure
12-crown-4 ether	0.6-0.75	12-C-4	2D	
15-crown-5 ether	0.85-1.1	15-C-5	2D	
cryptand 2.2.2	1.4*	C2.2.2	3D	
dicyclohexyl-18-crown-6 ether	1.3-1.6	DC-18-C-6	2D	

* cavity dimension is a fixed size since the structure of cryptand is more rigid and restricted due to its three-dimensional arrangement of donor atoms, O and N.

The model solutions of Sc single element were prepared in different concentrations (25 to 100 mg/mL) from the corresponding analytical Sc standard of 1000 mg/L in 2% HNO₃ at pH of solution from 1 to 5 as summarized in Tables S1 and S2. The macrocyclic compounds in different concentrations (0.001 to 0.01 mol/L) were dissolved in 1,2-dichloroethane. The solvent C₂H₄Cl₂ was chosen because it is moderately polar ($\epsilon = 9.7$) leading to negligible partition of MCs between water and organic phase (Manuel Aguilar Sanjuán and Cortina, 2008). Equal volumes (10 mL) of the organic phase and aqueous Sc model solutions were contacted and mixed in a

separatory funnel for 15 min in order to reach the equilibrium. The extraction steps are illustrated in Fig. 5.

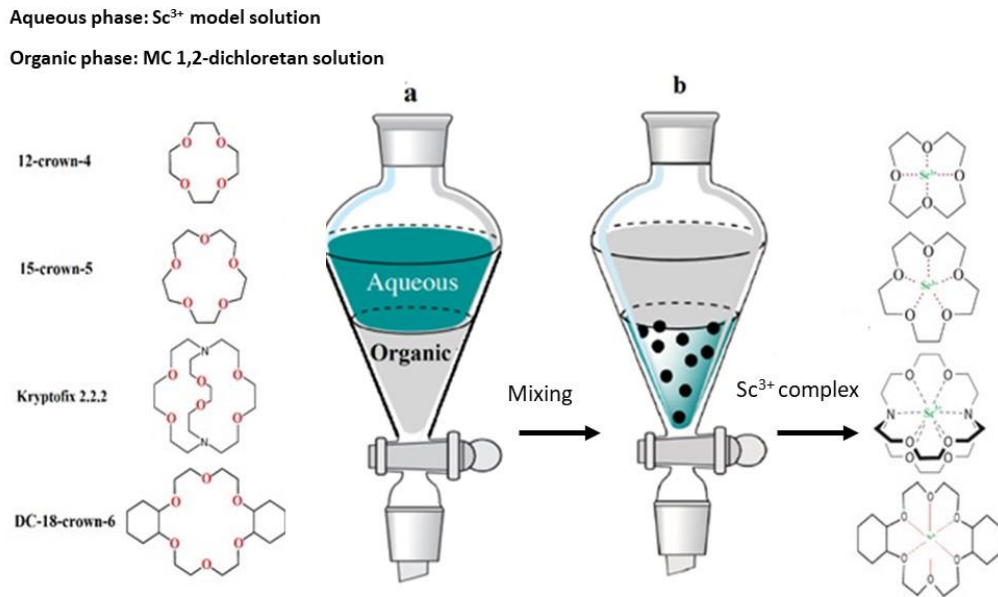


Fig. 5. Representation of Sc³⁺ extraction by macrocyclic compounds and its encapsulation (a) mixing, (b) phase separation steps. Black circles represent Sc ions in the organic phase.

The organic phase contained the extracted Sc. The next step was the recovery of Sc from the organic phase. Back extraction or stripping experiments were conducted by contacting 10 mL of Sc-loaded organic phase with 10 mL of hydrochloric or nitric acid stripping solutions for 15 min in a separatory funnel. The separated aqueous phase after extraction and back extraction was analysed by ICP-OES method.

The Sc, Y, La, and Ce (25 mg/L of each element in aqueous medium) multielements extraction experiments were made by 0.008 mol/L C2.2.2 at different pH of the REEs solutions.

The extraction efficiency (E, %) was calculated by Eq. (3) (Hu et al., 2020):

$$E = \frac{C_i - C_f}{C_i} \cdot 100\% \quad (3)$$

where, C_i and C_f are initial and final concentrations of the target metal in the aqueous phase (mg/L).

3. RESULTS AND DISCUSSION

3.1. Functionalized carbon nanotubes for hydrocarbon removal from water

3.1.1. Results of SEM analysis

Fig. 6. illustrates the TEM record on the MWCNTs as provided by the manufacturer.

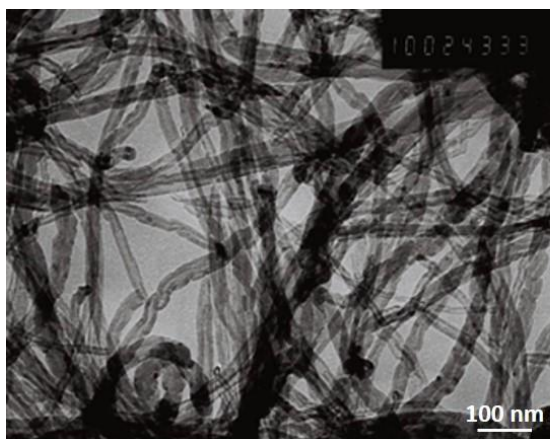


Fig. 6. The transmission electron microscopic (TEM) record of the MWCNTs (by courtesy of the MWCNTs manufacturer).

It can be seen that the MWCNTs are molecular size tubes, which are approximately 10,000 times thinner than a human hair. The MWCNTs consist of rolled-up sheets, in which case the primary building units are hexagonal carbon formations. The SEM record taken by the author (Fig. 7a) was in agreement with the one offered by the manufacturer.

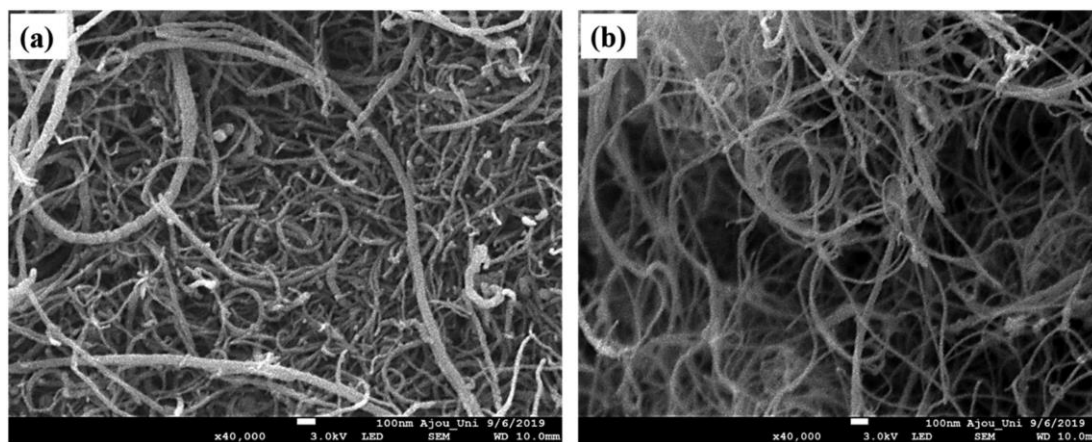


Fig. 7. The scanning electron microscopic (SEM) record of the (a) raw MWCNTs, (b) μ EMWCNTs at magnification: x 40.000 (taken by the author).

SEM and TEM analyses revealed interesting morphological features in the Timesnano MWCNTs as it had a mixture of smooth walled nanotubes with continuous hollow cores that were mainly bundles and ropes as can be seen. For μ EMWCNTs, Fig. 7a and b showed that microemulsification preserved the shape of the nanotubes.

3.1.2. Results of the morphological analysis

The MWCNTs had a length of 5–20 μ m; the outer average diameter was 10–20 nm with a purity of > 95%. The specific surface areas and pore size distributions of samples MWCNTs and μ EMWCNTs are presented in Table 2. In the case of the raw MWCNTs sample, the measurements were carried out at 30 and 160 °C. The pretreatment temperature has no significant effect on the weight loss of each sample. The weight loss of the MWCNTs sample during the pretreatment at 160 °C in a vacuum before the nitrogen sorption was 0.32 m/m % (Table 2).

Table 2. The specific surface area (S_{BET}), pore volume (V), and average pore volume (D_{av}) of the MWCNTs and μ EMWCNTs samples.

Sample and pretreatment temperature, T °C	Mass loss (m/m %)	S_{BET} (m^2/g)	S_{BJH} (m^2/g)	S_{micro} (m^2/g) ^a	$V_{1.7-300}$ (cm^3/g) ^b	V_{micro} (cm^3/g) ^c	D_{av} (nm) ^d
MWCNTs, 30 °C	0.21	155	159	14.7	0.7781	0.0067	13.1
MWCNTs, 160 °C	0.32	156	158	15.2	0.6847	0.0069	12.5
μ EMWCNTs, 65 °C	0.32	98	110	0	0.7026	0	18.3

^a The specific surface area of micropores (< 2 nm);

^b Pore volume according to Barrett, Joyner and Halenda (BJH) theory for pores having a diameter between 1.7 and 300 nm;

^c Volume of micropores (< 2 nm);

^d Average pore diameter, nm.

A similar mass loss was observed for μ EMWCNTs during the pretreatment at 65 °C under a vacuum. The mass loss is an indication of the desorption of the adsorbed gases/components from the surface of the sample. These results are in accord with the results of the thermoanalytical investigations (Section 3.1.4.) in which mass losses up to 200 °C temperature were lower than 0.5 m/m % for both samples. The adsorption and desorption isotherms of the samples are presented in Fig. 8.

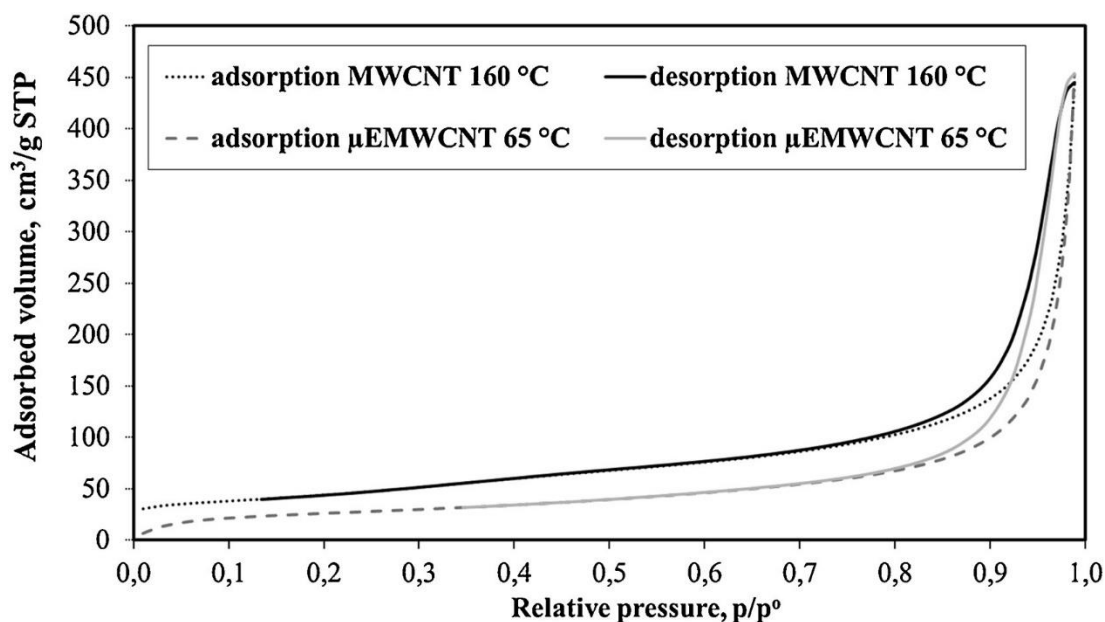


Fig. 8. Nitrogen adsorption and desorption isotherms of the raw and modified multiwalled carbon nanotubes.

The samples exhibited a 4th type of isotherms (Sing, 1985). The presence of a hysteresis loop of type H1 is an indication of capillary condensation and presence of meso- and macropores with regular shape (Sing, 1985). Also, it is an indication of the existence of non-capped pores of carbon nanotubes. According to the structure of carbon nanotubes by SEM image (Fig. 7), the pore shape can be described as nearly cylindrical channels. This is also confirmed by the BET and BJH surface values (Table 2). The BJH method, based on the Kelvin equation, assumes that the pores have a cylinder shape (Sing, 1985). According to our results, the BET and BJH surface areas of the samples are quite similar, indicating the uniform occurrence of tubular pores in the carbon nanotubes before modification ($S_{\text{BET}} = 156 \text{ m}^2/\text{g}$ and $S_{\text{BJH}} = 158 \text{ m}^2/\text{g}$). After the microemulsion modification the tubular structure remained with less uniformity ($S_{\text{BET}} = 98 \text{ m}^2/\text{g}$ and $S_{\text{BJH}} = 110 \text{ m}^2/\text{g}$). It can be concluded that the BET specific surface area of the raw MWCNTs decreased as a result of the surface modification. Nevertheless, the pore shape is preserved after the functionalization of the MWCNTs, and the average pore diameter was increased. The BHJ method can also be used to calculate the cumulative pore volume of pores between 1.7 and $\approx 100 \text{ nm}$ and the pore size distribution (Figs. 9 and 10 and Table 2).

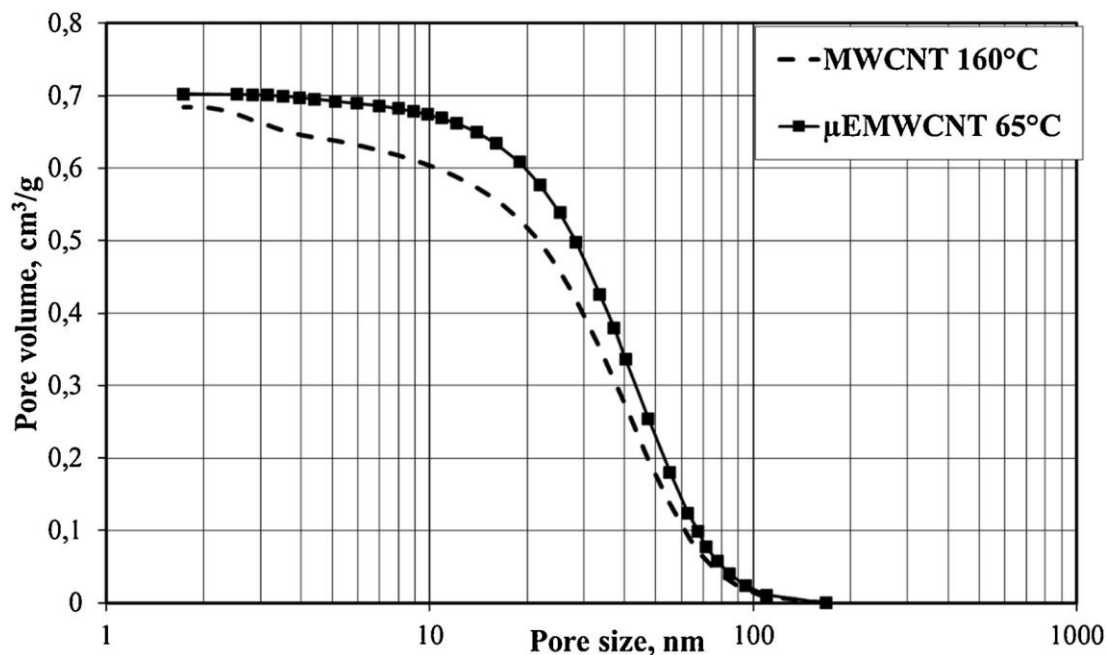


Fig. 9. Cumulative mesopore volume distribution of raw and microemulsified MWCNTs.

In the case of the untreated samples, the D_{av} of the MWCNTs was 12.5 nm, while in the case of μ EMWCNTs the pore diameter was 18.3 nm. In addition to this, it was also observed that the micropores have disappeared after the microemulsion treatment (Fig. 10). The BJH pore distribution plot shows two maxima at ~ 2.7 nm and ~ 40 nm in the mesoporous region attributed to inner and outer pore diameters (Fig. 10). Li et al. observed a little bit higher inner pore diameter for MWCNTs (3.3–3.5 nm) (Li et al., 2004), and it can be due to the apertures between the walls of the MWCNTs that are formed when they twist together tightly. Pores having a width between 20–60 nm are present in higher amounts in the investigated samples (Fig. 10).

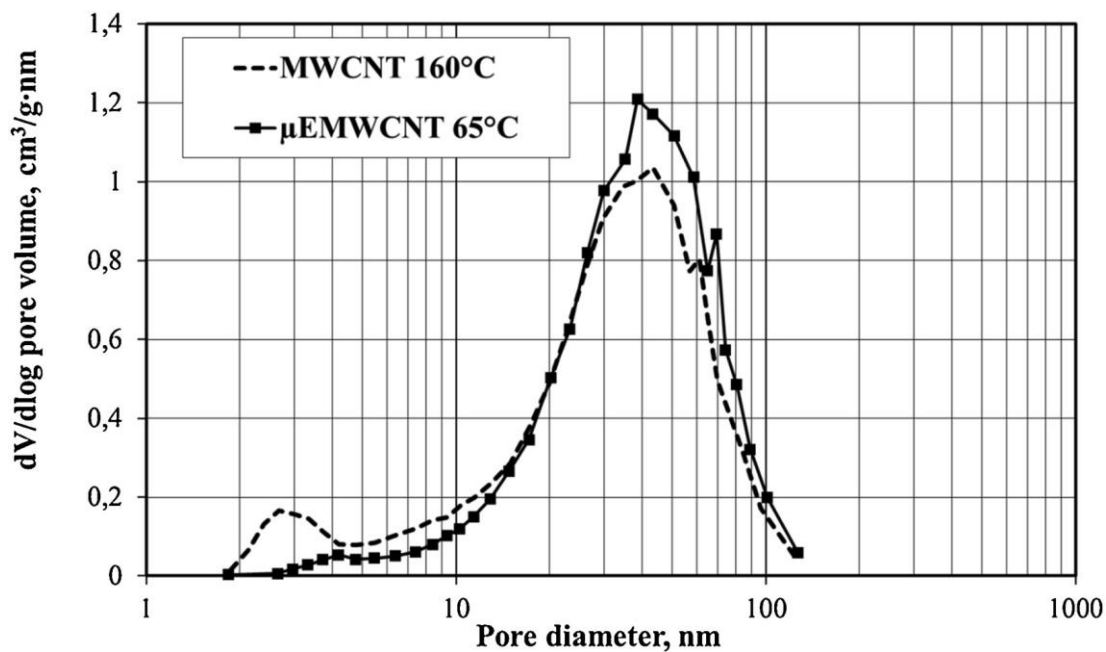


Fig. 10. Logarithmic pore volume distribution of multiwalled carbon nanotubes calculated based on the BJH theory.

3.1.3. Results of the XRD investigations

X-ray diffraction investigations were carried out on the raw MWCNTs and the μ EMWCNTs to determine the crystalline structures of the carbon nanotubes (Fig. 11).

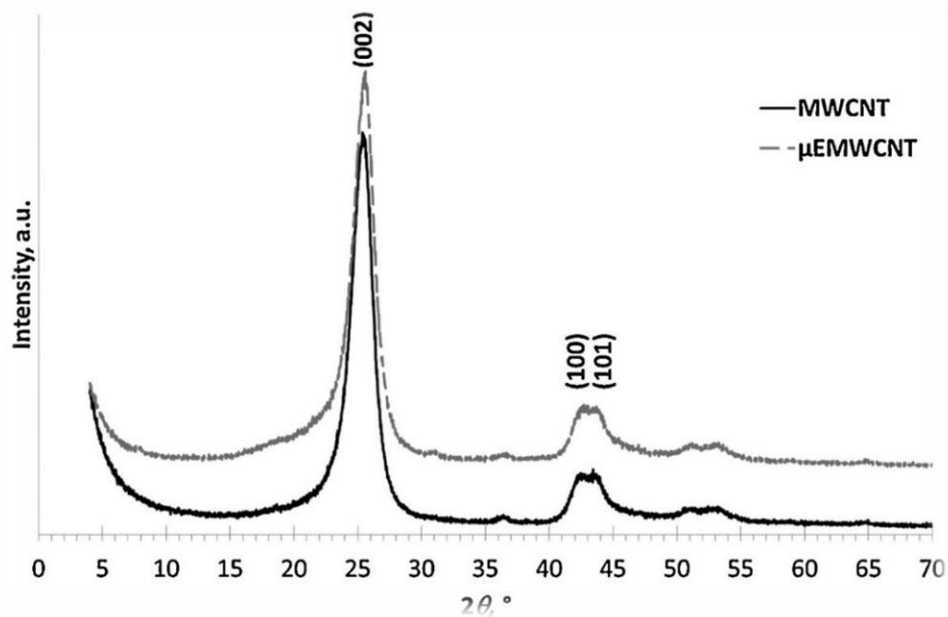


Fig. 11. XRD patterns of raw MWCNTs and μ EMWCNTs samples.

As can be seen in Fig. 11, two main characteristic peaks at $2\theta = 25.3^\circ$ and $\sim 43^\circ$ can be observed. MWCNTs can be formed from rolled graphene sheets with their interlayer distance similar to that of graphite ($d_{(002)} = 0.335$ nm) (Yusa and Watanuki, 2005). The most intensive peak appears at $2\theta = 25.3^\circ$ and it can be attributed to the (002) plane of the single graphene layer of hexagonal structure with d-spacing between 0.34 to 0.39 nm (Ovejero et al., 2006). This graphene sheet distance remains almost the same, even in the case of the μ EMWCNTs ($d_{(002)} = 0.350$ nm). The second main peak with two maxima at $2\theta \sim 43^\circ$ is observed for both samples, and it can be due to the reflections of the diffraction sheets of the nanotubes (100) and (101). This peak shows the reflection within the graphene hexagonal layer (Rebelo et al., 2016).

3.1.4. Results of thermoanalytical investigations

TG and DTG measurements were carried out in argon flow to determine the thermal stability and purity of raw MWCNTs and to investigate the effect of emulsification. The decomposition curves of MWCNTs and μ EMWCNTs are given in Fig. 12, while the mass loss data are summarized in Table 3.

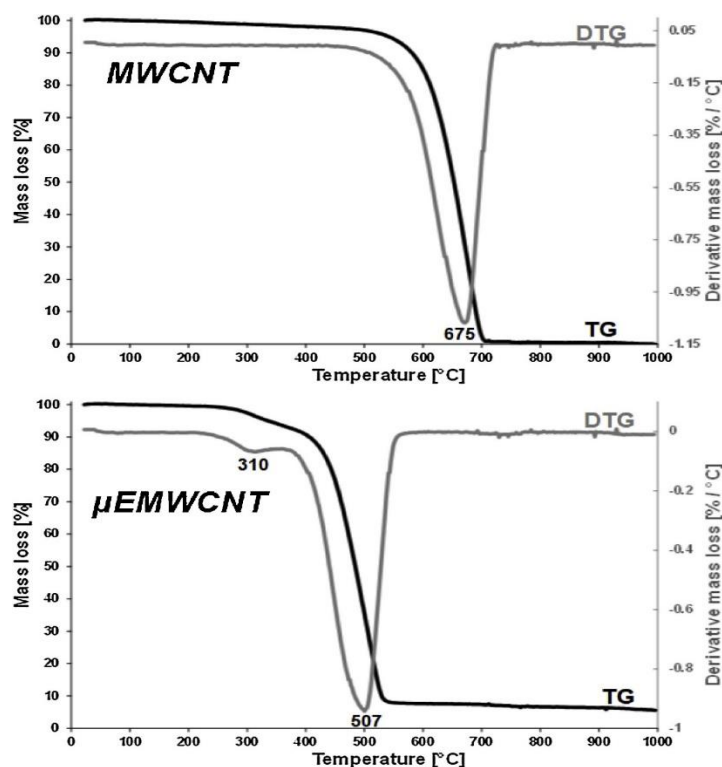


Fig. 12. TG and DTG curves of raw MWCNTs and μ EMWCNTs samples.

Table 3. Mass loss data of samples MWCNTs and μ EMWCNTs during thermoanalytical studies.

Sample	T _{initial} (°C)	T _{max} (°C)	T _{final} (°C)	Mass loss (m/m%)	Reason of step
raw MWCNTs	24	-	200	0.49	water desorption
	480	675	720	96.59	MWCNTs decomposition
	720	-	1000	0.79	loss of residual carbonaceous materials
	Sample mass: 4.276 mg				Total mass loss: 100%
μ EMWCNTs	22	-	200	0.36	water/adsorbed microemulsion
	200	310	376	7.04	adsorbed microemulsion
	376	507	575	84.89	MWCNTs decomposition
	575	-	1000	2.20	impurities of the coconut oil
	Sample mass: 4.428 mg				Total mass loss: 94.49%

In Fig. 12 a single major mass loss step (480–720 °C, $\Delta m = -96.59$ m/m%) is observed for the raw MWCNTs sample, which is typical in the decomposition temperature range of MWCNTs (Lehman et al., 2011). At 1000 °C, the total mass loss of 100% indicates that there is no metal catalyst residue present in the sample used during the production of MWCNTs by the CVD method (Hirsch, 2002).

Two major mass loss steps can be observed in the DTG curve of the μ EMWCNTs (Fig. 12). The step between 200 and 376 °C can be attributed to the loss of adsorbed myristic and lauric acid ($\Delta m = -7.04$ m/m%). The decomposition of the μ EMWCNTs can be observed between 376 and 575 °C ($\Delta m = -84.89$ m/m%). The significant decrease in the decomposition temperature indicates a functionalized surface and/or the structural defect sites in the μ EMWCNTs sample (Lehman et al., 2011). Up to 1000 °C, the overall mass loss is 94.49 m/m %, while the residual mass is 5.51 m/m %. This latter figure can be due to the presence of impurities introduced during the microemulsion modification. During TGA analysis the K⁺ substituent from microemulsion pretreatment might be converted to metal oxide (K₂O) at high temperature.

3.1.5. Results of Raman spectroscopic measurements

Raman spectroscopy can be expediently used for the determination of characteristic features of carbon nanotubes. The Raman spectra of SWCNTs are well interpreted and are usually used for the interpretation of the more complicated MWCNTs. The radial breathing mode (RBM, between 120 and 350 cm^{-1}) corresponds to the radial expansion-contraction of carbon atoms in the radial direction. The D-band (around 1350 cm^{-1}) is typical for graphite-like materials and stems from the presence of structural defect sites and edge carbon atoms at the end of nanotubes (Chernyak et al., 2017). The G-band (around 1600 cm^{-1}) indicates the tangential vibrations of carbon atoms. The overtone of D-band (G' band) can be found around 2600 cm^{-1} and is indicative of the long-range order in the structure (Dresselhaus et al., 2005; Lehman et al., 2011). The Raman spectra of MWCNTs and μ EMWCNTs are given in Fig. 13.

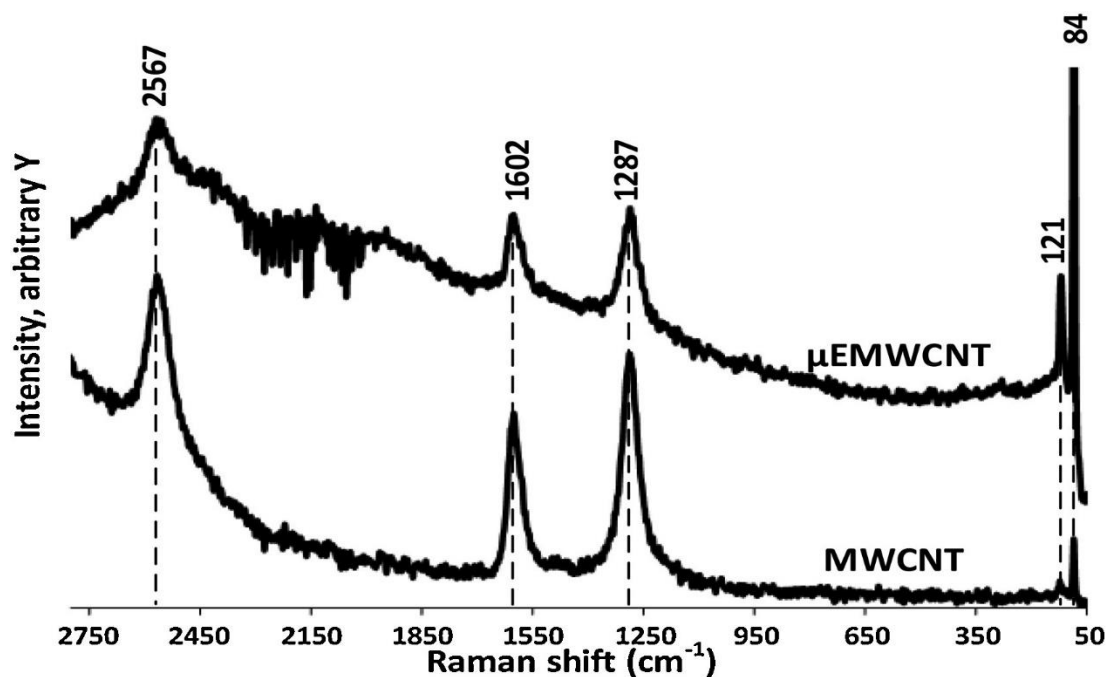


Fig. 13. Raman spectra of samples MWCNTs and μ EMWCNTs.

The well-separated D-band (1287 cm^{-1}), G-band (1602 cm^{-1}), and G' band (2567 cm^{-1}) can be observed in the Raman spectra, which are characteristic of tubular CNTs. The 121 cm^{-1} vibration can be attributed to the radial breathing mode. The peak positions remain unchanged after modification. However, the D and G' band intensities are sensitive to impurities (DiLeo et al., 2007). The structural quality and

purity of CNTs are usually estimated using the $\frac{I_D}{I_G}$ band intensity ratios. However, the G-band intensity is sensitive to carbon impurities, while the $\frac{I_{G'}}{I_D}$ intensity ratios could be more accurately used for quality and purity assessment (DiLeo et al., 2007). The calculated I_D/I_G and $I_{G'}/I_D$ values of MWCNTs were 1.32 and 1.31, while for the μ EMWCNTs, the ratios were 1.01 and 1.28, respectively. The decreasing intensity ratio values indicate a slightly increased disorder/impurity in the MWCNTs structure as a result of microemulsion modification. The μ EMWCNTs exhibited significant changes in the CH bending vibrations as compared to the raw MWCNTs, indicating the existence of intermolecular $CH \cdots \pi$ interactions between the carbon nanotubes side wall and lauric/miristic acid.

3.1.6. UV–Vis spectrophotometric results on toluene sorption test

Toluene was selected for the UV–Vis spectrophotometric studies since the change in toluene concentration in an organic phase such as hexane or cyclohexane can easily be followed by UV–Vis spectrophotometry in the range between 265–270 nm (Agilent Technologies, Inc., 2020; Berlman, 1971). The results of UV–Vis spectrophotometric investigations are summarized in Fig. 14 and in Table 4. Similar absorbance spectra were reported for toluene in 2-propanol (Edinger et al., 2016).

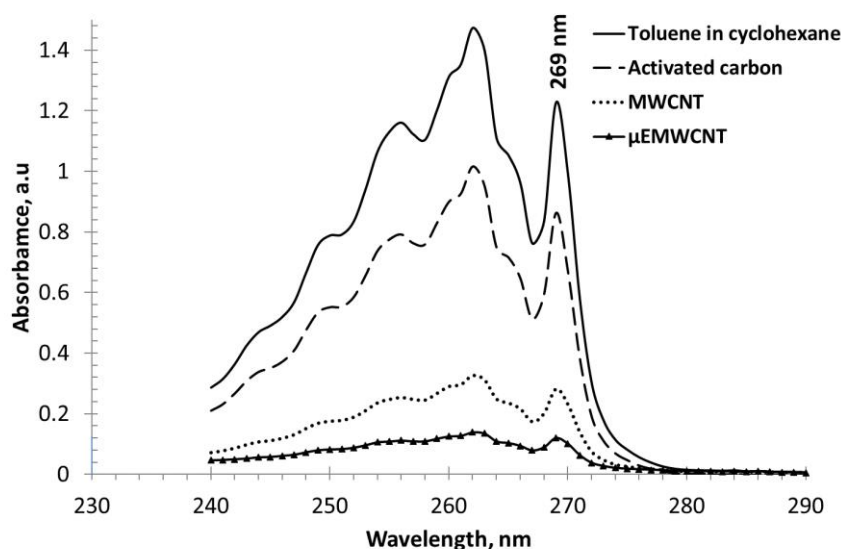


Fig. 14. UV–Vis spectrophotometric results of toluene samples before and after treatment with MWCNTs and μ EMWCNTs.

Table 4. UV–Vis spectrophotometric results of MWCNTs and μ EMWCNTs used for the removal of toluene after 30 min adsorption test.

Sample	Abs. λ : 269 (nm)	Abs. λ : 240-278 (nm)	C_f (mg C/L)	RE (%)	q_t (g/g)
Blank	1.23	22.76	500	-	-
Activated carbon (Chemviron)	0.86	15.60	350	30 ± 5	1.5
Raw MWCNTs	0.28	4.86	114	77 ± 7	3.86
μ EMWCNTs	0.12	1.87	49	90 ± 7	4.51

The change in the toluene concentration is proportional to the absorbance. Using this test, the toluene removal efficiency from the toluene-water mixture over raw MWCNTs and μ EMWCNTs can be investigated. Several UV peaks were recorded in the range of 240–280 nm. The stronger peak appearing at 269 nm was chosen to determine and monitor the concentration of toluene during the experimental runs. Toluene in cyclohexane in Fig. 14 was used only as a reference to illustrate the identification of the toluene. It can be seen in Fig. 14 and Table 4. that the toluene concentration decreased significantly after treatment over μ EMWCNTs (the peak at 269 nm decreases) in comparison with MWCNTs and activated carbon. Moreover, the peak areas in the 240–278 nm range, have been decreased as well. It can be seen in Fig. 14 that the removal efficiency of Chemviron did not approach that of the μ EMWCNTs since activated carbon achieved a removal efficiency up to 30%, only. Based on the experimental results summarized in Table 4, it can be concluded that the μ EMWCNTs proved to be more efficient for the removal of toluene from the toluene-water mixture (90%) in comparison with the untreated MWCNTs (77%).

3.1.7. GC results of the sorption test

Undecane as model hydrocarbon and kerosene were used to study the hydrocarbon removal efficiency over raw MWCNTs and μ EMWCNTs, and the results were compared with that obtained over commercial activated carbons. The measurement data are presented in Table 5.

Table 5. Undecane and kerosene removal efficiencies over MWCNTs, μ EMWCNTs and commercial activated carbon sorbents after 30 min adsorption test.

Sample	Hydrocarbon concentration (mg/L)	RE (%)	q_t (g/g)
Undecane (n-C ₁₁ H ₂₄)			
Blank/Initial	500	-	-
Raw MWCNTs	214	57 ± 5	7.2
μ EMWCNTs	30	94 ± 5	13.3
Kerosene (n-C ₁₀ -C ₁₆)			
Blank/ Initial	560	-	-
Raw MWCNTs	352	35 ± 5	4.8
μ EMWCNTs	22	96 ± 5	13.1
Chemiviron Carbon F300	240	55 ± 5	7.6
Norit GAC 1240 EN	399	27 ± 5	6.6

Higher undecane removal efficiency (94%) was achieved over μ EMWCNTs sorbent as on MWCNTs (57%). Kerosene removal from water by adsorption method was around 35% in the presence of MWCNTs. By using μ EMWCNTs, this value increased up to 96%; however, it is higher than that obtained over the widely used commercial Chemviron Carbon sorbent (55%). Of the two activated carbon sorbents the lower hydrocarbon removal efficiency was obtained over Norit GAC 1240EN (27%). The adsorption capacity of μ EMWCNTs is much higher than that of conventional activated carbon (AC), which was at about 0.150 g/g (Okiel et al., 2011).

3.1.8. Kinetic studies over μ EMWCNTs

A series of adsorption batch tests were carried out as a function of time at room temperature to investigate the equilibrium sorption capacity of μ EMWCNTs for toluene. In each run, 10 mg of μ EMWCNTs were added into a 100 mL toluene-water stock solution, with a concentration of 500 mg/L. The main objective of the equilibrium studies was to determine the maximum capacity of μ EMWCNTs for toluene removal under the studied conditions and accordingly, to make a comparison with raw MWCNTs. Fig. 15 shows the adsorption kinetics of toluene. The toluene uptake reached equilibrium in approximately 60 min.

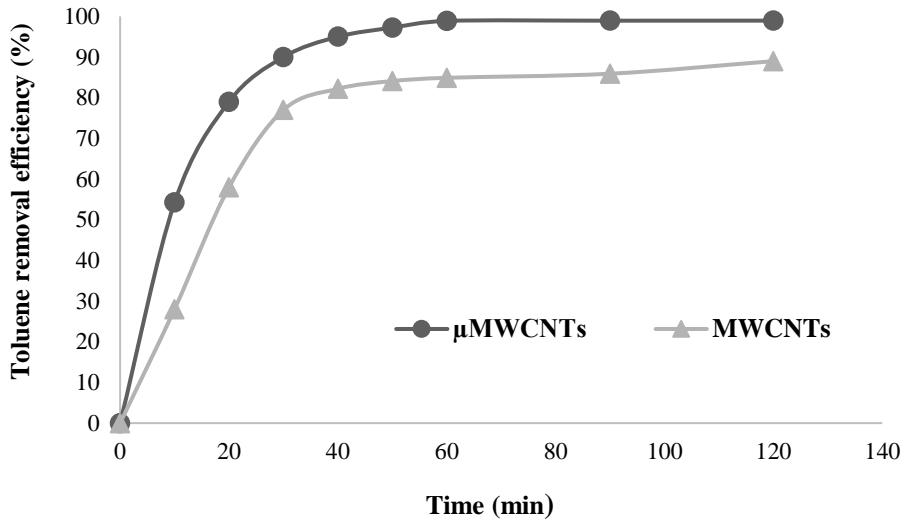


Fig. 15. The change in toluene removal efficiency of μEMWCNTs and raw MWCNTs as a function of contact time.

It can also be seen in Fig. 15 that the adsorbed amounts of toluene increased rapidly with time and then reached equilibrium in about 60 min. At this time, on μEMWCNTs the maximum uptake of toluene is 4.94 g/g, which is higher than that on the raw MWCNTs (4.05 g/g). It is essential to determine the rate at which toluene is removed from aqueous solutions to scale up the adsorption process. In order to determine the kinetics of the adsorption, the pseudo-first order and pseudo-second order equations as well as intraparticle diffusion (Huang et al., 2018; Lin and Wang, 2009; Wu, 2007) were taken into consideration (Eqs. (4-6)).

$$\ln(q_e - q_t) = \log q_e - k_1 t \quad (4)$$

$$\frac{t}{q_t} = \frac{1}{k_2 q_e^2} + \frac{t}{q_e} \quad (5)$$

$$q_t = k_p t^{1/2} + C \quad (6)$$

where: q_e (g/g) is the equilibrium uptake, k_1 (1/min) is the adsorption rate constant of the first-order model, k_2 (g/g·min) is the rate constant of the second-order model, k_p (g/g·min^{0.5}) is the intraparticle diffusion rate constant, and parameter C is a constant (g/g).

Table 6, in conjunction with Figs. 16-18 summarizes the models applied for the interpretation of the kinetic data and the correlation coefficients (R^2) for each

model obtained by non-linear regression analysis for toluene adsorption over μ EMWCNTs. The criterium $R^2 > 0.8$ had to be fulfilled (Simonin, 2016).

Table 6. Kinetic parameters of the pseudo-first order, pseudo-second and intra-particle diffusion models for toluene adsorption by μ EMWCNTs.

Kinetic models:		Pseudo-first order model		
k_1 (min^{-1})	$q_{e, \text{cal}}$ (g/g)	$q_{e, \text{exp}}$ (g/g)	R^2	
0.0456	1.3169	4.9445	0.8519	
		Pseudo-second order model		
k_2 (g/g·min)	$q_{e, \text{cal}}$ (g/g)	$q_{e, \text{exp}}$ (g/g)	R^2	
0.0303	5.2854	4.9445	0.9976	
		Intraparticle diffusion		
k_p ($\text{mg/g}\cdot\text{min}^{0.5}$)	C (g/g)	R^2		
0.4366	1.2925	0.5831		

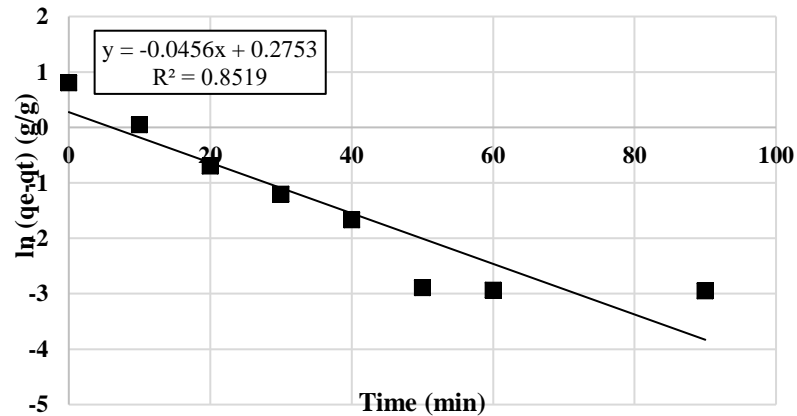


Fig. 16. Adsorption kinetics of toluene over μ EMWCNTs, pseudo-first order plot.

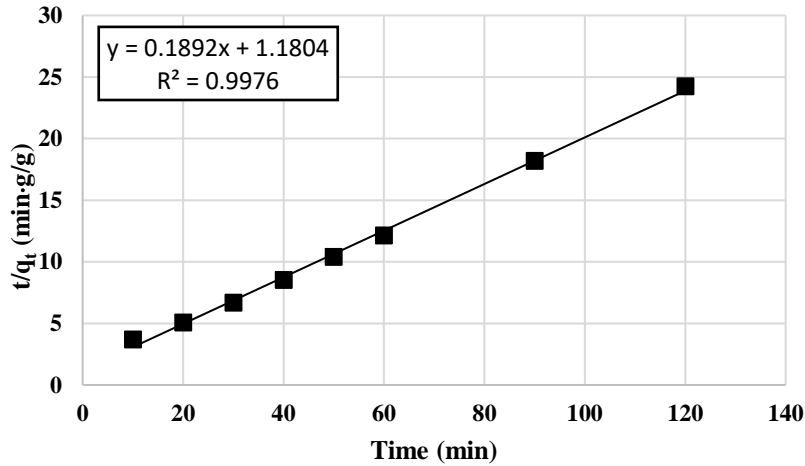


Fig. 17. Adsorption kinetics of toluene over μ EMWCNTs, pseudo-second order plot.

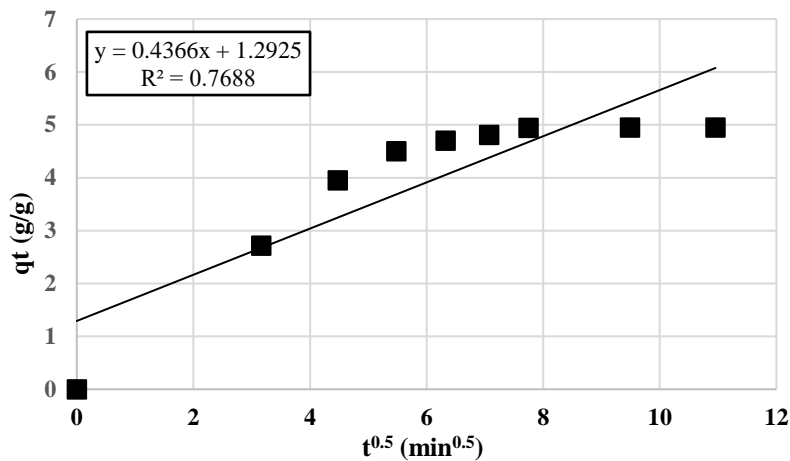


Fig. 18. Adsorption kinetics of toluene over μ EMWCNTs, intraparticle diffusion plot.

Figs. 16-18 show plots of the pseudo-first order, pseudo-second order and intra-particle diffusion models for toluene adsorption by μ EMWCNTs. From these figures and the data summarized in Table 6 it can be seen that optimum fitting can be obtained with k_2 because it gives a value for $q_{e,cal}$ that is in good agreement with $q_{e,exp}$. Thus, the pseudo-second order model is the best-correlating model. These results are based on the assumption that the rate-limiting step is chemisorption involving valency forces through sharing or exchanging electrons between sorbent and sorbate. This conclusion, in agreement with several adsorption studies, stated that the pseudo-second order model provides the best correlation for several systems (Eweida et al., 2023; Ho and McKay, 1999). Also the pseudo-second order model was found to be

the best fitted kinetic model for the sorption of *f*-elements (Kumar et al., 2017; Sengupta and Gupta, 2017) as well as for radioactive actinide metals, e.g. penta and hexavalent neptunium, on modified MWCNTs (Sengupta et al., 2017). Those results confirmed the potential of MWCNTs as adsorbents.

Kinetic studies were also used to prove the chemisorption over μ EMWCNTs by calculating the activation energies in the temperature range of 25–60 °C. The effect of temperature on the adsorption rate of toluene over μ EMWCNTs was investigated at 25, 45 and 60 °C. Fig. 19 presents the effect of temperature on the adsorption capacity value. At higher temperature (60 °C), the maximum adsorption capacity was reached in a shorter time (40 min), while at 25 °C, it reached the maximum value in 60 min. Moreover, the 40 min adsorption capacity at 25 and 60 °C was 4.73 and 4.97 g/g, respectively. The effect of changing the temperature on the equilibrium capacity of the μ EMWCNTs can be attributed to the decrease in solution viscosity at a higher temperature, which in turn, will increase the rate of diffusion of toluene across the external boundary layer and in the internal pores of the μ EMWCNTs.

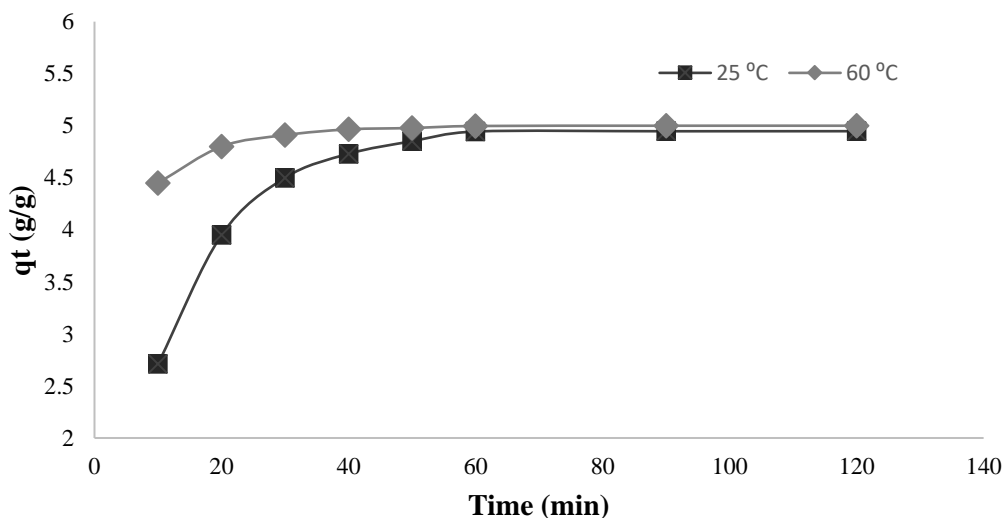


Fig. 19. Kinetic analysis of the temperature effect over μ EMWCNTs (amount of adsorbent: 10 mg/in 100 mL toluene-water solution, 500 mg/L).

The magnitude of the activation energy gives an indication for the type of adsorption, which is generally physisorption or chemisorption. Low activation energies (<40 kJ/mol) are characteristic of physisorption, while higher activation energies (>40 kJ/mol) suggest chemisorption process (Anirudhan and Radhakrishnan,

2008). To validate the assumption of the chemisorption process, activation energy was estimated on the basis of rate constant measurements at three temperatures. Table 7 depicts the pseudo-second order kinetic parameters for adsorption at 25, 45, and 60 °C.

Table 7. Kinetic parameters of the pseudo-second order model as a function of temperature for toluene adsorption over μEMWCNTs.

Temperature (°C / K)	k ₂ (g/g·min)	q _{e, cal} (g/g)	q _{e, exp} (g/g)	R ²
25 / 298	0.03032	5.2854	4.940	0.9976
45 / 313	0.09098	5.4732	4.820	0.9999
60 / 333	0.19350	5.9777	4.970	0.9999

From the pseudo-second order rate constant k₂ (Table 7), the activation energy for the adsorption of toluene on μEMWCNTs was calculated using the Arrhenius equation (Eq. (7)):

$$\ln k_2 = \ln A_0 - \frac{E_a}{RT} \quad (7)$$

where: E_a is the activation energy of the adsorption in J/mol, R is the ideal gas constant, 8.3145 J/K·mol, A₀ is the Arrhenius constant. By plotting ln k₂ versus 1/T (Fig. 20), and from the slope and the intercept, the values of E_a and A₀ can be obtained.

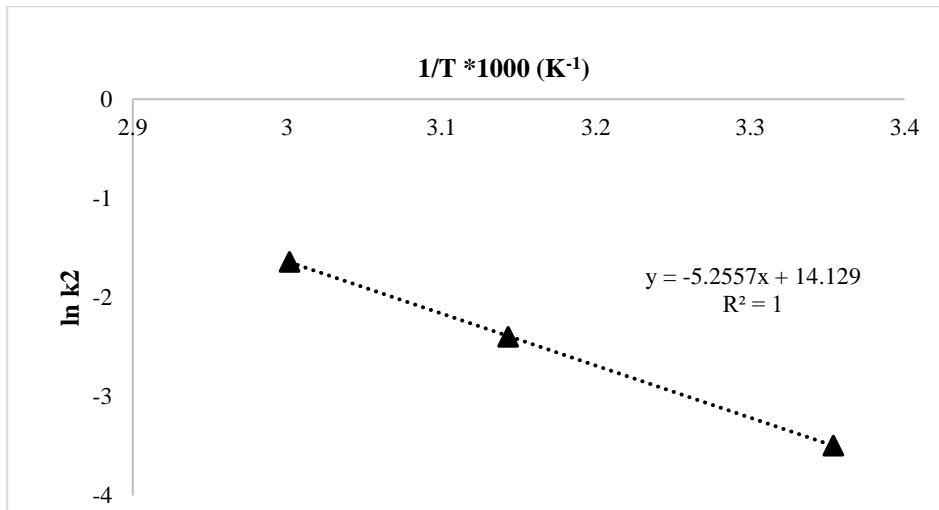


Fig. 20. Arrhenius plot of ln k₂ vs. 1/T to determine the activation energy of the adsorption.

The calculated activation energy of the adsorption is 43.73 kJ/mol, which supports our assumption that the sorption process is chemisorption.

3.1.9. Microemulsification mechanism of MWCNTs

The non-covalent functionalization of the MWCNTs involved surface attachment of saponified coconut oil $\text{CH}_3(\text{CH})_n\text{COO}^-\text{K}^+$ ($n=10,12$) surfactant on the hydrophobic surface of MWCNTs via Van der Waals forces and/or π - π interactions (Jun et al., 2018). The use of surfactant results in significant increase in the dispersion of CNTs in aqueous solutions. Interaction between the surfactant and MWCNTs is generally weak, resulting in weaker stability as compared to covalent functionalization (Jun et al., 2018).

For the non-covalent functionalization of the MWCNTs saponified coconut oil $\text{CH}_3(\text{CH})_n\text{COO}^-\text{K}^+$ was used as given before. It has a hydrophilic part (polar head group (COO^-K^+)) on the hydrophobic part (long carbon chain tail ($\text{C}_n = 10,12$)) (Vaisman et al., 2006). The mechanism of attachment of surfactant molecule to MWCNTs can be illustrated as shown in Fig. 21 (Yurekli et al., 2004).

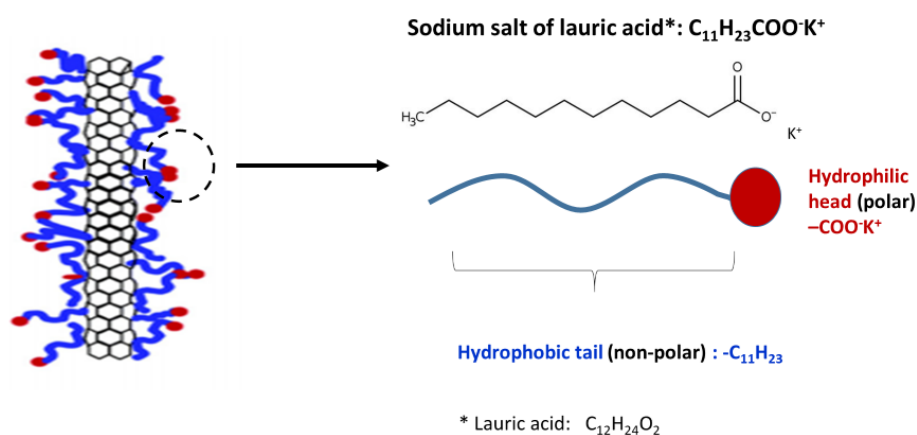


Fig. 21. Schematic representation of the random adsorption of surfactant molecules on MWCNTs. Red circles are the polar head groups (COO^-K^+) with long alkane tail indicated by blue colour.

The μ EMWCNTs, decorated with the surfactant molecules, have two distinct parts. The hydrophilic polar section gets into contact with the aqueous phase and the nonpolar hydrophobic tail joins the hydrocarbon molecules.

3.1.10. Mechanism of hydrocarbon adsorption over MWCNTs

Different mechanisms can be considered during organic chemical and MWCNTs interactions, such as hydrophobic interactions, π - π bonds, electrostatic interactions, and hydrogen bonds. The sorption mechanism is supposed to be different for different types of organic chemicals (such as polar and non-polar). Toluene was chosen to study the mechanism of adsorption over MWCNTs. In case of raw MWCNTs the surface acts as the electron donor and the aromatic ring of toluene functions as electron acceptor (Fig. 22) (Cai, 2011).

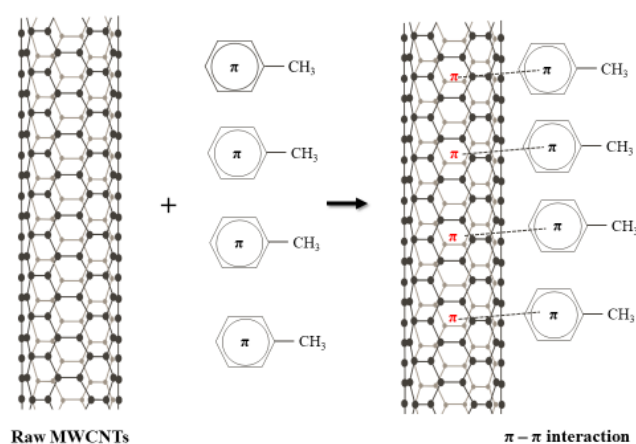


Fig. 22. Proposed mechanism of toluene sorption over raw MWCNTs.

The proposed sorption of toluene on the surface of the μ EMWCNTs is depicted in Fig. 23. In case of μ EMWCNTs the carboxylic oxygen atom of the MWCNTs surface acts as electron donor and the aromatic ring of toluene as electron acceptor.

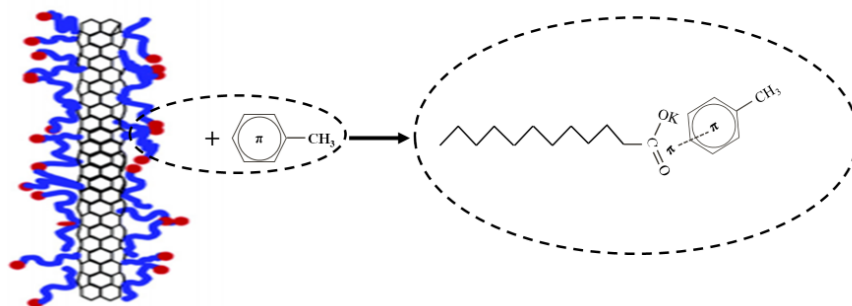


Fig. 23. The mechanism of the surface functionalization and sorption of toluene over MWCNTs.

The adsorption affinity over modified MWCNTs is enhanced by the $-C=O$ group and this interaction is assumed to be stronger than for raw MWCNTs. The given mechanism in Fig. 23 is in agreement with the adsorption mechanism of organic pollutants on CNTs (Lu et al., 2008; Pan and Xing, 2008).

The most probable mechanism of non-polar paraffin molecule sorption on μ EMWCNTs is via $CH\cdots\pi$ interaction as described in the literature (Umadevi and Sastry, 2014). It is worth mentioning that the hydrocarbon removal efficiency values obtained by various analytical techniques are in harmony. The obtained results confirm that the MWCNTs could earn a significant potential in hydrocarbon depollution control of waters.

3.2. V_2O_5 , CeO_2 and their MWCNTs nanocomposites modified for the removal of methylene blue dye from water

3.2.1. Results of the X-ray diffraction study

Fig. 24. shows XRD results for the samples of $V_2O_5:CeO_2$, raw MWCNTs, oxidized MWCNTs, V/MWCNTs, Ce/MWCNTs and V:Ce/MWCNTs. $V_2O_5:CeO_2$ nanoparticles prepared by the hydrothermal method and annealed at 500 °C showed the reflections of both oxides, namely V_2O_5 and CeO_2 . In the case of vanadia nanoparticles, the main diffraction peaks of (200), (010), (110), (101), (310), (011), (301), (020) and (320) appear at 15.04°, 20.04°, 21.80°, 26.20°, 31.00°, 32.40°, 34.20°, 41.20° and 48.00° 2θ , respectively. These peaks relate to the scherbinaite orthorhombic crystalline structure of vanadium pentoxide (JCPDS Card No. 41-1426). The main diffraction peaks of CeO_2 are (111), (200), (220) and (311) at 28.60°, 32.20°, 47.40° and 56.51° 2θ , respectively. These peaks confirm the form of cerianite, having face-centered cubic structure (JCPDS Card No. 34-0394).

In mixed composites, the constituent V_2O_5 orthorhombic crystalline structure dominates over the CeO_2 equivalent. Furthermore, with high probability the presence of some $CeVO_4$ (with Ce^{3+} and V^{5+}) crystallites were observed at 18.20° and 24.20° 2θ (Brătan et al., 2011; Riaz et al., 2021), originating from the thermal reaction of the two metal oxide phases (Yin and Hasegawa, 2023). Also, the transformation of V_2O_5 to V_2O_3 is accompanied with the segregation of the $CeVO_4$ phase (Riaz et al., 2021). Formation of $CeVO_4$ was reported after the thermal treatment of the precipitate at 400

°C obtained by co-precipitation from the corresponding vanadia and ceria precursors (Brătan et al., 2011).

The oxidized MWCNTs, V/MWCNTs, Ce/MWCNTs and V:Ce/MWCNTs samples were treated at 200 °C. On the basis of the XRD results, it can be seen that the graphene layers of MWCNTs are preserved after acid treatment and deposition of metal oxides. It is in agreement with Raman results showing the presence of the graphite G band in all investigated sample (See Section 3.2.5.). The diffraction peaks at 25.3° and ~43° 2θ of metal oxide-modified MWCNTs are the (002), (100) and (101) reflections of graphite, as indexed by the JCPDS Card No. 01-071-4630. Similar findings were reported (Abdel-Ghani et al., 2015; Oh et al., 2010).

The peaks corresponding to CeO₂ and V₂O₅ in Ce/MWCNTs and V/MWCNTs could not be detected because of their low amounts and/or well-dispersion on the nanotube surface. The major crystalline phase with regard to the graphene layers of the MWCNTs was recorded for all multiwalled carbon nanotubes. The presence of some crystals of individual oxides was detected for samples V:Ce/MWCNTs.

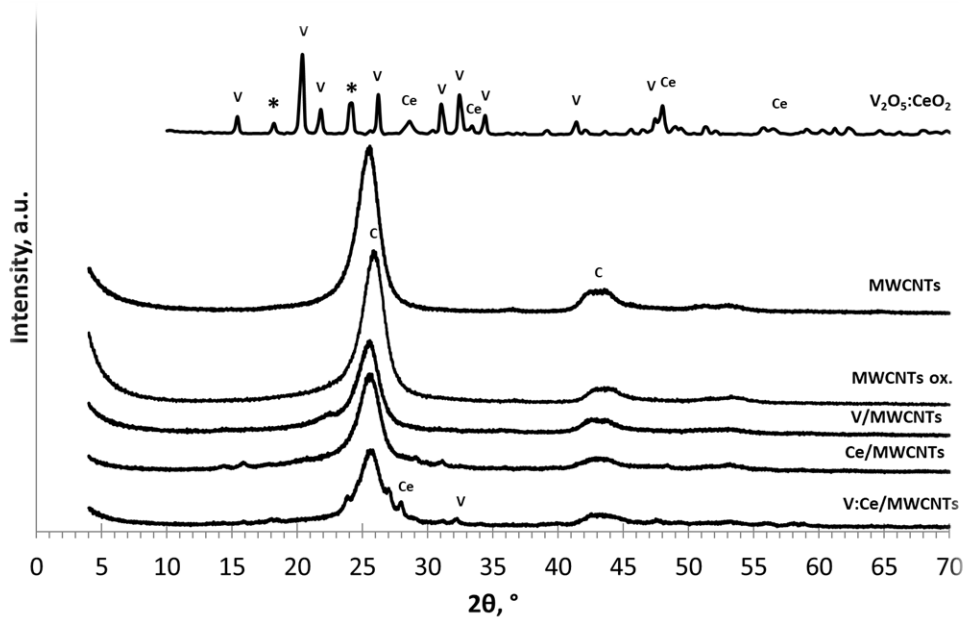


Fig. 24. XRD results for fresh and modified MWCNTs, where V, Ce, C and * denote the V₂O₅, CeO₂ graphite and CeVO₄ crystalline phases.

3.2.2. Electron spectroscopy and energy dispersive X-ray spectroscopy results

SEM records for metal oxides are shown in Fig. 25a-c. Fig. 25a shows the surface morphology of V_2O_5 nanopowder, identified in the form of nanoflakes close to 65-80 nm in thickness, which is in agreement with the reported atomic force microscopic (AFM) data (Asim et al., 2009; Margoni et al., 2017). Fig. 25b shows that the surface morphology of the CeO_2 powder adopts a different shape including nanorods and irregular octahedra with a diameter of 60-70 nm (also confirmed by AFM analysis). Irregular CeO_2 octahedral nanocrystals could be obtained by precipitation of a Ce(III) salt with sodium hydroxide at $pH > 5$. CeO_2 nanotubes, nanowires, and nanorods could be fabricated from $Ce(OH)_3$ intermediates (Lin et al., 2012). Fig. 25c shows the $V_2O_5:CeO_2$ nanocomposite in which the vanadium pentoxide is preserved in the form of nanoflakes.

SEM and TEM records for raw MWCNTs and for metal oxide-modified MWCNTs are shown in Figs. 26 and 27. It can be observed that the size of the carbon nanotubes remains within the nanoscale range and the shape of carbon nanotubes was not significantly affected during thermal modification of MWCNTs in the presence of nanoparticles (Fig. 27a-c). The preservation of the initial structure of MWCNTs was reported after oxidation treatment of carbon nanotubes with 10 M H_2SO_4/HNO_3 or 10M HNO_3 (Sezer and Koç, 2019).

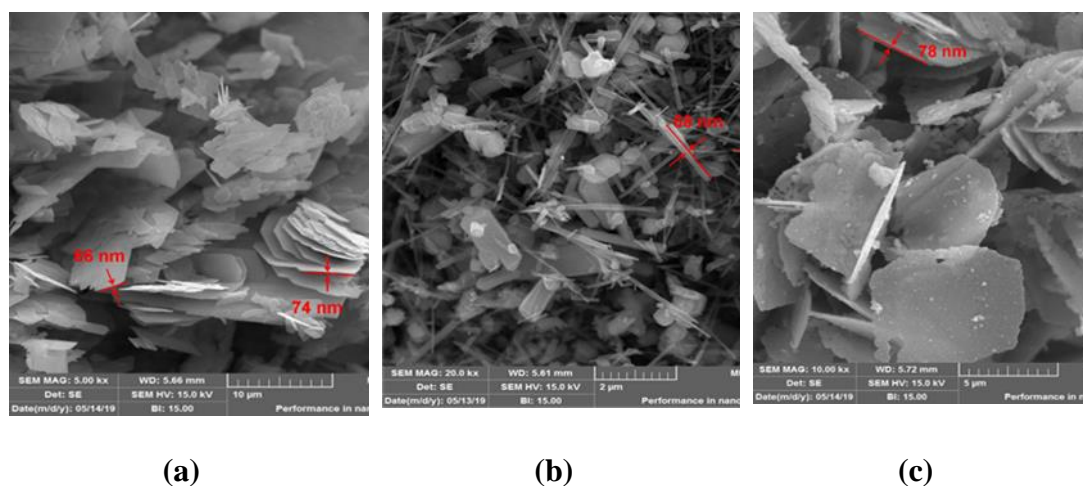


Fig. 25. SEM images between 2 and 10 μm : (a) V_2O_5 , (b) CeO_2 , (c) $V_2O_5:CeO_2$.

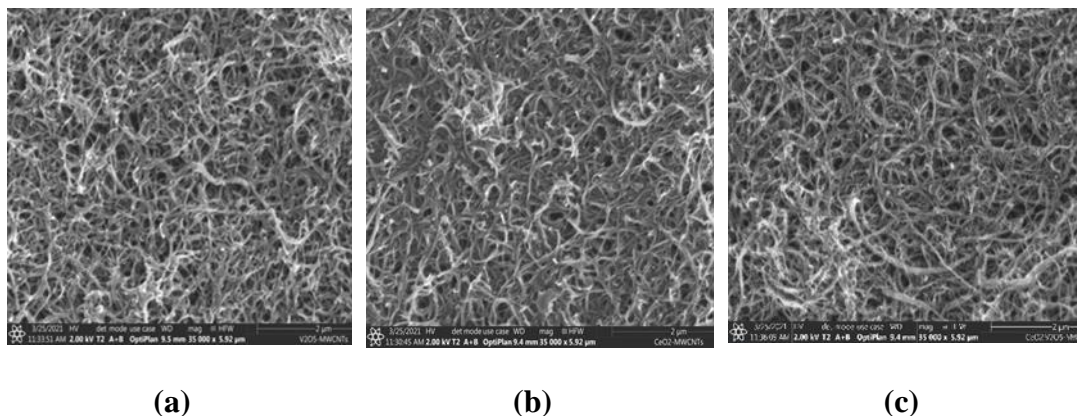


Fig. 26. SEM images on scale of 2 μm : (a) V/MWCNTs, (b) Ce/MWCNTs, (c) V:Ce/MWCNTs.

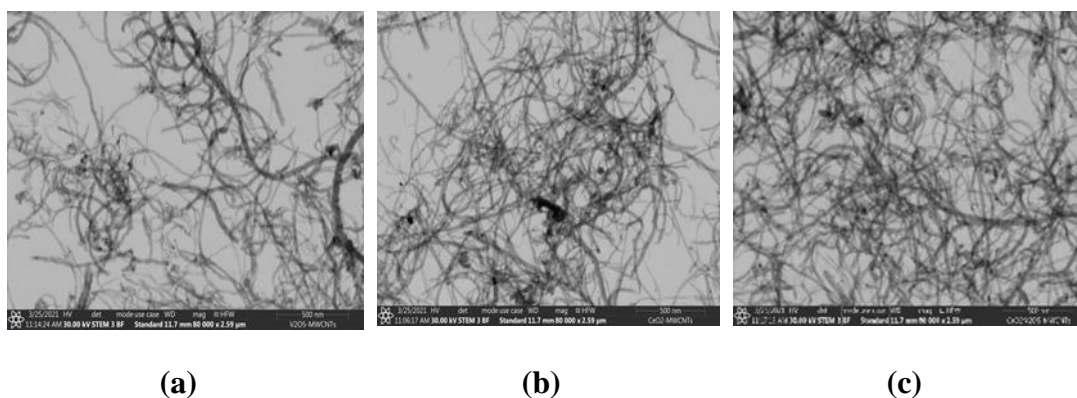


Fig. 27. TEM images on a scale of 500 nm: (a) V/MWCNTs, (b) Ce/MWCNTs, (c) V:Ce/MWCNTs.

EDX analyses were carried out to determine the amounts of carbon, vanadium and/or cerium on the surface of the samples. The analyses were made on three different areas of the specimens to determine the average composition of the near-surface layer. EDX results confirm the supposition that the metal oxides were deposited on the surface of the carbon nanotubes, but were not uniformly distributed. The metal oxides amounts in the samples varied in the following ranges: V(2.3-4.6 m/m%)/MWCNTs, Ce(4.0-7.4 m/m%)/MWCNTs and V(1.2-6.0 m/m%):Ce(0.4-2.1 m/m%)/MWCNTs samples.

3.2.3. Atomic force microscopy results

The three-dimensional AFM images of V_2O_5 , CeO_2 and $\text{V}_2\text{O}_5:\text{CeO}_2$ nanoparticles after annealing at 500 $^\circ\text{C}$ are shown in Fig. 28. The morphological

images of V_2O_5 , CeO_2 and $V_2O_5:CeO_2$ nanoparticles clearly depict that the average grain sizes were found to be 70.3, 56.9 and 71.4 nm as shown in Fig. 28a-c, respectively. The addition of cerium dioxide to vanadium pentoxide resulted in a slight increase in the particles size distribution range from 40-100 nm to 55-120 nm.

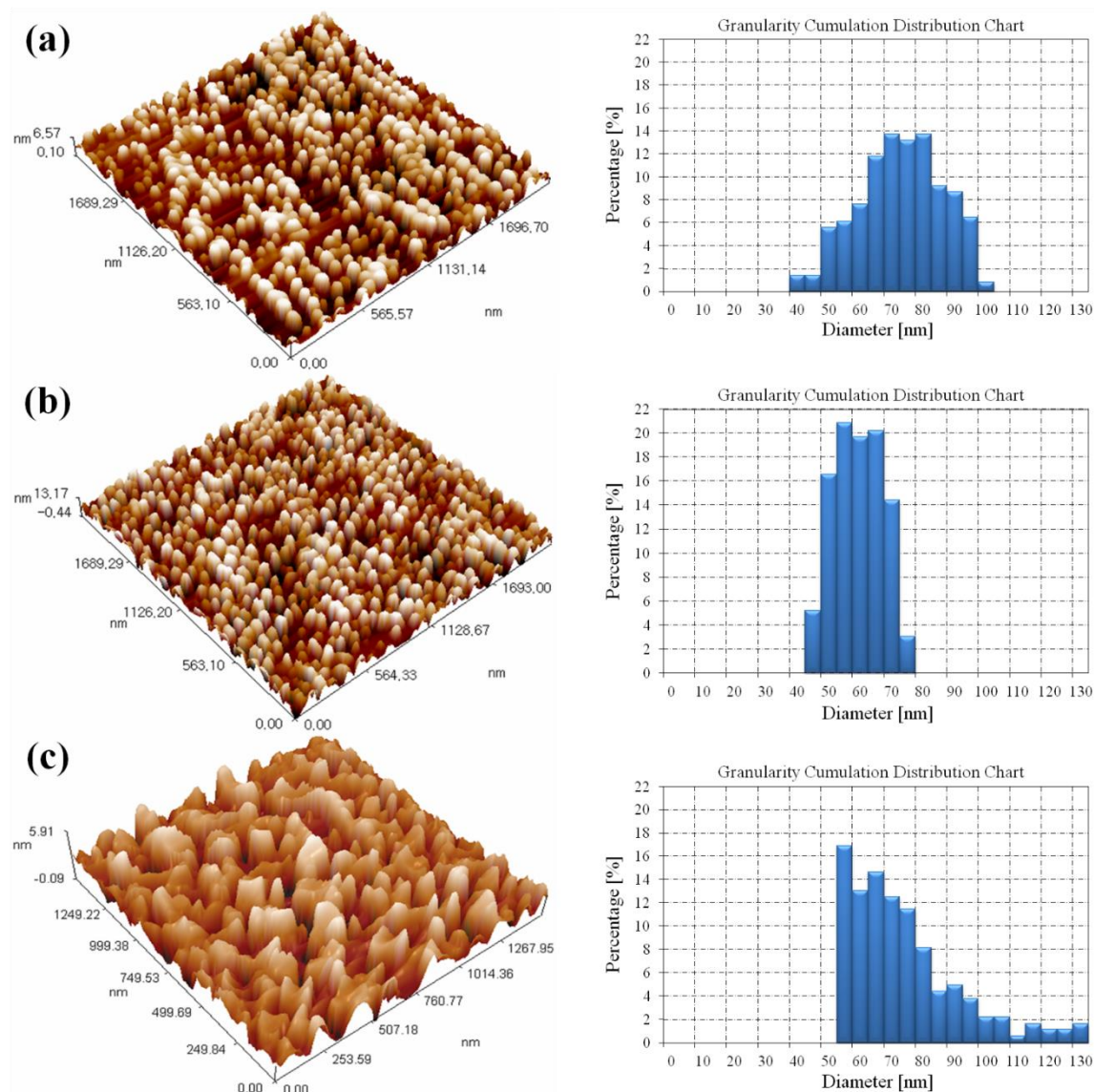


Fig. 28. AFM records of (a) V_2O_5 , (b) CeO_2 and (c) $V_2O_5:CeO_2$ composites at an annealing temperature of 500 °C.

3.2.4. Raman spectroscopy results

The distinctive features of the MWCNTs can be identified by Raman spectroscopy (Fig. 29). The radial breathing mode (RBM) corresponds to the in-phase,

radial movement of the carbon atoms within the structure of CNTs. This mode is located between 75 and 300 cm^{-1} from the excitation line. It is usually not present in the Raman spectra of MWCNTs (Costa et al., 2008; Lehman et al., 2011). However, two separate RBM bands were observed at 121 and 143 cm^{-1} . Since the position of an RBM band is sensitive to the diameter of the CNTs, it can be utilized to estimate their overall, average diameter (Costa et al., 2008; Jorio and Saito, 2021). The 121 and 143 cm^{-1} bands indicate the presence of two small, slightly different diameters with averages of 2.1 and 1.8 nm, respectively.

The band at 1284 cm^{-1} can be assigned to the presence of defect sites in the sp^2 carbon structure (D-band). The position of the D-band depends on the diameter and chirality of the carbon structure as well as on the applied laser wavelength (Jorio and Saito, 2021). The D-band can be deconvoluted into two bands centered on the same wavenumber for small crystallites of CNTs (Puech et al., 2019).

The peak at 1598 cm^{-1} is attributed to the vibrations of the sp^2 carbon structure (G-band). Splitting of the G-band (G^+G^-) is not observed, as expected for MWCNTs (Murphy et al., 2006). Although RMB shows the feature of SWCNTs (Costa et al., 2008), it is therefore tempting to conclude that the carbon nanotubes studied have a double-walled structure.

The band at 2561 cm^{-1} (G' -band) is the overtone of the D-band, but contrary to the D-band, it indicates the long-range order of the structure arising from defect-free sp^2 carbon atoms (Costa et al., 2008; Lehman et al., 2011).

As a result of being treated with strong acids, structural defect sites are introduced in the form of carboxyl, carbonyl and hydroxyl groups via oxidation of the carbon structure (Murphy et al., 2006; Osswald et al., 2007). After oxidative treatment, the RBM band at 143 cm^{-1} disappeared (1.8 nm pores disappeared), moreover, the D- and G' -bands shifted slightly to higher wavenumbers (1289 and 2566 cm^{-1} , respectively), indicating the successful surface modification (Fig. 6. MWCNTs (ox.)). The decreased population of micropores ($\varnothing \leq 2$ nm) is also shown by the BET analysis (Section 3.2.6.).

The peak intensity or area ratios of the D- and G-bands $\left(\frac{I_D}{I_G}; \frac{A_D}{A_G}\right)$ can be used to estimate the quality of the CNT structure and the extent of surface modification via the presence of defect sites (Jorio and Saito, 2021; Puech et al., 2019). Alternatively, the

G'- and D-band ratios ($\frac{I_{G'}}{I_D}; \frac{A_{G'}}{A_D}$) can be used for a more accurate estimation (DiLeo et al., 2007). The calculated intensity ratios follow a similar trend to the area ratios (Table S1). After oxidative treatment, the $\frac{I_D}{I_G}; \frac{A_D}{A_G}$ values decreased, while the $\frac{I_{G'}}{I_D}; \frac{A_{G'}}{A_D}$ values increased (Table S3), indicating a slightly more disordered structure as a result of acid-treatment (Murphy et al., 2006) and removing carbon impurities e.g. metal CVD catalyst residuals (see TG Section 3.2.5).

No major spectral changes were observed once the nanocomposites had been prepared (Table S1, Fig. 9. Ce/, V/, V:Ce/MWCNTs). Most probably, due to their low surface concentration, no new peaks appear in accordance with the Raman scattering of V₂O₅ (Shvets et al., 2019) or CeO₂ (Schilling et al., 2017) polymorphs. However, based on their $\frac{I_D}{I_G}$ and $\frac{I_{G'}}{I_D}$ ratios, the structural order of the Ce and V:Ce nanocomposites showed decrease as compared to the MWCNTs (Table S3) in correlation with deposited metal oxide amount. The calculated Raman values, provided in Table S3, correlate very well with the TG/DTG results of Fig. 30.

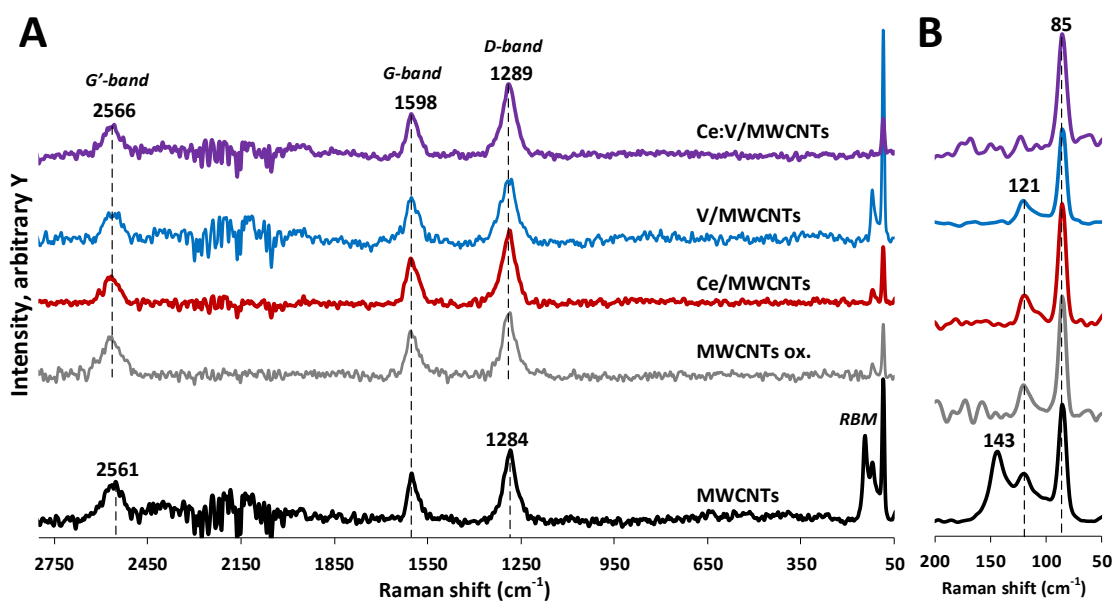


Fig. 29. Raman spectra of the MWCNTs samples: (A) normalized to the G'-, G- and D-bands intensity in the 2750-50 cm⁻¹ region, (B) normalized to the RBM bands in the 200-50 cm⁻¹ region.

3.2.5. Thermogravimetric analysis results

The raw MWCNTs sample used for surface modification shows two notable mass loss regions (Fig. 30). A minor mass loss is observed up to 190 °C as the surface adsorbed water is removed, while a major mass loss step is found between 440-750 °C, indicating the thermal decomposition of the carbon structure (Table S4. MWCNTs). After annealing to 1000 °C the residual mass indicates the impurity of the MWCNTs sample (m=10.4%), which is due to the presence of catalyst residues from the production of CNTs. The observed amount of catalyst impurity is well within the acceptable range reported in the literature (cc. 6-43%) (DiLeo et al., 2007; Shah and Tali, 2016).

As a result of surface treatment using strong acids, the MWCNTs structure is oxidized via the introduction of oxygenated surface functional groups (carboxyl, carbonyl, hydroxyl) (Sezer and Koç, 2019). The improved hydrophilic nature due to the modified surface properties of the acid treated MWCNTs sample is indicated by the increased amount of adsorbed water (Fig 30. MWCNTs (ox.), Table S4. MWCNTs (ox.), 21-155 °C). Oxidation of the carbon backbone results in the presence of defect sites eventuating in the lower thermal stability of the functionalized CNTs (Bom et al., 2002). The elimination of the introduced surface carboxyl groups are observed in the second step (155-366 °C), while a small mass loss between 366-500 °C could be attributed to the decomposition of other, thermally more stable surface functional groups (Sezer and Koç, 2019). The major decomposition was found between 500-730 °C. As compared to the pristine MWCNTs, the shift to higher starting temperature and the narrower decomposition curve indicates the purification effect of acid treatment, mostly via the removal of carbon impurities. The significantly smaller residual mass (m=1.5%) is due to the removal of catalyst residuals during acid treatment (Sezer and Koç, 2019). Consequently, the acid treatment resulted in a purified MWCNTs sample.

Small changes are observed upon the addition of CeO₂ to the oxidized MWCNTs (Fig. 30. Ce/MWCNTs, Table S4. Ce/MWCNTs). No thermal decomposition process is expected due to the presence of pre-annealed CeO₂ particles. Cerium(IV) oxide shows structural stability at temperatures up to 1600 °C (Riaz et al., 2021). Therefore, the differences could be related to the interactions of the lanthanide-oxide nanoparticles and the carbon nanostructure. The slightly higher temperature maximum (257 °C vs 226 °C) of the second stage could indicate a possible interaction

between the CNTs surface carboxyl groups and the introduced CeO₂ resulting in the increased thermal stability of the surface moieties. The thermal stability of the MWCNTs backbone has not changed considerably (628 °C vs 623 °C), however the increased mass loss of the third stage (360-485 °C) could be indicative of the increased ratio of MWCNT particles having slightly smaller thermal stability. This effect could be related to the thermal activation of CeO₂ catalyst at elevated temperatures, resulting in a slightly enhanced pyrolysis of CNTs (Trovarelli, 1996; Vita, 2020).

Similar changes can be observed in case of V₂O₅ nanoparticle addition (Fig. 30. V/MWCNTs, Table S4. V/MWCNTs). No additional mass loss is expected due the addition of previously heat-treated V₂O₅ particles (Bom et al., 2002). The thermal stability of the second stage increased further ($T_{\max}=268$ °C), indicating the slightly stronger interaction of vanadium-pentoxide particles with the functionalized CNTs surface. Compared to the MWCNTs oxidized sample, major changes can be observed in the thermal stability of the CNTs backbone: the mass loss ratio of the third stage has increased and the maxima has shifted to 388 °C, while the prominent decomposition stage has also shifted to 498 °C from 628 °C. Only a small mass loss at 638 °C indicates the presence of MWCNTs particles with their original thermal stability. These changes can be indicative of the thermally activated catalytic properties of V₂O₅ nanoparticles (Wachs, 2013) resulting in enhanced pyrolysis and lower thermal stability of MWCNTs.

The simultaneous presence of CeO₂ and V₂O₅ particles resulted in a further decrease of MWCNTs thermal stability (Fig. 30. V:Ce/MWCNTs, Table S4. V:Ce/MWCNTs). The thermal decomposition of the MWCNTs backbone slightly shifted to the lower temperature regions, where 3 overlapping stages can be identified (316-422 °C, 422-545 °C, 545-700 °C). The observed shift to lower thermal stability can be explained by the increased catalytic activity due to the simultaneous presence of CeO₂ and V₂O₅ catalysts (Tamin et al., 2022; Zeleke and Kuo, 2019). Overall, the addition of V₂O₅ particles significantly decreased the thermal stability of MWCNTs.

The residual masses after heating to 1000 °C can be utilized to estimate the metal-oxide content of the samples (Table S4). Considering the residual mass of MWCNTs (ox.) sample (m=1.5%), the estimated oxide contents for the Ce/, V/ and V:Ce/MWCNTs samples are 11.9%, 3.7% and 8.5%, respectively. The metal oxide amount for the Ce/MWCNTs sample is different from the values obtained by EDX

(see SEM-EDX Section 3.2.2.). The difference can be explained by the higher uncertainty of EDX, since the analytical signal originates from a smaller volume (in a scale of μm^3) and conclusions to the overall composition bears greater errors due to the possible inhomogeneity of the sample (Notthoff et al., 2013).

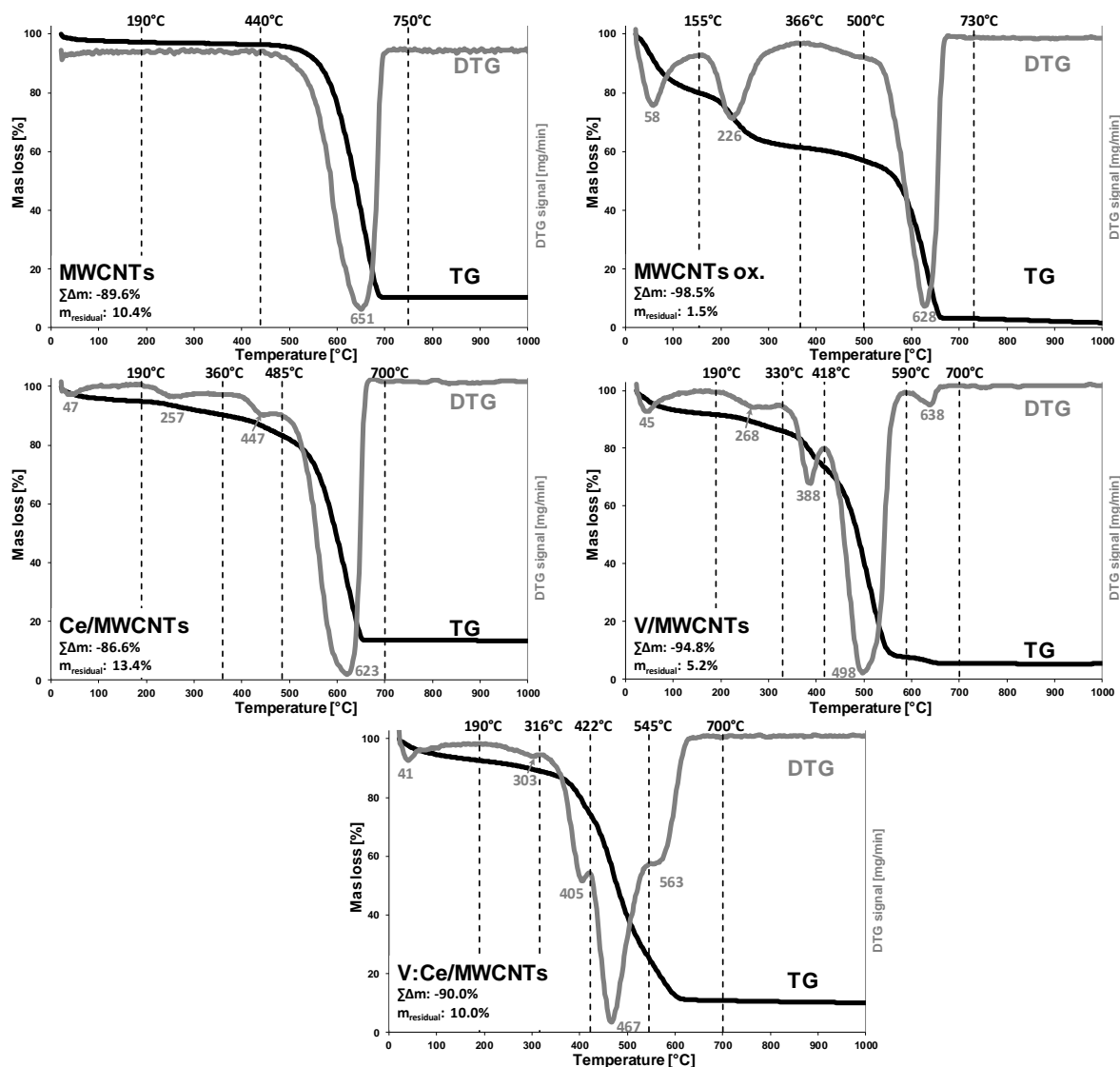


Fig. 30. Thermogravimetric (TG/DTG) curves of the raw and modified MWCNTs samples.

3.2.6. Low-temperature nitrogen adsorption results

The surface area, pore volume as well as average pore size values of the raw, acid-treated and metal oxide-modified MWCNTs samples are presented in Table 8.

The total surface area of raw MWCNTs was $156 \text{ m}^2/\text{g}$ which is higher than reported by the supplier ($120 \text{ m}^2/\text{g}$). Newly prepared samples with masses of 0.5-1.0 g previously outgassed in a vacuum at $160 \text{ }^\circ\text{C}$ were used for the nitrogen adsorption experiments. The mass of the sample was reduced during the outgassing procedure before the BET analysis. The highest reduction in mass was observed in the case of oxidized MWCNTs ($7.9 \text{ m/m}\%$) (Table 8). It can be assumed that some moisture and/or residual acid remained in the bulk of the sample after the acid treatment.

The treatment of MWCNTs with a $3\text{H}_2\text{SO}_4:1\text{HNO}_3$ acid mixture resulted in splitting of the tubes (Chernyak et al., 2017). This can create new openings in the channels of the tubes, hence increasing their total volume (Table 8). Meanwhile, the acid treatment applied resulted in a significant decrease in the micropore volume of MWCNTs (ox.). The acid treatment of MWCNTs could form carboxyl and hydroxyl functional groups which might block the small pore openings (Birch et al., 2013). This can also have an impact on the total pore size distribution (Fig. 31). The number of smaller pores (2-3 nm) decreases and that of larger pores (20-40 nm) slightly increases during the acid treatment of MWCNTs and metal oxide-modified MWCNTs samples. It results in a slight decrease in S_{BET} from 156 to $140 \text{ m}^2/\text{g}$ and from 140 to $115 \text{ m}^2/\text{g}$, respectively.

CeO_2 shows a relatively higher surface area ($69 \text{ m}^2/\text{g}$) among the metal oxides. The pore volume and surface area of the micropores of CeO_2 nanoparticles exhibit also higher values than those of V_2O_5 and $\text{CeO}_2:\text{V}_2\text{O}_5$. V_2O_5 has the lowest surface area of $3 \text{ m}^2/\text{g}$ and the $\text{CeO}_2:\text{V}_2\text{O}_5$ nanocomposite has a surface area of $9 \text{ m}^2/\text{g}$ as shown in Table 8. The surface area of mixed metal oxides depends on the proportions of the individual oxides and on the interactions between the constituent oxides. The surface area is an important factor in the studied adsorption steps.

As a result of the deposition of metal oxides over the oxidized MWCNTs, the pore volumes and pore diameters of the metal oxide-modified samples were decreased (Table 8) in comparison with acid-treated MWCNTs. In addition to this, it was also observed that the micropores were completely blocked and disappeared after the deposition of CeO_2 or $\text{CeO}_2:\text{V}_2\text{O}_5$ as shown in Table 8. In the case of the addition of V_2O_5 to MWCNTs, the surface area of the micropores decreased by some 50%. The pore size distributions of these preparations are shown in Fig. 31. Two pore size regions, namely 2-3 and 20-40 nm, were identified for all samples. Both types of pore

sizes have enough space to let MB molecules in. The 3D dimensions of the MB molecule are $1.29 \text{ nm} \times 0.77 \text{ nm} \times 0.74 \text{ nm}$ (Xia et al., 2019). A bigger size of MB molecule can also be found in the literature, having length between 1.38 nm and 1.45 nm, and the width is approximately 0.95 nm (Khan et al., 2022). The number of smaller pores (2-3 nm) decreases and that of larger pores (20-40 nm) slightly increases during the acid treatment of MWCNTs and in the case of the metal oxide-modified MWCNTs samples.

Table 8. Weight loss during outgassing; total and micropore surface area, S_{BET} and S_{micro} ; volume of pores between 1.7 and 300 nm diameter and micropore volume, $V_{1.7-300 \text{ nm}}$ and V_{micro} ; average pore size, D_{av} values of fresh MWCNTs, acid-treated MWCNTs and metal oxide-modified MWCNTs.

Samples	Weight loss (m/m%)	S_{BET} (m^2/g)	S_{micro} (m^2/g)	$V_{1.7-300}$ (cm^3/g)	V_{micro} (cm^3/g)	D_{av} (nm)
MWCNTs	0.1	156	25.4	0.6577	0.0109	16.1
MWCNTs (ox.)	7.9	140	13.6	1.0384	0.0052	28.2
V_2O_5	0.8	3.0	0	0.0073	0	13.4
CeO_2	0.5	69.4	15.5	0.1676	0.0069	13.4
$\text{V}_2\text{O}_5:\text{CeO}_2$	3.5	8.8	0.5	0.0368	0.0001	15.0
V/MWCNTs	1.3	135	6.9	0.8439	0.0018	24.5
Ce/MWCNTs	4.5	115	0	0.7002	0	24.1
V:Ce/MWCNTs	6.9	129	0	0.8545	0	25.8

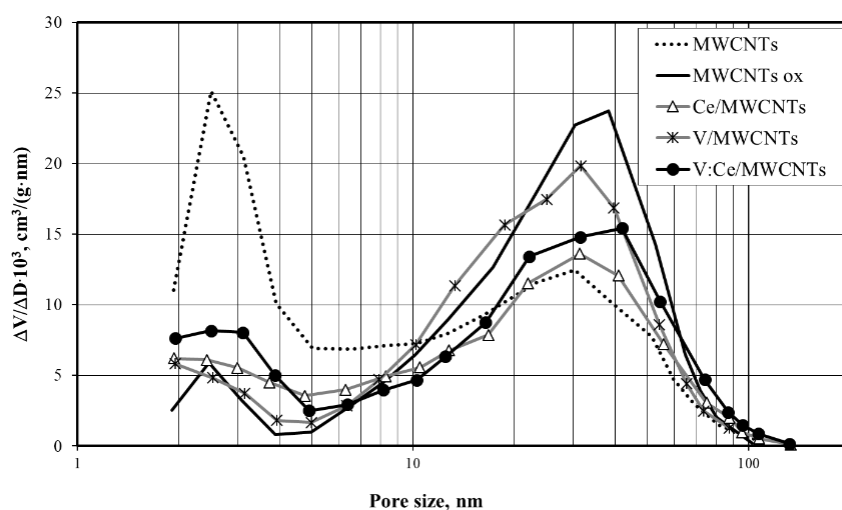


Fig. 31. Pore volume distribution of fresh, oxidized and metal oxide-modified MWCNTs samples.

3.2.7. Results of methylene blue adsorption over metal oxide-doped MWCNTs

A study was carried out on mixed metal oxides as well as raw and metal oxide-doped MWCNTs as a function of time over 35 min. Measurements were taken in every 5 min. The initial MB concentration, volume of the MB solution and mass of the samples were 20 mg/L, 20 mL and 4.5 mg, respectively. The chosen solution pH was 7, since the reported data indicates increasing removal efficiency with rising pH values (Song et al., 2021). Increasing the pH from 4.0 to 10.0, the negative surface charge on the MWCNTs is increased, leading to a stronger interaction between the MWCNTs and the MB molecules (Alqadami et al., 2018).

The raw MWCNTs showed very weak ability to adsorb MB molecules (Fig. 32 and 33). The acidic treatment introduced hydrophilic groups on MWCNTs surface such as carboxylic, carbonyl and hydroxyl ones, thus in some extent altering the MB adsorption. The doping with single metal oxides significantly increased the removal efficiency (by 45-57%). Moreover, the MB concentration reached its minimum when both V_2O_5 and CeO_2 were present in the MWCNTs (Fig. 32 V:Ce/MWCNTs).

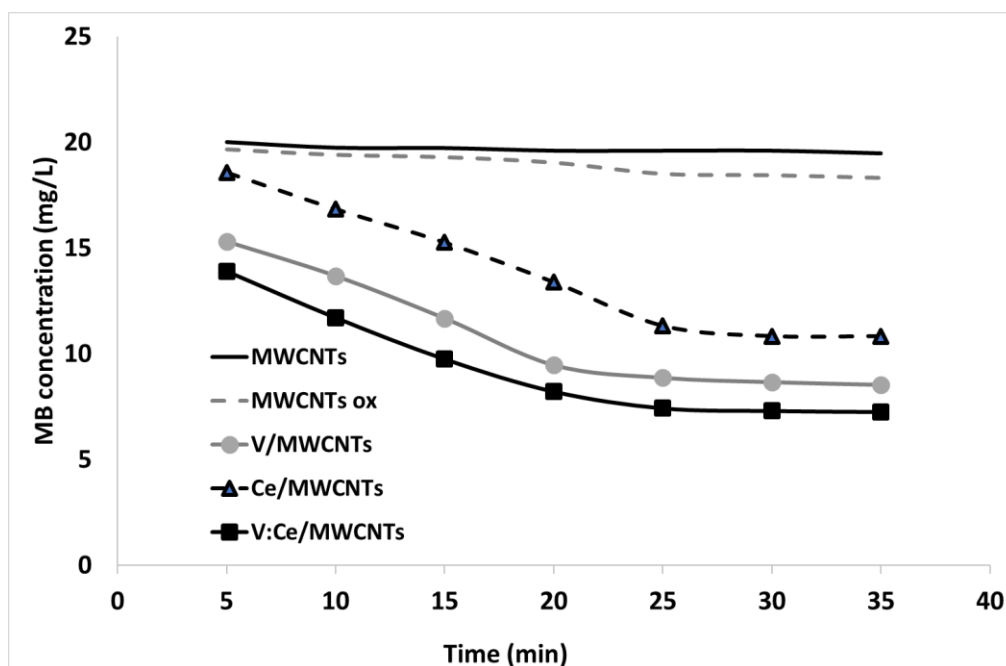


Fig. 32. MB concentration vs. contact time curves of the studied samples ($C_0 = 20$ mg/L, $V = 20$ mL, $m_{ads} = 4.5$ mg, pH 7).

As can be seen in Fig. 33, the V:Ce/MWCNTs exhibit the highest MB removal efficiency from water in comparison with raw, oxidized and single metal oxide-doped MWCNTs.

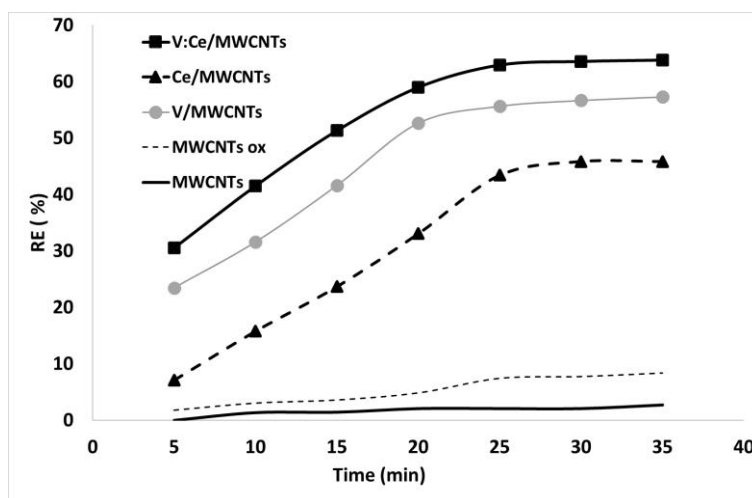


Fig. 33. MB removal efficiency against contact time using raw, oxidized and metal oxide nanocomposite-doped MWCNTs ($C_0 = 20$ mg/L, $V = 20$ mL, $m_{ads} = 4.5$ mg, pH 7).

Fig. 32 and Table 9 show that the decrease in MB concentration and increase in the removal efficiency over time with regard to the studied samples were noticeable in the case of metal oxide-doped MWCNTs for the first 25 min. After 25 min, the adsorption capacity of the samples increased slowly and did not change significantly. Due to the quick occupation of the adsorption sites, the rate of adsorption was high at the earlier stage of the process, but later on the MB molecules could still diffuse into the interior of the nanotubes. Deng et al. observed similar phenomena for herbicide diuron adsorption onto MWCNTs (Deng et al., 2012).

Table 9. Removal efficiency (RE) and adsorption capacity (q_t) of MWCNTs samples during MB removal from water over different preparations after 35 min ($C_0 = 20$ mg/L, $V = 20$ mL, $m_{ads} = 4.5$ mg, pH 7).

Adsorbents	RE (%)	q_t (mg/g)
MWCNTs	2.68	2.39
MWCNTs (ox.)	8.37	7.44
V/MWCNTs	57.30	50.93
Ce/MWCNTs	45.85	40.76
V:Ce/MWCNTs	63.77	56.69

It was noted that the V:Ce/MWCNTs had moderate adsorption capacity in comparison to other carbon-based adsorbents listed in Table 10.

Table 10. Comparison of the experimental adsorptive capacity of carbon-based adsorbents for methylene blue dye.

Adsorbent	Conditions of MB adsorption	Capacity <i>experimental/calculated</i> (mg/g)	Reference
bamboo-based AG	100-500 mg/L 200 mg, pH 7	99.8-441 / 100-454.4	(Hameed et al., 2007)
graphene oxide	312 mg/L 150 mg, pH 6	709-714 /-	(Yang et al., 2011)
CNTs	40 mg/L 150 mg, pH 10	80.2 / 95.30	(Selen et al., 2016)
sulfonic acid-CNTs	250 mg/L 50 mg/L 10 mg, pH 7	236.5 / - 78.2 / -	(Lei et al., 2021)
Fe ₂ O ₃ -MWCNTs	20 mg/L, 50mg pH 6	42.3 / -	(Qu et al., 2008)
MWCNTs/Fe ₃ O ₄	20-200 mg/L, 20mg, pH 4-10	118.3 / 204.2	(Song et al., 2021)
graphene/Fe ₃ O ₄	10-25 mg/L, 10 mg, pH 2-11	24.7-35.4 / 43.8	(Ai et al., 2011)
V:Ce/MWCNTs	20 mg/L, 4.5 mg, pH 7	56.7 / -	<i>This work</i>

The effect of the amount of adsorbent was studied over the two best-performing composite samples, namely V/MWCNTs and V:Ce/MWCNTs, exhibiting the highest MB removal efficiencies of 57.3 and 63.8 mg/g, respectively. These samples also exhibited the highest adsorption capacities of 50.9 and 56.7 mg/g, respectively (Table 10). Different amounts of adsorbents from 1.5 to 10.0 mg were added to the MB solution and the removal of MB was followed for 25 min at room temperature. The results showed that the optimum adsorbent masses were 6.0 and 9.0 mg for the V/MWCNTs and V:Ce/MWCNTs samples, respectively (Fig. 34).

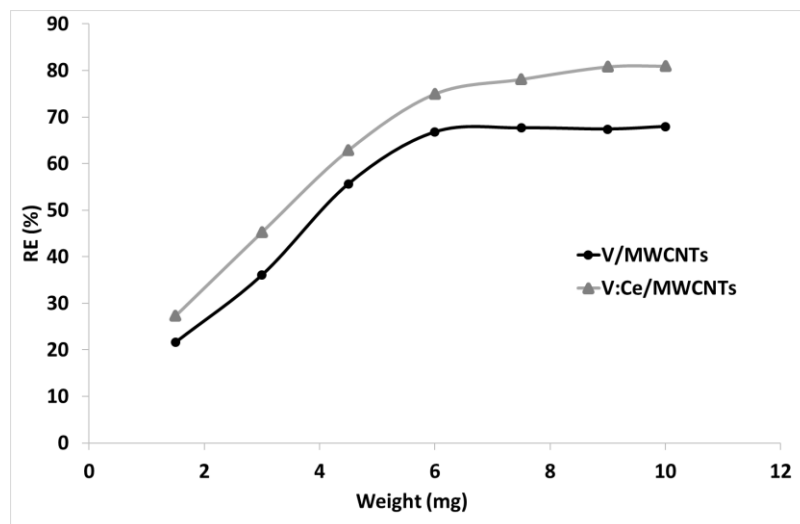


Fig. 34. Effect of adsorbent dosage on MB removal efficiency over V/MWCNTs and V:Ce/MWCNTs ($C_0 = 20$ mg/L, $V = 20$ mL, pH 7).

The effect of temperature on the MB removal efficiency was studied within the temperature range of 15 to 65 °C over V:Ce/MWCNTs samples. The reaction time was 25 min, the mass of the adsorbent was 9 mg, the shaking speed was 240 rpm, the MB concentration was 20 mg/L and the volume of the solution was 20 mL. A comparison of the adsorption values at different temperatures shows that the adsorption capacity increased from 45 to 82 mg/g as the temperature increased from 15 to 45 °C. This can be due to the increased mobility of the dye molecules with the increase of the temperature. In addition, the higher temperature leads to lower viscosity enabling a faster diffusion of the adsorbate through the external boundary layer as well as inside the pores. Similar results have been reported (Selen et al., 2016). A further increase in temperature (> 45 °C) does not have a positive effect on adsorption. This supports that the adsorption is an exothermic process and more favourable at lower temperatures (Song et al., 2021).

3.2.8. Mechanism of MB adsorption over metal oxide-doped MWCNTs

The three main interaction mechanisms between MB and CNTs are reported as π - π interactions, hydrogen bonding and electrostatic interactions (Sajid et al., 2022). For raw MWCNTs, a π - π interaction can form between bulk π systems on CNTs surfaces and the phenyl ring of MB (Fig. 35a). When the MWCNTs are oxidized by acids, covalent sidewall functionalization of the nanotubes with -OH, -COOH and

-C=O groups occurs. A stronger electrostatic interaction can form between negatively charged carboxyl groups (-COO⁻) and the cationic methylene blue (Mallakpour et al., 2021) (Fig. 35b). Also, π - π donor-acceptor interactions can occur between delocalized π electrons of the phenyl ring of MB and the carbonyl groups (Sajid et al., 2022). Hydrogen bonds could also be formed between the lone pair of electrons on the nitrogen atom and the hydrogen atom at the end of the tubes or at defect sites (not shown) (Mallakpour and Tabesh, 2021).

Adding of metal oxides to CNTs leads to modification of adsorptive properties of the adsorbent surface (M. Oliveira et al., 2023). The presence of semiconductor metal oxides on the surface of MWCNTs might induce an electron transfer from nanoparticles to nanotubes (electron injection) (Ai et al., 2011; Duan et al., 2016; Zeleke and Kuo, 2019). This leads to the enhancement of adsorptivity of cationic MB through π - π interactions between the MB molecules and the aromatic rings of the tubular graphene layer.

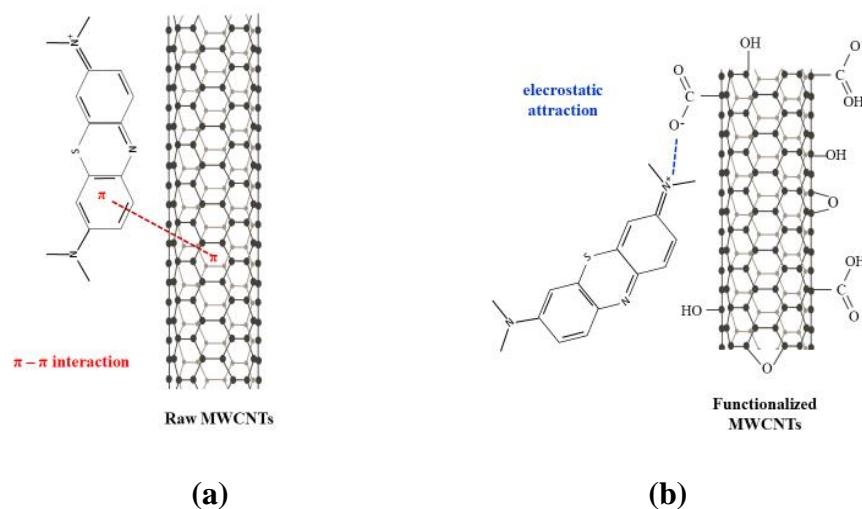


Fig. 35. The proposed adsorption mechanism between MB and raw MWCNTs (a) and between MB and oxidized MWCNTs (b).

3.3. Macrocyclic compounds for selective recovery of rare earth scandium element from aqueous media

3.3.1. Results of extraction with varying concentrations of macrocyclic compounds

Macrocyclic compounds can form stable complexes with metal ions. In the preliminary extraction experiments, Sc was extracted with varying concentrations (0.001–0.01 mol/L) of cryptand 2.2.2, 12-crown-4, 15-crown-5 and DC18-crown-6. 25 mg/L ($5.5 \cdot 10^{-4}$ mol/L) Sc model solution was used at pH 2. The experimental data are shown in Fig. 36 and summarized in Table S1.

The results showed that the extraction efficiency was quantitative above 0.004 mol/L C2.2.2, 12-C-4, and 15-C-5 concentrations. In case of C2.2.2 of 0.004 mol/L (Fig. 36a) the extraction efficiency was 17%, while at 0.006 mol/L concentration the extraction efficiency increased to 85%. Thus, Sc extraction into the organic phase becomes significant at about 0.008 mol/L and increases rapidly above this value, as shown in Fig. 36a. The maximum extraction efficiency (over 99%) appears to occur at around 0.01 mol/L. The extraction with 12-C-4 and 15-C-5 follows the same tendency but reaches a lower value: 59% and 53%, respectively (Fig. 36b-c).

The impact of the increasing DC18-C-6 concentration is different from that of C2.2.2, 15-C-5, and 12-C-4 and has the lowest extraction values, $E_{\max} = 15\%$ (Fig. 36d). Cryptand 2.2.2 - in contrast to crown ethers - binds the guest ions via both the nitrogen and oxygen donors. The two tertiary amine nitrogen atoms make the compound a fairly strong base and increase the cryptand extraction ability towards metal cations. Macrocyclic compounds have similar structures, but cryptands are more selective and stronger when considering their ability to form complexes with metal ions.

The low DC18-C-5 ability to bind Sc^{3+} ion can be attributed to its cavity being too large (1.3-1.6 Å, Table 1) to bind the cation having the size of 0.745-1.116 Å (Table 11). At the same time, the level of complexation with 12-C-4 was also lower. The 12-C-4 cavity (0.6-0.75 Å) is too small to accommodate the cation, therefore the rate of complexation was lower in comparison with cryptand, C2.2.2. In this case sandwich-type complexes might form with regard to two crowns per metal ion present in the complex (Jong and Reinhoudt, 1980).

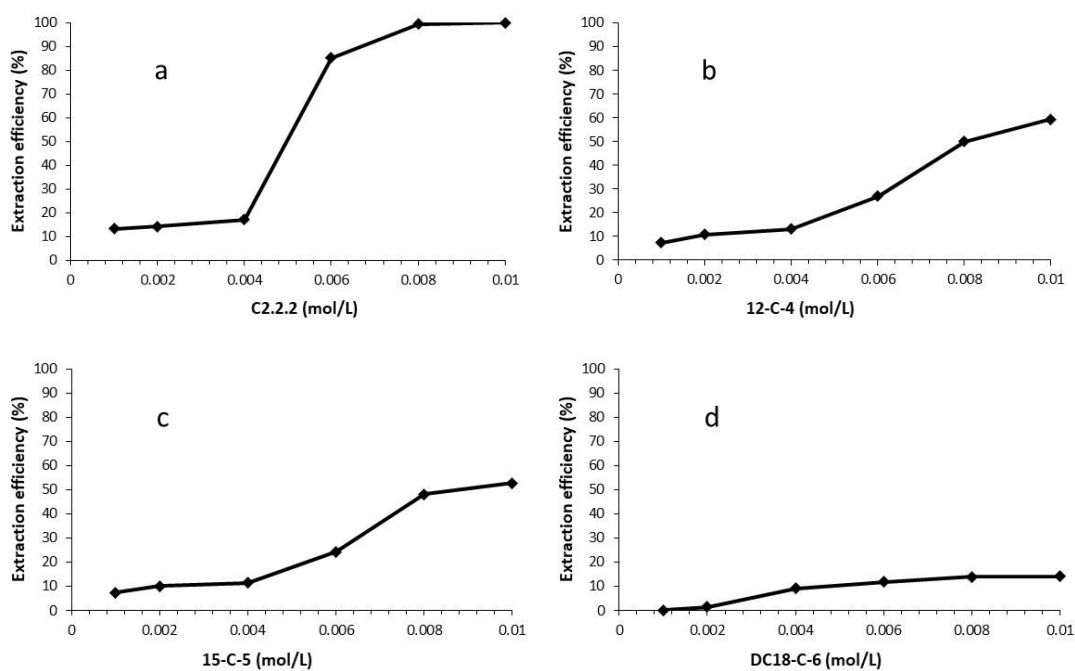


Fig. 36. Sc ion extraction efficiency as functions of (a) cryptand 2.2.2, (b) 12-crown-4, (c) 15-crown-5 and (d) DC18-crown-6 concentrations ($C_{Sc^{3+}} = 25$ ppm, $V = 25$ mL, pH 2).

Table 11. Ionic radii of Sc, Y, La, Ce Group 3 elements according their coordination number.

Elements	Atomic mass	Ionic radii (Å)	
		6 / 8 / 12-fold coordination (Lide et al., 2008)	6-fold coordination (Greenwood and Earnshaw, 1997)
Sc ³⁺	44.96	0.745/0.87/1.116	0.745
Y ³⁺	88.91	0.900/1.015/1.220	0.900
La ³⁺	138.91	1.045/1.18/1.320	1.032
Ce ³⁺	140.12	1.010/1.14/1.290	-

3.3.2. Extraction of Sc ions as a function of pH

To investigate the impact of pH on the extraction efficiency of Sc from the aqueous phase with MCs, extraction experiments were made in the pH range of 1–5 as shown in Fig. 37. The acidic pH range was used to avoid the hydrolysis and precipitation of Sc (Brown and Ekberg, 2016). In these experiments, the concentration of the macrocyclic compounds in the organic phase was set to 0.01 mol/L while the Sc

ions concentrations in the aqueous phase were 25, 50, 75, and 100 mg/L (Fig. 37a-d, Table S2).

With all types of MC extractants at $\text{pH} < 2$, Sc was not appreciably extracted. At the same time, the extraction efficiency increased rapidly above $\text{pH} 2$ applying different Sc^{3+} concentration. With all concentrations of C2.2.2, 12-C-4, 15-C-5 high extraction values (95-99%) were reached above $\text{pH} 3$. This is due to the increasing tendency of metal ions to form complexes with increasing pH .

The extraction of 25 mg/L Sc solution with DC18-C-6 (Fig. 37d) showed that the pH change was ineffective in improving the extraction efficiency as compared with 15-C-5, 12-C-4, and C2.2.2. The maximum extraction efficiency was only 25.8 % at $\text{pH} 5$. According to these results with DC18-C-6, it made no sense to continue the extraction experiments with different Sc ion concentrations.

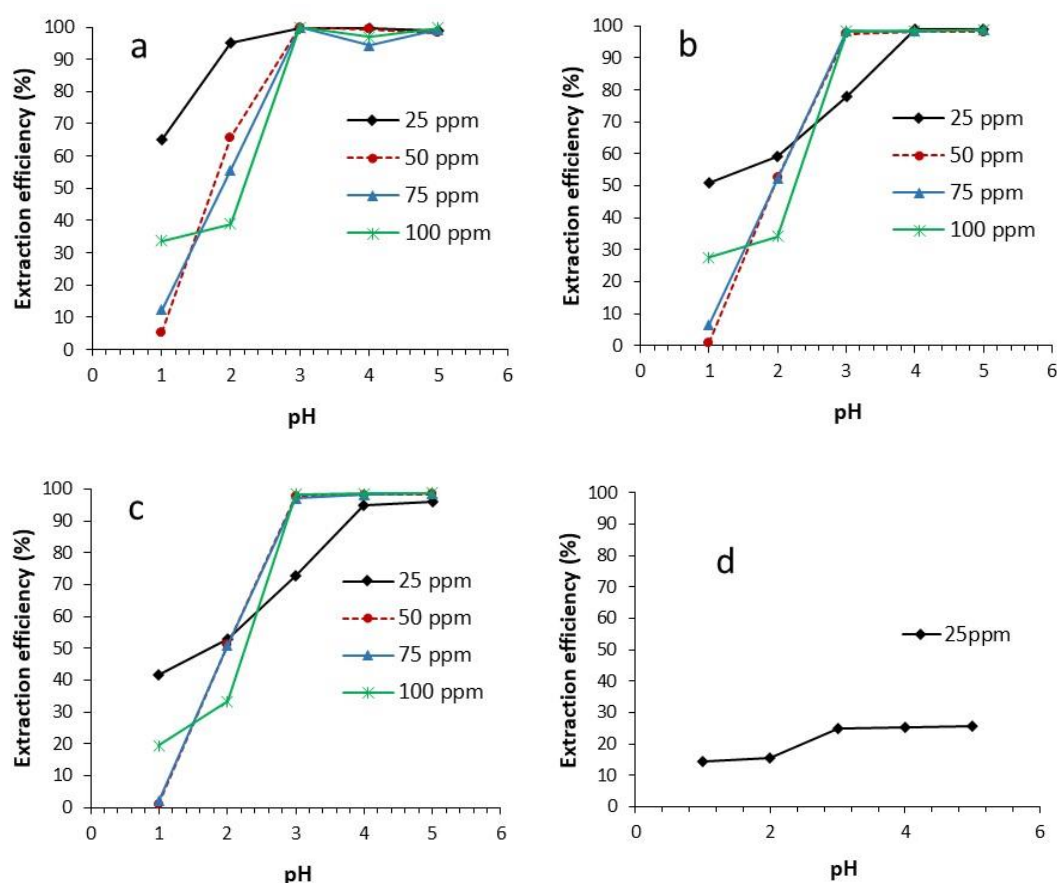


Fig. 37. Extraction efficiency of Sc as a function of function of pH at 0.01 mol/L of (a) cryptand 2.2.2, (b) 12-crown-4, (c) 15-crown-5 and (d) DC18-crown-6.

3.3.3. Stripping of Sc with inorganic acids

After the extraction, Sc was stripped with inorganic acids. Stripping Sc from macrocyclic compounds was studied using hydrochloric and nitric acids with different concentrations. Both acids at concentrations of 0.1, 0.5, and 1.0 mol/L were effective. The preliminary results of back-extraction/stripping indicated the high efficiency of the extraction. According to spectrophotometric Sc³⁺ determination the results showed that HCl and HNO₃ were efficient in Sc³⁺ recovery (> 95%), as shown in Table 12.

Table 12. Effect of HCl and HNO₃ concentration on Sc ion recovery from solution of pH 2.

Stripping agent concentration (mol/L)	Sc ion recovery (%)	
	HCl (pH value)	HNO ₃ (pH value)
0.1	95.7 (pH 1.03)	96.0 (pH 1.19)
0.5	97.0 (pH 0.41)	96.3 (pH 0.54)
1.0	99.1 (pH 0.12)	99.5 (pH 0.26)

3.3.4. Results of extraction of REEs from multielement model solution

In chapter 3.3.3 above the results of the Sc extraction process with different macrocyclic compounds and the impact of the process operating variables were discussed. Of the investigated macrocyclic compounds, cryptand 2.2.2 (0.008 mol/L) was selected as extractant for REEs multielement solution (Sc, Y, La, Ce) due to its high performance for Sc³⁺ extraction. These elements have been selected to extract because of their similarity in physico-chemical properties to Sc. In addition, these REEs occur together in bauxite ore as well as in industrial wastes such as red mud (Juzsakova et al., 2018; Salman et al., 2021). Also, these elements usually are co-extracted during the recovery process of individual REEs (Cotton, 2006).

Scandium, yttrium, lanthanum are trivalent in aqueous solutions (Brown and Ekberg, 2016). Cerium exists in two main oxidation states, Ce³⁺ and Ce⁴⁺. The dominating oxidation state of cerium in aqueous solutions is Ce³⁺ (Cotton, 2006; Greenwood and Earnshaw, 1997).

The solution of REEs in diluted nitric acid was used in this study. All four elements form nitrates. Sc³⁺ and Y³⁺ have 9- and 10-fold coordination in [M(NO₃)₅]²⁻

complexes (Greenwood and Earnshaw, 1997). Lanthanum and cerium exhibit high coordination numbers having 11-fold coordination in nitrate complexes (Cotton, 2006).

The effective ionic radii of rare earth ions depends on their coordination number as shown in Table 11. The metal cations mentioned above with coordination numbers between 9 and 11 (ionic radii between ~ 0.87 and 1.32 \AA) in nitric acid solution fit well into the cavity of the chosen macrocyclic extractant, C2.2.2 ($r = 1.40 \text{ \AA}$).

The binding affinity/selectivity can be manipulated by changing the pH. The multielement extraction result showed a selective separation towards Sc ions having high E value of 97% at pH 2, as compared with Y = 18%, La = 10%, and Ce = 9%, as shown in Fig. 38.

The bicyclic C2.2.2 cryptand with tertiary N atoms – connected through $\text{C}_2\text{H}_4\text{OCH}_2\text{OCH}_2$ chains – shows chemical characteristics similar to the ether- or amine – containing ones (Hamilton, 1984). The two tertiary amine nitrogen atoms make the compound a quite strong base (Marcus, 2004). Sc – as the least basic element – showed stronger binding affinity towards C2.2.2 than the rest of the elements (Greenwood and Earnshaw, 1997).

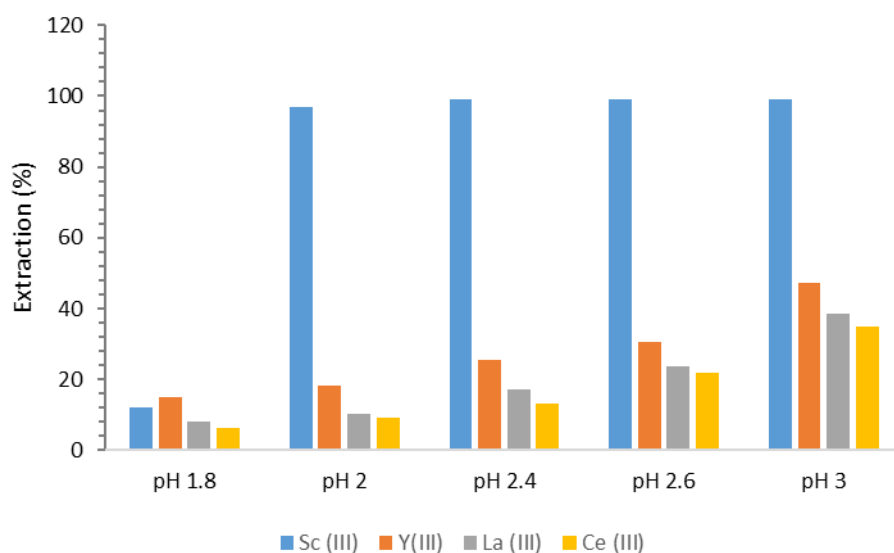


Fig. 38. Effect of pH on the extraction efficiency of REEs metal ions (25 mg/L Sc, Y, La, Ce in aqueous solution; organic phase: 0.008 mol/L C2.2.2; A/O : 10 mL/10 mL, shaking time: 10 min, RT).

3.3.5. Extraction and stripping mechanism

Recovery of REEs from multielement model solutions can be done with inorganic acids like hydrochloric or nitric acids, at $\text{pH} < 2$. The stripping agent and its concentration has an important effect on the selectivity of the process as shown above. The recovery of Sc^{3+} can be achieved between 58 and 100% efficiency, as compared to that of Y^{3+} , La^{3+} and Ce^{3+} (23 - 50%) (Salman et al., 2022). The exact value of recovery depends on type and concentration of the acid used for stripping.

During the cation interaction with cryptand 2.2.2, the cation is transported from the aqueous phase and can be coordinated in the cavity of the cryptand by six oxygen and two nitrogen atoms (Marcus, 2004). Because C2.2.2 is a diprotic base, its ability to complex metal ions in aqueous solutions is highly influenced by the pH of the medium. At $\text{pH} < 2$, the C2.2.2 will be protonated (as shown in Fig. 39), and the binding constant for metal cations will be severely reduced relative to that of the neutral C2.2.2 due to charge repulsion.

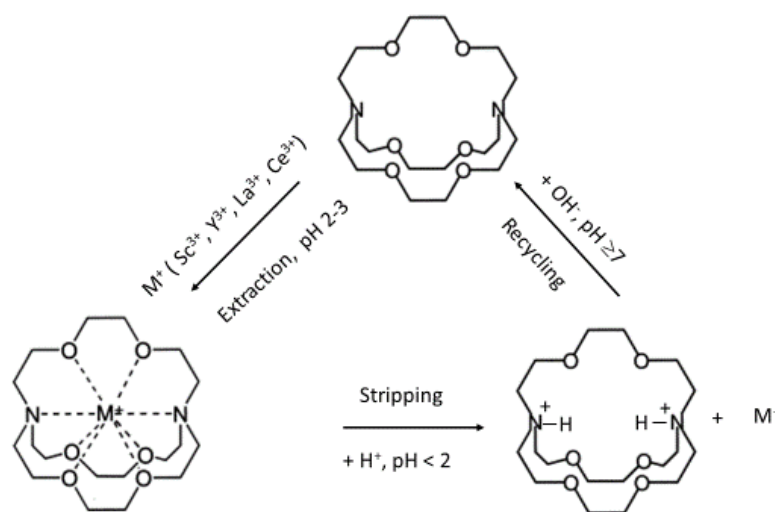


Fig. 39. Effect of the pH on the metal ions extraction ability of cryptand 2.2.2 and its protonation.

The protonation of C2.2.2-type cryptands occurs through proton transfer from the acid solutions (Auffinger and Wipff, 1991). It was shown that acids are able to catalyse decomplexation of metal cryptates in the endo-endo form (Auffinger and Wipff, 1991). Hence, stripping or displacement of guest cations from the macrocyclic molecules usually occurs in acidic environments (Gandhi and Khopkar, 1993; Luo et

al., 2004). The experimental data confirm the supposition that the pH of the solution can alter the binding affinity of cryptand. The extraction of M^{3+} was quantitative at $pH \geq 2$. Then different metal cations can differently compete to be encapsulated by cryptand, between pH 2-3.

On the other hand, stripping of REE cations from the cryptand organic phase was quantitative at $pH < 2$, since the proton concentration is high enough to displace cations from the cavity. It was reported that deprotonation of the N-H⁺ group of cryptand 1.1.1 starts from $pH \sim 7$ (Alibrandi, 2008) and ends in the alkaline range. This observation makes the cryptand regeneration and its further reuse possible (Fig. 39).

3.3.6. Flowchart for scandium recovery from red mud

The red mud contains the following main components: iron oxide (Fe_2O_3) 12-48 m/m%, calcium oxide (CaO) 2-42 m/m%, aluminum oxide (Al_2O_3) 12-26 m/m%, silica (SiO_2) 8-43 m/m%, titania (TiO_2) 4-18 m/m%, sodium oxide (Na_2O) 2-11 m/m% and rare earth elements in minor amounts (0.1-0.3 m/m%) (Juzsakova et al., 2018). The total amount of REEs estimated in the Hungarian red mud is about 1500-2500 ppm (Lakatos et al., 1978; Szépvölgyi and Kótai, 2012).

The major elements concentrations of red mud should be diminished before the extraction of REEs. As it was shown, the extraction step can involve extraction of REEs with cryptand (this study), crown ethers or organophosphorus compounds (e.g. di-(2-ethylhexyl) phosphoric acid, tributyl phosphate) (Lakshmanan and Vijayan, 2018) or with solid extractants (Zhang et al., 2019). Due to the limited capacity of MCs and solid adsorbent particles, liquid-liquid and solid-liquid extraction methods are recommended for the final step of the recovery procedure, when the solution mainly contains the REE target metals (e.g. Sc, La, Ce).

Application of the selective leaching method using inorganic acids can minimize Al (56%), Ca (73%), Mg (89%), Mn (65%), Na (51%), Ti (63%), Si (1%) dissolution from red mud (but not Fe (91 wt%)) at atmospheric pressure and relatively low temperature, 80 °C (Juzsakova et al., 2023). At the same time leaching results in the selective and effective dissolution of rare earth metals (e.g. Sc 50-70 % or 50-70 ppm).

The major elements of red mud such as iron can be efficiently removed by reduction at high temperature followed by magnetic separation (Grudinsky et al., 2022). The dissolved iron from HCl media can also be efficiently separated by organic solvent extraction with diethyl ether (Tunkasiri et al., 1992).

In order to separate the rare earth metals - and other metal components that may dissolve - it is advisable to use the ion exchange process. An ion exchange technique, using strongly acidic cation exchange resins (e.g. AmberChrom 50WX8), is suitable for the efficient separation of various metals from red mud (Acikara, 2013; Molchanova et al., 2019). During the ion exchange process, the various metal ions (M^{n+}) including REEs from red mud leachate are competing with counter ions (H^+) for the functional group of an ion exchanger/resin. The most common strategy to elute bound metals from the resin is pH manipulation of the eluent: increasing the ionic strength (e.g. increasing the molarity of acid) can displace metal ions that are more highly charged/ stronger bound. As a result, fractions rich in different metals are obtained. In the product fractions obtained during ion-exchange, the rare earth metals are present in the same order of magnitude as the main elements, which results in a significant enrichment of target elements, such as Sc, as compared to the initial leachate composition (Juzsakova et al., 2023).

Adjusting the pH between 1 and 2, Sc ions can quantitatively be precipitated from solution with oxalic ions (Nawab et al., 2022). This is the usual way of the quantitative analysis of lanthanides after calcination of the oxalate precipitate (Silva et al., 2019; Strauss, 2016). The next purification step of the desired fraction containing high amount of Sc can be done by liquid-liquid extraction with macrocyclic or organophosphorus compounds and by solid-liquid extraction.

The knowledge gained on the ability of MCs to encapsulate REEs has been utilized in designing the solid phase applied for recovery of Sc ions by solid phase extraction (Salman et al., 2020). This extraction is an ecologically friendly alternative technology, efficiently simplifying the procedure of Sc^{3+} extraction and decreasing the costs as compared to solvent or liquid film extractions (Dai et al., 2022). Novel hybrid nanoparticles and natural amorphous SiO_2 nanoparticles were modified with 3-aminopropyl triethoxysilane (APTES) as chemical linker and cryptand 2.2.2 as supramolecular ligand for scandium extraction. The extraction efficiency on these hybrid nanomaterials from 15-75 mg/L Sc^{3+} solutions varied between 81.3 and 96.7%.

Moreover, the stripping/back extraction with 0.1 mol/L HCl recovered Sc from the solid phase with an efficiency ranged from 95.0 to 96.5% (Salman et al., 2020). The proposed flowchart for the recovery of scandium, iron and other metals from red mud are shown in Fig. 40.

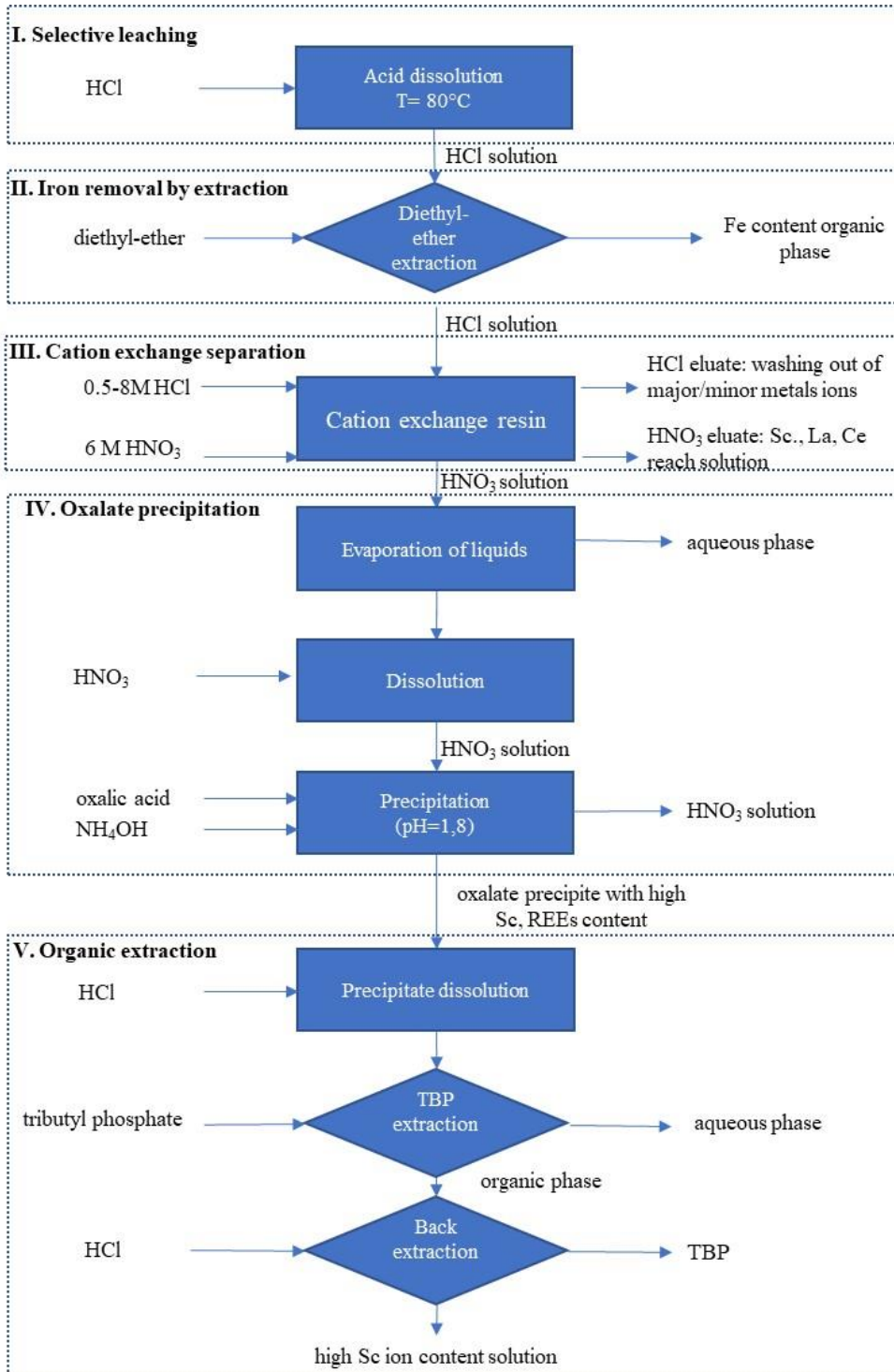


Fig. 40. Flowchart for the recovery of scandium, iron and other metals from red mud.

It should be emphasized that red mud as a resource of individual rare earth metals alone cannot be an attractive option. From an economic point of view, it is necessary to consider the complex processing of red mud. The recovery of Sc should be combined with the separation of Fe, Al, Ti, Mn main/minor as well as other rare earths elements, e.g. Y, La, Ce.

CONCLUSIONS

This work has shown the feasibility of preparing valuable hydrocarbon adsorbents using functionalization techniques such as microemulsion treatment of MWCNTs and doping the MWCNTs by nanometal oxides. The adsorption behaviour of functionalized MWCNTs underlines the structural and hydrophobic properties stemming from functionalization via microemulsion treatment, and the impacts of this modification on hydrocarbon adsorption capacity. The experimental results proved that the μ EMWCNTs are good hydrocarbon adsorbents. The adsorption capacities of μ EMWCNTs are higher than that of MWCNTs for all model hydrocarbons. The q_t of μ EMWCNTs is in the range of 4.5 to 13.3 g/g, while the q_t of MWCNTs is in the range of 3.8–7.2 g/g.

The kinetic studies illustrated that the pseudo-second order model is the best-correlating one for toluene removal over μ EMWCNTs with equilibrium removal capacity reaching up to 4.9 g/g and a rate constant of $k_2 = 0.0303$ g/g·min. This result is based on the assumption that the rate-limiting step is chemisorption involving valency forces through the sharing or exchange of electrons between sorbent and sorbate. Thus, this model provided the best correlation of the data. The activation energy (43.73 kJ/mol) calculated on the basis of the kinetic measurements supports the notion that chemisorption occurs instead of physisorption.

The result showed that the novel metal oxide-doped MWCNTs adsorbents are nanosized materials having the graphene layers as the major crystalline phase. The EDX and TGA studies confirmed the successful deposition/attachment of metal oxides onto the MWCNTs surface. The deposition of V_2O_5 (2-5 wt%), CeO_2 (4-12 wt%) and $V_2O_5:CeO_2$ (2-8 wt%) over the oxidized MWCNTs caused the blockage of micropores. At the same time, the surface area remained relatively high (115-135 m^2/g) for adsorption treatment. The experimental results showed that adsorption capacity and removal efficiency of MWCNTs for methylene blue increased after adding metal oxides nanocomposites over MWCNTs (ox.) from 7.4 to 56.7 mg/g and 8.4 to 63.8% respectively. The studied microemulsified MWCNTs and metal oxides-modified MWCNTs can be considered as potential adsorbents for organic molecule depollution control and could open new avenues for their application.

Recovering rare earth metals from secondary sources such as red mud is a challenging task. Since scandium is a highly valuable element, the aim of this work was to devise and test novel techniques involving the use of macrocyclic compounds (crown ethers, cryptand) for the encapsulation of metal ions in cage-like structures for the separation. In this study, the extraction of Sc by cryptand 2.2.2 and crowns (12-C-4, 15-C-5, and DC18-C-6) from model acid solutions containing Sc has been successfully proposed and highlighted. The results clearly show that C2.2.2, 12-C-4 and 15-C-5 exhibited excellent Sc^{3+} extraction abilities as compared to DC18-C-6 under the same conditions. The extraction ability of these compounds can be due to the compatibility between the macrocyclic compounds ring sizes and the ionic radii of Sc ions. The Sc^{3+} extraction efficiency obtained by C2.2.2, 12-C-4, 15-C-5 achieved a high percentage (> 95%) depending on the pH value of aqueous solutions at different scandium concentrations.

Novel analytical procedures have been developed for the recovery of Sc from the acidic leachates of Hungarian red mud including: iron removal with diethyl-ether; main elements separation from REEs via cation exchange; Sc, Ce, La oxalates precipitation and purification applying solvent extraction (using organo-phosphorous or macrocyclic compounds) or solid phase extraction (with organophosphorous compound-modified solid support).

NEW SCIENTIFIC FINDINGS, DSC THESIS

The adsorption properties of surface-modified MWCNTs and nanometal-modified MWCNTs necessitate the understanding of (i) the surface chemical properties stemming from the functionalization of MWCNTs, and (ii) the impacts of this pretreatment on pollutants removal from water. The interpretation of processes occurring on the surface of newly synthesized adsorbents can contribute to the remediation of contaminated water bodies.

The red mud contains several valuable metals including iron oxide (33-40%), titania (4-6%), vanadia (0.2-0.4%), rare earth elements (REEs) (1500-2500 ppm), etc. Therefore, it can be considered as a potential secondary metals resource. The recovery of scandium was aimed at from the red mud since the scandium is a very important element for the electronic industry to produce high-intensity lights source and to prepare high strength alloys for spacecraft industry. The liquid-liquid extraction of the scandium cation by macrocyclic compounds from model REEs solutions was studied. The result showed that cryptand as an organic extractant could be of potential value in the separation and purification of Sc^{3+} in rare earth elements processing industry. Moreover, the recycling of REEs is considered as part of the complex utilization of red mud, leading to a reduction in the storage volume of wet red mud and mitigation its hazardous impact to the environment. The main results are summarised in the thesis points below.

THESIS POINTS

4.1. Microemulsified carbon nanotubes ($\mu\text{EMWCNTs}$) for the removal of hydrocarbons (undecane, kerosene and toluene) from water:

4.1.1. I concluded that the functionalization of MWCNTs via non-covalent microemulsification has no effect on crystal structure. This fact is evidenced by the XRD. Raman spectroscopic studies confirmed the interaction between the carbon nanotubes and the functional groups of the fatty acid esters used for the modification. The thermogravimetric studies showed that during microemulsification treatment fatty acid esters (esterified mainly with lauric

acid) were connected onto the surface of the MWCNTs. The BET study revealed that microemulsification resulted in a decrease in the specific surface area of MWCNTs by 37% due to the blocking of micropores. This result also proves the successful incorporation of functional groups into the MWCNTs pores. The disappearing of micropores does not have significant impact on the removal efficiency of hydrocarbon pollutants from water [P1-2].

4.1.2. I proved that the microemulsion technique as a type of non-covalent surface functionalization has a beneficial effect on MWCNTs' hydrophobic properties without the need for additional functionalization and substitution steps to attach hydrocarbon side chains. This statement was proved by batch adsorption tests, GC, UV-Vis results. The adsorption capacity of μ EMWCNTs was higher than that of MWCNTs for all model hydrocarbon-water solutions investigated (alkanes and aromatic hydrocarbons). Moreover, the adsorption capacity of μ EMWCNTs towards kerosene was two and three times higher than that obtained over commercial Chemiviron Carbon F300 and Norit GAC 1240 EN activated carbon-based adsorbents, respectively [P1].

4.1.3. I proposed that one of the most probable ways of sorption of non-polar, alkane molecules on raw MWCNTs is via $\text{CH}\cdots\pi$ interaction. The $\text{CH}\cdots\pi$ link is one of the weak non-covalent hydrogen bonds. In case of raw MWCNTs interaction occurs between the H atoms of the saturated hydrocarbons (undecane, kerosene) and the carbon atoms of MWCNTs (Fig. 1.) [P1-2].

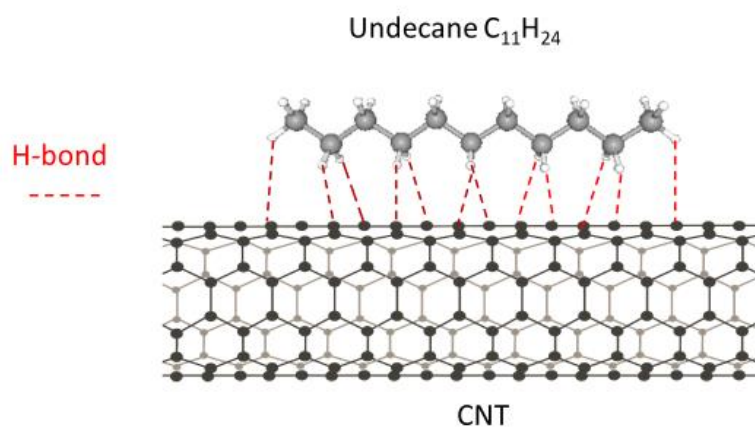


Fig. 1. Adsorption of undecane over MWCNTs.

4.1.4. I concluded that the adsorption affinity of toluene over μ EMWCNTs increases by the involvement of the $-C=O$ groups and by aromatic π - π bonds. The sorption of the toluene on the surface of the μ EMWCNTs can be given, as depicted in Fig. 2. It is in harmony with the adsorption mechanisms of organic pollutants over CNTs reported earlier [P1].

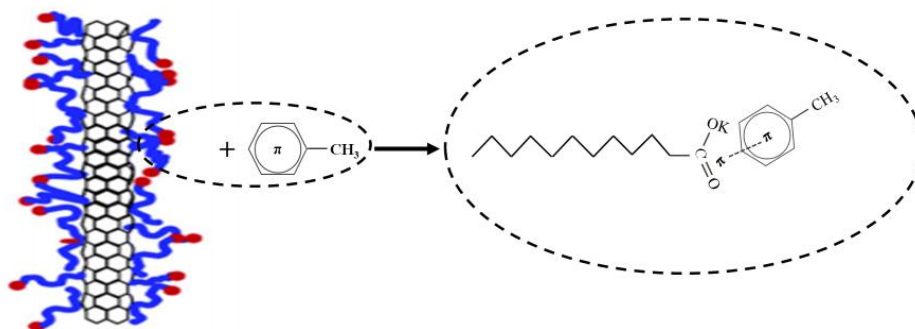


Fig. 2. The mechanism of the surface functionalization and sorption of toluene over μ EMWCNTs.

4.1.5. I observed that the experimental data of toluene adsorption over μ EMWCNTs fitted well to the second-order kinetic model ($R^2 \geq 0.99$). Moreover, the calculated activation energy of the adsorption is 43.73 kJ/mol, which supports the assumption that the sorption process is chemisorption [P1].

4.2. Nanometal oxide-doped MWCNTs composites for the removal methylene blue dye from water:

4.2.1. I confirmed the successful doping of metal-oxide nanocomposites over MWCNTs surfaces while preserving the crystalline phase and morphology of the graphene layers (confirmed by TGA, BET, XRD, SEM-EDX, and TEM). The deposition of V_2O_5 , CeO_2 and $V_2O_5:CeO_2$ mixture over the oxidized MWCNTs caused the blockage of some micropores. Meanwhile, the surface area available for adsorption treatment remained relatively high (115–135 m^2/g) [P3].

- 4.2.2.** I observed that the adsorption capacity (q_t) and removal efficiency (RE) of MWCNTs with regard to the removal of methylene blue from water increased after adding $V_2O_5:CeO_2$ over MWCNTs (q_t increased from 2.4 to 56.7 mg/g and RE increased from 2.7 to 63.8%) [P3].
- 4.2.3.** For raw MWCNTs, I concluded that a π - π -type interaction can form between the π bonds in methylene blue and the π bonds of the multiwalled carbon nanotubes. When the MWCNTs are oxidized with acids covalent sidewall functionalization of the nanotubes with $-OH$, $-COOH$, $-C=O$ groups occurs. Stronger electrostatic interactions can form between the carboxyl group and the cationic methylene blue. A bond could also be formed between the electron pair of the nitrogen atom and the hydrogen atom at the end of the tubes or at defect sites. Therefore, in the case of oxidized MWCNTs adsorption can follow a mixed mechanism (π - π and electrostatic interactions) [P3].
- 4.2.4.** The nanotube surface exhibits polar groups (like hydroxyl or carboxyl ones) after acidic treatment, which are able to interact with the nanometal oxides during the deposition of metal-oxides over MWCNTs surface. The presence of semiconductor metal-oxides nanocomposites (CeO_2 , V_2O_5) on the surface of MWCNTs induces the electron transfer from nanoparticles into nanotube (electron injection). This leads to enhanced MB adsorption through π - π interactions between the MB molecules and the aromatic rings of the tubular graphene layer [P3-4].

4.3. Scandium recovery based on molecular recognition methodology:

- 4.3.1.** I proposed the macrocyclic compounds (crown ethers, cryptand) for the encapsulation of REE ions in cage-like structures. It has been shown that the incorporation of Sc^{3+} into an 0.008 mol/L C2.2.2. cryptand extractant solution was feasible from model acid solution containing 25 mg/L Sc, Y, La, Ce of each. The binding affinity/selectivity can be manipulated by changing the pH. Application of cryptand extractant showed a selective separation towards Sc^{3+} ions having high extraction value of 97% at pH 2, as compared to Y = 18%, La = 10% and Ce = 9%. The results support the observation that the high extraction ability of C2.2.2 for Sc^{3+} from REEs solutions can be due to its molecular recognition ability. On other hand, the molecules of cryptand are

three-dimensional structures and is able to encapsulate the guest ions and form stable complexes. This could be of potential value in the separation and purification of Sc in REEs processing [P5-6].

- 4.3.2.** The knowledge gained in the field of REE extraction with macrocyclic compounds has been implemented to develop new types of solid phases for solid-liquid extraction techniques. Novel hybrid nanoparticles, SiO₂ nanoparticles modified with 3-aminopropyl triethoxysilane (APTES) as chemical linker and cryptand 2.2.2 as supramolecular ligand is suitable for scandium adsorption from model solution of 15-75 mg of Sc/L. Moreover, the stripping/back extraction with 0.1 mol/L of HCl re-covered Sc from solid phase with efficiency ranged from 93.1 to 97.8% [P7].
- 4.3.3.** I proposed reliable and efficient analytical techniques for the recovery of Sc from the acidic leachates of Hungarian red mud including: iron removal with diethyl-ether; main elements separation from REEs via cation exchange; Sc, Ce, La oxalates precipitation and purification applying solvent extraction (using organo-phosphorous or macrocyclic compounds) or solid phase extraction (with organo-phosphorous compound-modified solid support) [P8-10]. By this techniques at about 35-40 % of Sc can be recovered by processing of red mud in the laboratory-scale system. Flowchart for the recovery of scandium, iron and other metals from red mud is shown in Fig. 3 [R11].

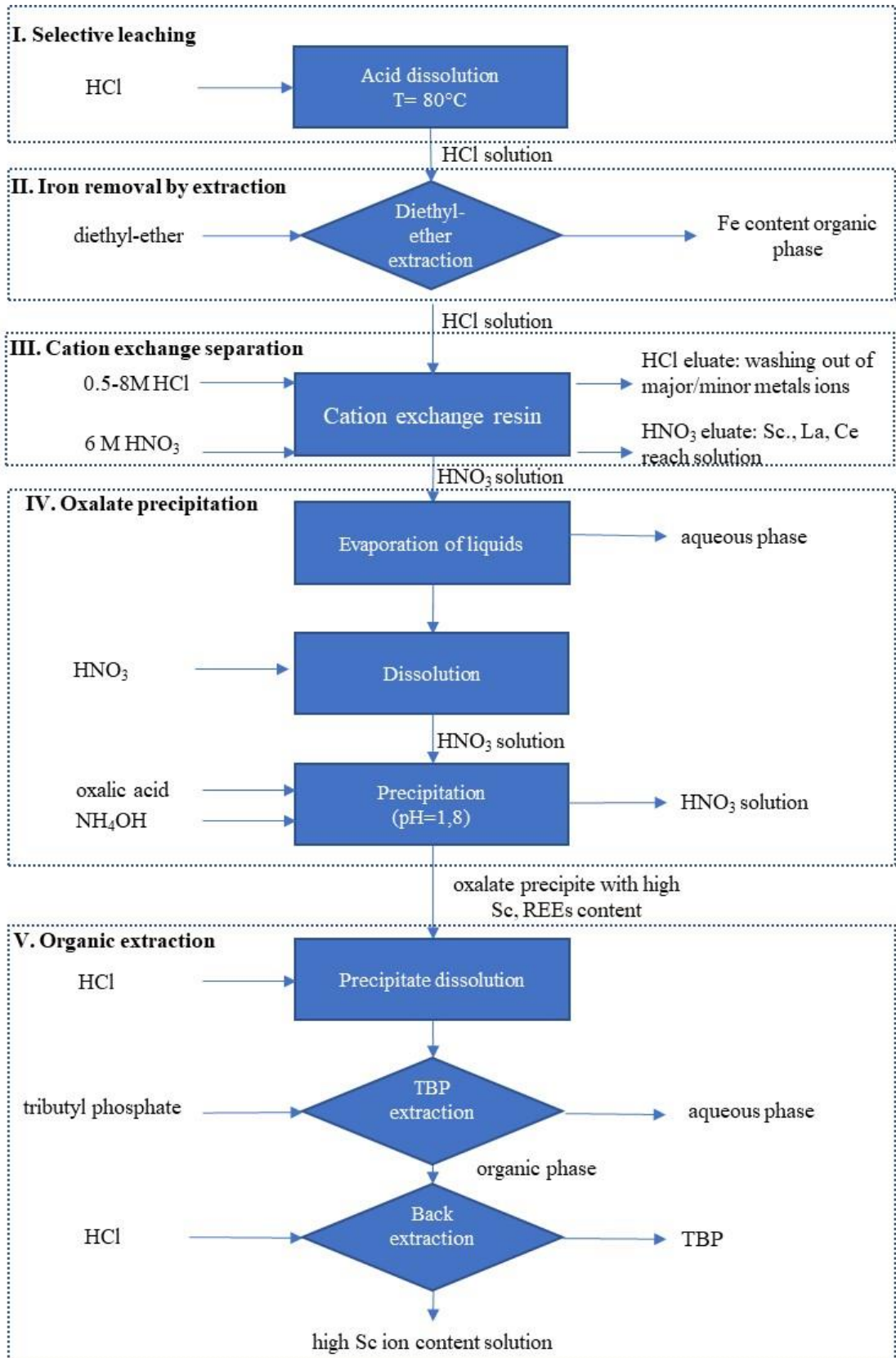


Fig. 3. Flowchart for the recovery of scandium from red mud.

PUBLICATIONS FORMING THE BASES OF THE THESES

Papers in international journals [P] and project report [R]:

- P1. Al-Jammal, N., Abdullah, T.A., **Juzsakova, T.**, Zsirka, B., Cretescu, I., Vágvolgyi, V., Sebestyén, V., Le Phuoc, C., Rasheed, R.T., Domokos, E., 2020. Functionalized carbon nanotubes for hydrocarbon removal from water. *Journal of Environmental Chemical Engineering* 8, 103570. <https://doi.org/10.1016/j.jece.2019.103570>
- P2. Abdullah, T.A., **Juzsakova, T.**, Hafad, S.A., Rasheed, R.T., Al-Jammal, N., Mallah, M.A., Salman, A.D., Le, P.C., Domokos, E., Aldulaimi, M., 2022. Functionalized multi-walled carbon nanotubes for oil spill cleanup from water. *Clean Techn Environ Policy* 24, 519–541. <https://doi.org/10.1007/s10098-021-02104-0>
- P3. Abdullah, T.A., **Juzsakova, T.**, Le, P.C., Le H.S., Adelikhah M., Rasheed, R.T., Salman, A.D., Domokos, E., Kułacz, K., Nguyen, X.C., 2022. Nanocomposites over modified multiwalled carbon nanotubes for the removal of cationic dye from water, *Total Environment Research Themes*, 3–4, 2022, 100005, doi:10.1016/j.totert.2022.100005
- P4. Abdullah, T.A., **Juzsakova, T.**, Rasheed, R.T., Salman, A.D., Adelikhah, M., Cuong, L.P., Cretescu, I., 2021. V₂O₅ nanoparticles for dyes removal from water. *Chem J Mold* 16, 102–111. <https://doi.org/10.19261/cjm.2021.911>
- P5. Salman, A.D., **Juzsakova, T.**, Jalhoom, M.G., Le, P.-C., Abdullah, T.A., Cretescu, I., Domokos, E., Nguyen, V.-H., 2022. Potential Application of Macrocyclic Compounds for Selective Recovery of Rare Earth Scandium Elements from Aqueous Media. *J. Sustain. Metall.* 8, 135–147. <https://doi.org/10.1007/s40831-021-00484-7>
- P6. Salman, A.D., **Juzsakova, T.**, Jalhoom, M.G., Ibrahim, R.I., Domokos, E., Al-Mayyahi, M.A., Abdullah, T.A., Szabolcs, B., Al-Nuzal, S.M.D., 2022. Studying the extraction of scandium(III) by macrocyclic compounds from aqueous solution using optimization technique. *Int. J. Environ. Sci. Technol.* 19, 11069–11086. <https://doi.org/10.1007/s13762-022-03917-2>
- P7. Salman, A.D., **Juzsakova, T.**, Jalhoom, M.G., Le Phuoc, C., Mohsen, S., Adnan Abdullah, T., Zsirka, B., Cretescu, I., Domokos, E., Stan, C.D., 2020. Novel hybrid nanoparticles: Synthesis, functionalization, characterization, and their application in the uptake of scandium (III)Ions from aqueous media. *Materials* 13, 5727. <https://doi.org/10.3390/ma13245727>
- P8. Salman, A.D., **Juzsakova, T.**, Rédey, Á., Le, P.-C., Nguyen, X.C., Domokos, E., Abdullah, T.A., Vagvolgyi, V., Chang, S.W., Nguyen, D.D., 2021. Enhancing the recovery of rare earth elements from red mud. *Chemical Engineering & Technology* 44, 1768–1774. <https://doi.org/10.1002/ceat.202100223>
- P9. Salman, A.D., **Juzsakova, T.**, Jalhoom, M.G., Abdullah, T.A., Le, P.-C., Viktor, S., Domokos, E., Nguyen, X.C., La, D.D., Nadda, A.K., Nguyen, D.D., 2022. A selective hydrometallurgical method for scandium recovery from a real red mud leachate: A comparative study. *Environmental Pollution* 308, 119596. <https://doi.org/10.1016/j.envpol.2022.119596>

- P10. Salman, A.D., **Juzsakova, T.**, Mohsen, S., Abdullah, T.A., Le, P.-C., Sebestyen, V., Sluser, B., Cretescu, I., 2022. Scandium Recovery Methods from Mining, Metallurgical Extractive Industries, and Industrial Wastes. *Materials (Basel)* 15, 2376. <https://doi.org/10.3390/ma15072376>
- R11. **Juzsakova, T.**, Varga, B., Pap, T., 2023. Ritkaföldfémek kinyerése és másodlagos nyersanyagok előállítása a vörösiszap komplex hasznosítása keretében/ Utilization of the red mud to recover rare earth element, Final project report, GINOP-2.2.1-15-2017-00106. Pannon Egyetem, Veszprém

International articles and conference proceedings related to the topic:

1. Al-Jammal, N., **Juzsakova, T.**, 2017. Review on the effectiveness of adsorbent materials in oil spills clean up, in 7th Int. Conf. International Council of Environmental Engineering Education (ICEEE), Budapest, 131–138. ISBN: 97896344906301
2. **Juzsakova, T.**, Al-Jammal, N., Cretescu, I., Sebestyén, V., Le Phuoc, C., Domokos, E., Rédey, Á., Stan, C.D., 2018. Case studies for clean technology development in the chemical industry using zeolite based catalysts. *Minerals* 8, 462. <https://doi.org/10.3390/min8100462>
3. Al-Jammal, N., **Juzsakova, T.**, Halmágyi, T., Sebestyén, V., Zsirka, B., Domokos, E., Cretescu, I., Rédey, Á., 2019. Study on dealuminated zeolitic tuff for hydrocarbon removal from water, *Environ. Eng. Manag. J.*, 188, 1809 <https://doi.org/10.30638/eemj.2019.172>
4. Al-Jammal, N., **Juzsakova, T.**, Zsirka, B., Sebestyén, V., Németh, J., Cretescu, I., Halmágyi, T., Domokos, E., Rédey, Á., 2019. Modified Jordanian zeolitic tuff in hydrocarbon removal from surface water. *Journal of Environmental Management* 239, 333–341. <https://doi.org/10.1016/j.jenvman.2019.03.079>
5. Salman, A.D., **Juzsakova, T.**, Ákos, R., Ibrahim, R.I., Al-Mayyahi, M.A., Mohsen, S., Abdullah, T.A., Domokos, E., 2021. Synthesis and surface modification of magnetic Fe₃O₄@SiO₂ core-shell nanoparticles and its application in uptake of scandium (III) ions from aqueous media. *Environ Sci Pollut Res* 28, 28428–28443. <https://doi.org/10.1007/s11356-020-12170-4>
6. Thuy, L.T.X., Suong, L.T., Cuong, L.P., **Juzsakova, T.**, 2020. Application of activated carbon and PGα21Ca to remove methylene blue from aqueous solution, In: *Sustainable Development of Water and Environment, ICSDWE 2020. Environmental Science and Engineering*, Jeon, H.-Y. (Ed.), Springer, pp. 11. https://doi.org/10.1007/978-3-030-45263-6_14
7. Abdullah, T.A., Nguyen, B.S., **Juzsakova, T.**, Rasheed, R.T., Hafad, S., Mansoor, H., Al-Jammal, N., Salman, A.D., Awad, H.A., Domokos, E., Le, P.C., Nguyen, V.H., 2021. Promotional effect of metal oxides (MxOy = TiO₂, V₂O₅) on multi-walled carbon nanotubes (MWCNTs) for kerosene removal from contaminated water, *Materials Letters* 292, 129612 <https://doi.org/10.1016/j.matlet.2021.129612>
8. Abdullah, T.A., **Juzsakova, T.**, Rasheed, R.T., Salman, A.D., Sebestyen, V., Domokos, E., Sluser, B., Cretescu, I., 2021. Polystyrene-Fe₃O₄-MWCNTs nanocomposites for toluene removal from water. *Materials* 14, 5503. <https://doi.org/10.3390/ma14195503>
9. Abdullah, T.A., **Juzsakova, T.**, Mansoor, H., Salman, A.D., Rasheed, R.T., Hafad, S.A., Mallah, M.A., Domokos, E., Cuong, N.X., Nadda, A.K., Chang,

- S.W., Le, P.C., Nguyen, D.D., 2022. Polyethylene over magnetite-multiwalled carbon nanotubes for kerosene removal from water. *Chemosphere* 287, 132310. <https://doi.org/10.1016/j.chemosphere.2021.132310>
10. Abdullah, T.A., **Juzsakova, T.**, Rasheed, R.T., Mallah, M.A., Salman, A.D., Le, P.C., Jakab, M., Zsirka, B., Kułacz, K., Sebestyén, V., 2022. V₂O₅, CeO₂ and their MWCNTs nanocomposites modified for the removal of kerosene from water, *Nanomaterials* 12(2) 189, <https://doi.org/10.3390/nano12020189>
11. Abdullah, T.A., **Juzsakova, T.**, Le, P.-C., Kułacz, K., Salman, A.D., Rasheed, R.T., Mallah, M.A., Varga, B., Mansoor, H., Mako, E., Zsirka, B., Nadda, A.K., Nguyen, X.C., Nguyen, D.D., 2022. Poly-NIPAM/Fe₃O₄/multiwalled carbon nanotube nanocomposites for kerosene removal from water. *Environmental Pollution* 306, 119372. <https://doi.org/10.1016/j.envpol.2022.119372>
12. **Juzsakova, T.**, Salman, A.D., Abdullah, T.A., Rasheed, R.T., Zsirka, B., Al-Shaikhly, R.R., Sluser, B., Cretescu, I., 2023. Removal of methylene blue from aqueous solution by mixture of reused silica gel desiccant and natural sand or eggshell waste. *Materials* 16, 1618. <https://doi.org/10.3390/ma16041618>

International conference lectures related to the theses:

1. **Juzsakova, T.**, Sebestyén, V., Al-Jammal, N., Németh, J., Domokos, E., Rédey, Á.: Follow up of the removal efficiency of oil contaminations in surface waters by environmental assessment, 7th International Council of Environmental Engineering Education International Conference, Óbuda University, Budapest, November 17-18, 2016.
2. **Juzsakova, T.**, Al-Jammal, N., Németh, J., Sebestyén, V., Fráter, T., Rédey, Á.: Environmentally Friendly Chemical Technology Developments/Környezetbarát kémiai technológia fejlesztések, XIII. Kárpát-medencei Környezettudományi Konferencia, Kolozsvár, Románia, 2017. április 5-8.
3. **Juzsakova, T.**, Cretescu, I., Al-Jammal, N., Domokos, E., Nemeth, J., Sebestyén, V., Rédey, Á.: Clean technology development in the chemical industry, 9th International Conference on Environmental Engineering and Management, Bologna, Italy, September 6-9, 2017.
4. **Juzsakova, T.**, Al-Jammal, N., Ifju, Zs., Domokos, E., Nemeth, J., Rédey, Á.: Development of microemulsified multiwall carbon nanotubes as adsorbents for oil spills clean up, 9th International Conference on Environmental Engineering and Management, Bologna, Italy, September 6-9, 2017.
5. **Juzsakova, T.**, Ifju, Zs., Al-Jammal, N., Cretescu, I., Sebestyén, V., Domokos, E., Rédey, Á.: Carbon nanotubes for environmental mitigations, International Joint Conference on Environment and Light Industry, Budapest, November 24-25, 2017.
6. **Juzsakova, T.**, Sebestyén, V., Nemeth, J., Cretescu, I., Rédey, Á., Domokos, E.: Technological optimization in the inorganic chemical industry, International Joint Conference on Environment and Light Industry, Budapest, November 24-25, 2017.
7. **Juzsakova, T.**, Domokos, E., Sebestyén, V., Rédey, Á.: Multiwalled carbon nanotubes for depollution of water, Environmental legislation, Safety Engineering and Disaster Management, ELSEDIM Conference, Babes-Bolyai University, Cluj-Napoca, Romania, May 17-19, 2018.
8. **Juzsakova, T.**, Al-Jammal, N., Cretescu, I., Sebestyén, V., Németh, J., Domokos, E., Rédey, Á.: Microemulsified carbon nanotubes for clean-up operations, 4th International Conference on Chemical Engineering, Innovative Materials and

- Processes for a Sustainable Development, Iasi, Romania, October 31-November 2, 2018.
9. **Juzsakova, T.**, Bakonyi, Z., Domokos, E., Rédey, Á.: New developments in red mud reprocessing and utilization, 4th International Conference on Chemical Engineering, Innovative Materials and Processes for a Sustainable Development, Iasi, Romania, October 31-November 2, 2018.
 10. Salman, A.D., **Juzsakova, T.**, Bakonyi, Z., Domokos, E.: New strategy for the recovery of rare earth elements (REEs) from Hungarian red mud, Conference on Global and Regional Environmental Protection, GLOREP 2018, Timisiora, Romania, November 15-17, 2018.
 11. Salman, A.D., **Juzsakova, T.**, Bakonyi, Z., Pap, T., Domokos, E.: Experimental investigation to recovery of rare earth elements (REEs) from Hungarian red mud using optimization technique, 9th International Conference on Climatic Changes and Environmental(Bio) Engineering, Óbuda University, Budapest, November 22-24, 2018.
 12. **Juzsakova, T.**, Al-Jammal, N., Abdullah, T.A., Cretescu, I., Viktor, S., Le Phuoc, C., Domokos, E.: Modified carbon nanotubes for water cleaning, 11th International Conference Air and Water-Components of the Environment, Cluj-Napoca, Romania, March 22-24, 2019.
 13. Salman, A.D., **Juzsakova T.**, Barbooti M.M.: Technological development for recovery of rare earth elements from red mud, Conference on postgraduate research in chemical engineering, CEPC3-2019, University of Technology, Baghdad, Iraq, May 5-7, 2019.
 14. Abdullah, T.A., **Juzsakova, T.**, Salman, A.D.: Hydrocarbons removal from water using MWCNTs as promising adsorbent material. 7th International Conference on Environmental Management, Engineering, Planning and Economics CEMEPE and SECOTOX, Mykonos Island, Greece, May 19-24, 2019.
 15. Salman, A.D., **Juzsakova T.**, Abdullah, T.A.: Process development for recovery of rare earth elements from red mud. 7th International CEMEPE and SECOTOX, Mykonos Island, Greece, May 19-24, 2019.
 16. Abdullah, T.A., **Juzsakova T.**, Rashed, T.R., Salman, A.D., Al-Asadi, M., Rizk, R.: Metal nanoparticles modified carbon nanotubes as adsorbent materials to remove hydrocarbons from water. Keynote, 13th International Conference on Chemical, Agricultural, Environmental and Biological Sciences (BCAEBs-19) Budapest, July 22-24, 2019.
 17. Rédey, Á., **Juzsakova T.**: Functionalized carbon nanotubes for hydrocarbon removal from water, 100 years from the founding of the School of Chemistry Taught in a Romanian in Cluj, „Chemia Napocensis-100”, Cluj-Napoca, October 9-12, 2019.
 18. Abdullah T.A., **Juzsakova T.**, Rasheed T.R., Le Phuoc, C., AL-Lami M., Domokos, E.: Removal of paraffin hydrocarbons from wastewater for petroleum industries using metal oxides nanoparticles modified MWCNTs, 25th International Conference on Chemistry, Cluj-Napoca, October 24–26, 2019.
 19. Abdullah, T.A., **Juzsakova, T.**, Rashed T. Rasheed, R.T., Salman, A.D., Al-Lami, M., Adelikhah, M., Domokos, E.: Removal of methylene blue from water using V₂O₅ and MnO₂ nanoparticles modified MWCNTs. 14th International Conference on Waste Management, Ecology and Biological Sciences, Budapest, Hungary, November 8-9, 2019.
 20. Salman, A.D., **Juzsakova, T.**, Domokos, E., Abdullah, T.A.: Recovery of rare earths from red mud by high-pressure acid leaching, Oral, International Joint Conference on Environmental and Light Industry Technologies IJCELIT 7, Óbuda University, Budapest, Hungary, November 21–22, 2019.
 21. **Juzsakova, T.**, Salman, A.D., Varga, B., Kulcsár, G., Lauer, J., Pap, T.: Rare earth metals separation from bauxite waste by ion exchange and solvent extraction techniques, *Keynote*, 13th ICEEE-2022, International Annual Conference on “Global

Environmental Development & Sustainability: Research, Engineering & Management”, Budapest, November 17-18, 2022.

22. **Juzsakova, T.:** Modification and characterization of advanced materials for environmental applications, Szeminárium, Department of Chemical Technology and Ecology, Shakarim University, Semey, Kazahsztán, October 31, 2023.

Hungarian conference presentations related to the theses:

1. Pozsgai, Cs., Tiber, B., Varga, B., Kulcsár, G., Pap, T., **Juzsakova, T.:** Ritkaföldfémek kinyerése vörösiszaból extrakciós eljárással / Recovery of rare earth elements from red mud by extraction techniques, Műszaki Kémiai Napok 2023 Konferencia Engineering Chemistry Conference, Veszprém, 2023. április 18-20.
2. Tiber, B., Pozsgai, Cs., Varga B., Kulcsár G., Pap T., **Juzsakova T.:** Ritkaföldfémek kinyerése vörösiszaból ioncsere eljárással / Recovery of rare earth elements from red mud by ion exchange techniques, Műszaki Kémiai Napok 2023 Konferencia Engineering Chemistry Conference, Veszprém, 2023. április 18-20.
3. **Juzsakova, T.,** Varga, B., Kulcsár, G., Pap, T.: Fémionok kinyerése vörösiszaból ioncserés elválasztással, XV. Környezetvédelmi Analitikai és Technológiai Konferencia és 63. Magyar Spektrokémiai Vándorgyűlés, Balatonszárszó, 2024. március 6-8.

REFERENCES

- Abdel-Ghani, N.T., El-Chaghaby, G.A., Helal, F.S., 2015. Individual and competitive adsorption of phenol and nickel onto multiwalled carbon nanotubes. *Journal of Advanced Research, Editors and International Board Member collection* 6, 405–415. <https://doi.org/10.1016/j.jare.2014.06.001>
- Acikara, Ö.B., 2013. Ion-Exchange Chromatography and Its Applications, in: *Column Chromatography*. IntechOpen. <https://doi.org/10.5772/55744>
- Afzaal, M., Hameed, S., Liaqat, I., Ali Khan, A.A., Abdul Manan, H., Shahid, R., Altaf, M., 2022. Heavy metals contamination in water, sediments and fish of freshwater ecosystems in Pakistan. *Water Practice and Technology* 17, 1253–1272. <https://doi.org/10.2166/wpt.2022.039>
- Agarwal, T., Sievert, A.C., Komini Babu, S., Adhikari, S., Park, E.J., Prasad, A.K., Advani, S.G., Hopkins, T.E., Park, A.M., Kim, Y.S., Borup, R.L., 2023. Enhancing durability of polymer electrolyte membrane using cation size selective agents. *Journal of Power Sources* 580, 233362. <https://doi.org/10.1016/j.jpowsour.2023.233362>
- Agilent Technologies, Inc., 2020. *Pharmaceutical Analysis Using UV-Vis: Compliance with USP Chapter <857>, and European Pharmacopoeia (Ph. Eur. Chapter 2.2.25)*.
- Ai, L., Zhang, C., Chen, Z., 2011. Removal of methylene blue from aqueous solution by a solvothermal-synthesized graphene/magnetite composite. *Journal of Hazardous Materials* 192, 1515–1524. <https://doi.org/10.1016/j.jhazmat.2011.06.068>
- Al-Ghouthi, M.A., Al-Degs, Y.S., 2011. New adsorbents based on microemulsion modified diatomite and activated carbon for removing organic and inorganic pollutants from waste lubricants. *Chemical Engineering Journal* 173, 115–128. <https://doi.org/10.1016/j.cej.2011.07.047>
- Alhalili, Z., 2023. Metal Oxides Nanoparticles: General Structural Description, Chemical, Physical, and Biological Synthesis Methods, Role in Pesticides and Heavy Metal Removal through Wastewater Treatment. *Molecules* 28, 3086. <https://doi.org/10.3390/molecules28073086>
- Alibrandi, G., 2008. Cryptand 111: A Chemical Device for Variable-pH Kinetic Experiments. *Angew. Chem.* 120, 3068–3070. <https://doi.org/10.1002/ange.200800180>
- Alosime, E.M., 2023. A review on surface functionalization of carbon nanotubes: methods and applications. *Discover Nano* 18, 12. <https://doi.org/10.1186/s11671-023-03789-6>
- Alqadami, A.A., Naushad, Mu., Alotman, Z.A., Ahmad, T., 2018. Adsorptive performance of MOF nanocomposite for methylene blue and malachite green dyes: Kinetics, isotherm and mechanism. *Journal of Environmental Management* 223, 29–36. <https://doi.org/10.1016/j.jenvman.2018.05.090>
- Anirudhan, T.S., Radhakrishnan, P.G., 2008. Thermodynamics and kinetics of adsorption of Cu(II) from aqueous solutions onto a new cation exchanger derived from tamarind fruit shell. *The Journal of Chemical Thermodynamics* 40, 702–709. <https://doi.org/10.1016/j.jct.2007.10.005>
- Anjum, H., Johari, K., Gnanasundaram, N., Appusamy, A., Thanabalan, M., 2019a. Impact of surface modification on adsorptive removal of BTX onto activated carbon. *Journal of Molecular Liquids* 280, 238–251. <https://doi.org/10.1016/j.molliq.2019.02.046>
- Anjum, H., Johari, K., Gnanasundaram, N., Appusamy, A., Thanabalan, M., 2019b. Investigation of green functionalization of multiwall carbon nanotubes and its application in adsorption of benzene, toluene & p-xylene from aqueous solution. *Journal of Cleaner Production* 221, 323–338. <https://doi.org/10.1016/j.jclepro.2019.02.233>
- Asim, N., Radiman, S., Yarmo, M.A., Banaye Golriz, M.S., 2009. Vanadium pentoxide: Synthesis and characterization of nanorod and nanoparticle V₂O₅ using CTAB micelle solution. *Microporous and Mesoporous Materials* 120, 397–401. <https://doi.org/10.1016/j.micromeso.2008.12.013>
- Auffinger, P., Wipff, G., 1991. Molecular dynamics simulations on the protonated 222. H⁺ and 222.2H⁺ cryptands in water: Endo versus exo conformations. *J Incl Phenom Macrocycl Chem* 11, 71–88. <https://doi.org/10.1007/BF01073686>
- Berlman, I.B., 1971. 6 - GRAPHS, in: Berlman, I.B. (Ed.), *Handbook of Fluorescence Spectra of Aromatic Molecules (Second Edition)*. Academic Press, pp. 107–415. <https://doi.org/10.1016/B978-0-12-092656-5.50011-3>
- Bharagava, R.N., Saxena, G., Mulla, S.I., 2020. Introduction to Industrial Wastes Containing Organic and Inorganic Pollutants and Bioremediation Approaches for Environmental Management, in: Saxena, G., Bharagava, R.N. (Eds.), *Bioremediation of Industrial Waste for Environmental*

- Safety: Volume I: Industrial Waste and Its Management. Springer, Singapore, pp. 1–18. https://doi.org/10.1007/978-981-13-1891-7_1
- Birch, M.E., Ruda-Eberenz, T.A., Chai, M., Andrews, R., Hatfield, R.L., 2013. Properties that Influence the Specific Surface Areas of Carbon Nanotubes and Nanofibers. *The Annals of Occupational Hygiene* 57, 1148–1166. <https://doi.org/10.1093/annhyg/met042>
- Bom, D., Andrews, R., Jacques, D., Anthony, J., Chen, B., Meier, M.S., Selegue, J.P., 2002. Thermogravimetric Analysis of the Oxidation of Multiwalled Carbon Nanotubes: Evidence for the Role of Defect Sites in Carbon Nanotube Chemistry. *Nano Lett.* 2, 615–619. <https://doi.org/10.1021/nl020297u>
- Botelho Junior, A.B., Espinosa, D.C.R., Vaughan, J., Tenório, J.A.S., 2021. Recovery of scandium from various sources: A critical review of the state of the art and future prospects. *Minerals Engineering* 172, 107148. <https://doi.org/10.1016/j.mineng.2021.107148>
- Bouzbib, M., Rohonczy, J., Sinkó, K., 2023. Effect of vanadium precursor on dip-coated vanadium oxide thin films. *J Sol-Gel Sci Technol* 105, 278–290. <https://doi.org/10.1007/s10971-022-05965-z>
- Brătan, V., Chesler, P., Todan, L., Zaharescu, M., Căldăraru, M., 2011. SURFACE PROPERTIES AND CATALYTIC OXIDATION ON V2O5-CeO2 CATALYSTS.
- Brown, P.L., Ekberg, C., 2016. Hydrolysis of metal ions. Wiley-VCH Verlag GmbH & KGaA, Weinheim.
- Buschmann, H.-J., 1988. The formation of 1:1 and 2:1 complexes of crown ethers and cryptands with K⁺ in acetonitrile and propylene carbonate. *Polyhedron* 7, 721–724. [https://doi.org/10.1016/S0277-5387\(88\)80044-5](https://doi.org/10.1016/S0277-5387(88)80044-5)
- Cai, H.N., Yaqi, 2011. Adsorption and Concentration of Organic Contaminants by Carbon Nanotubes from Environmental Samples, in: *Advances in Nanotechnology and the Environment*. Jenny Stanford Publishing.
- Cánovas, C.R., Macías, F., Pérez López, R., Nieto, J.M., 2018. Mobility of rare earth elements, yttrium and scandium from a phosphogypsum stack: Environmental and economic implications. *Science of The Total Environment* 618, 847–857. <https://doi.org/10.1016/j.scitotenv.2017.08.220>
- CE, 2003, n.d. Crown ether, Chemical Book [WWW Document]. URL https://www.chemicalbook.com/ProductCatalog_EN/201264.htm (accessed 6.15.23).
- Chassé, M., Griffin, W.L., O'Reilly, S.Y., Calas, G., 2019. Australian laterites reveal mechanisms governing scandium dynamics in the critical zone. *Geochimica et Cosmochimica Acta* 260, 292–310. <https://doi.org/10.1016/j.gca.2019.06.036>
- Chernyak, S.A., Ivanov, A.S., Maslakov, K.I., Egorov, A.V., Shen, Z., Savilov, S.S., Lunin, V.V., 2017. Oxidation, defunctionalization and catalyst life cycle of carbon nanotubes: a Raman spectroscopy view. *Phys. Chem. Chem. Phys.* 19, 2276–2285. <https://doi.org/10.1039/C6CP04657F>
- Chiang, Y.-C., Lin, W.-H., Chang, Y.-C., 2011. The influence of treatment duration on multi-walled carbon nanotubes functionalized by H2SO4/HNO3 oxidation. *Applied Surface Science* 257, 2401–2410. <https://doi.org/10.1016/j.apsusc.2010.09.110>
- Costa, S., Borowiak-Palen, E., Kruszy, M., Bachmatiuk, A., Kale, R.J., 2008. Characterization of carbon nanotubes by Raman spectroscopy.
- Cotton, S.A., 2006. Lanthanide and actinide chemistry, *Inorganic chemistry*. Wiley, Chichester, England ; Hoboken, NJ.
- Cusack, P.B., Courtney, R., Healy, M.G., O' Donoghue, L.M.T., Ujaczki, É., 2019. An evaluation of the general composition and critical raw material content of bauxite residue in a storage area over a twelve-year period. *Journal of Cleaner Production* 208, 393–401. <https://doi.org/10.1016/j.jclepro.2018.10.083>
- Dai, X., Thi Hong Nhung, N., Hamza, M.F., Guo, Y., Chen, L., He, C., Ning, S., Wei, Y., Dodbiba, G., Fujita, T., 2022. Selective adsorption and recovery of scandium from red mud leachate by using phosphoric acid pre-treated pitaya peel biochar. *Separation and Purification Technology* 292, 121043. <https://doi.org/10.1016/j.seppur.2022.121043>
- De Castro Dantas, T.N., Neto, A.A.D., De A. Moura, M.C.P., 2001. Removal of chromium from aqueous solutions by diatomite treated with microemulsion. *Water Research* 35, 2219–2224. [https://doi.org/10.1016/S0043-1354\(00\)00507-8](https://doi.org/10.1016/S0043-1354(00)00507-8)
- Deng, J., Shao, Y., Gao, N., Deng, Y., Tan, C., Zhou, S., Hu, X., 2012. Multiwalled carbon nanotubes as adsorbents for removal of herbicide diuron from aqueous solution. *Chemical Engineering Journal* 193–194, 339–347. <https://doi.org/10.1016/j.cej.2012.04.051>

- DiLeo, R.A., Landi, B.J., Raffaele, R.P., 2007. Purity assessment of multiwalled carbon nanotubes by Raman spectroscopy. *Journal of Applied Physics* 101, 064307. <https://doi.org/10.1063/1.2712152>
- Dresselhaus, M.S., Dresselhaus, G., Saito, R., Jorio, A., 2005. Raman spectroscopy of carbon nanotubes. *Physics Reports* 409, 47–99. <https://doi.org/10.1016/j.physrep.2004.10.006>
- Duan, Q., Lee, J., Liu, Y., Qi, H., 2016. Preparation and Photocatalytic Performance of MWCNTs/TiO₂ Nanocomposites for Degradation of Aqueous Substrate. *Journal of Chemistry* 2016, e1262017. <https://doi.org/10.1155/2016/1262017>
- Dubey, R., Dutta, D., Sarkar, A., Chattopadhyay, P., 2021. Functionalized carbon nanotubes: synthesis, properties and applications in water purification, drug delivery, and material and biomedical sciences. *Nanoscale Advances* 3, 5722–5744. <https://doi.org/10.1039/D1NA00293G>
- Edinger, P., Schneebeli, J., Struis, R.P.W.J., Biollaz, S.M.A., Ludwig, C., 2016. On-line liquid quench sampling and UV–Vis spectroscopy for tar measurements in wood gasification process gases. *Fuel* 184, 59–68. <https://doi.org/10.1016/j.fuel.2016.06.127>
- El-Hefny, N.E., El-Nadi, Y.A., Ahmed, I.M., 2011. 18-Crown-6 for the selective extraction and separation of cerium(IV) from nitrate medium containing some lanthanides. *International Journal of Mineral Processing* 101, 58–62. <https://doi.org/10.1016/j.minpro.2011.07.013>
- Eweida, B.Y., Omer, A.M., Tamer, T.M., Soliman, H.A.-E.M., Zaatot, A.A., Mohy-Eldin, M.S., 2023. Kinetics, isotherms and thermodynamics of oil spills removal by novel amphiphilic Chitosan-g-Octanal Schiff base polymer developed by click grafting technique. *Polym. Bull.* 80, 4813–4840. <https://doi.org/10.1007/s00289-022-04260-9>
- Faridbod, F., Ganjali, M., Dinarvand, R., Norouzi, P., Riahi, S., 2008. Schiff's Bases and Crown Ethers as Supramolecular Sensing Materials in the Construction of Potentiometric Membrane Sensors. *Sensors* 8, 1645–1703. <https://doi.org/10.3390/s8031645>
- Gambogi J., 2021. Scandium. U.S. Geological Survey, Mineral Commodity Summaries, (703) 648–7718.
- Gandhi, M.N., Khopkar, S.M., 1993. Liquid-liquid extraction of copper(II) with cryptand 222 with erythrosine B as the counter-ion. *Mikrochim Acta* 111, 93–101. <https://doi.org/10.1007/BF01240171>
- Ghosh, A., Dhiman, S., Gupta, A., Jain, R., 2022. Process Evaluation of Scandium Production and Its Environmental Impact. *Environments* 10, 8. <https://doi.org/10.3390/environments10010008>
- Ghosh, N., Das, S., Biswas, G., Haldar, P.K., 2022. Review on some metal oxide nanoparticles as effective adsorbent in wastewater treatment. *Water Science and Technology* 85, 3370–3395. <https://doi.org/10.2166/wst.2022.153>
- Gierczyk, B., 2013. Chapter One - NMR Studies of Crown Ether–Cyclodextrin Complexes, in: Webb, G.A. (Ed.), *Annual Reports on NMR Spectroscopy*. Academic Press, pp. 1–31. <https://doi.org/10.1016/B978-0-12-408097-3.00001-9>
- Greenwood, N.N., Earnshaw, A., 1997. *Chemistry of the Elements*. Elsevier. <https://doi.org/10.1016/C2009-0-30414-6>
- Grudinsky, P., Pasechnik, L., Yurtaeva, A., Dyubanov, V., Zinoveev, D., 2022. Recovery of Scandium, Aluminum, Titanium, and Silicon from Iron-Depleted Bauxite Residue into Valuable Products: A Case Study. *Crystals* 12, 1578. <https://doi.org/10.3390/cryst12111578>
- Haas, K.L., Franz, K.J., 2009. Application of Metal Coordination Chemistry To Explore and Manipulate Cell Biology. *Chem. Rev.* 109, 4921–4960. <https://doi.org/10.1021/cr900134a>
- Hameed, B.H., Din, A.T.M., Ahmad, A.L., 2007. Adsorption of methylene blue onto bamboo-based activated carbon: Kinetics and equilibrium studies. *Journal of Hazardous Materials* 141, 819–825. <https://doi.org/10.1016/j.jhazmat.2006.07.049>
- Hamilton, A.D., 1984. Crown Ethers and Cryptands, in: *Comprehensive Heterocyclic Chemistry*. Elsevier, pp. 731–761. <https://doi.org/10.1016/B978-008096519-2.00127-2>
- Hassan, A.A., Sajid, M., Tanimu, A., Abdulazeez, I., Alhooshani, K., 2021. Removal of methylene blue and rose bengal dyes from aqueous solutions using 1-naphthylammonium tetrachloroferrate (III). *Journal of Molecular Liquids* 322, 114966. <https://doi.org/10.1016/j.molliq.2020.114966>
- Hauke, F., Hirsch, A., 2010. Covalent Functionalization of Carbon Nanotubes, in: *Carbon Nanotubes and Related Structures*. John Wiley & Sons, Ltd, pp. 135–198. <https://doi.org/10.1002/9783527629930.ch6>
- Haxel, Gordon B, Hedrick, James B., Orris, Greta J., 2002. Rare Earth Elements—Critical Resources for High Technology | USGS Fact Sheet 087-02 [WWW Document]. URL <https://pubs.usgs.gov/fs/2002/fs087-02/> (accessed 5.17.23).

- Hedwig, S., Yagmurlu, B., Huang, D., von Arx, O., Dittrich, C., Constable, E.C., Friedrich, B., Lenz, M., 2022. Nanofiltration-Enhanced Solvent Extraction of Scandium from TiO₂ Acid Waste. *ACS Sustainable Chem. Eng.* 10, 6063–6071. <https://doi.org/10.1021/acssuschemeng.2c01056>
- Hirsch, A., 2002. Functionalization of single-walled carbon nanotubes. *Angewandte Chemie - International Edition* 41, 1853–1859. [https://doi.org/10.1002/1521-3773\(20020603\)41:11<1853::AID-ANIE1853>3.0.CO;2-N](https://doi.org/10.1002/1521-3773(20020603)41:11<1853::AID-ANIE1853>3.0.CO;2-N)
- Ho, Y.S., McKay, G., 1999. Pseudo-second order model for sorption processes. *Process Biochemistry* 34, 451–465. [https://doi.org/10.1016/S0032-9592\(98\)00112-5](https://doi.org/10.1016/S0032-9592(98)00112-5)
- Hoang, A.T., Nižetić, S., Cheng, C.K., Luque, R., Thomas, S., Banh, T.L., Pham, V.V., Nguyen, X.P., 2022. Heavy metal removal by biomass-derived carbon nanotubes as a greener environmental remediation: A comprehensive review. *Chemosphere* 287, 131959. <https://doi.org/10.1016/j.chemosphere.2021.131959>
- Hu, J., Zou, D., Chen, J., Li, D., 2020. A novel synergistic extraction system for the recovery of scandium (III) by Cyanex272 and Cyanex923 in sulfuric acid medium. *Separation and Purification Technology* 233, 115977. <https://doi.org/10.1016/j.seppur.2019.115977>
- Huang, C.-H. (Ed.), 2010. Rare earth coordination chemistry: fundamentals and applications. John Wiley & Sons, Singapore ; Hoboken, NJ.
- Huang, X., Yu, F., Peng, Q., Huang, Y., 2018. Superb adsorption capacity of biochar derived from leather shavings for Congo red. *RSC Adv.* 8, 29781–29788. <https://doi.org/10.1039/C8RA06370B>
- Ihsanullah, I., Jamal, A., Ilyas, M., Zubair, M., Khan, G., Atieh, M.A., 2020. Bioremediation of dyes: Current status and prospects. *Journal of Water Process Engineering* 38, 101680. <https://doi.org/10.1016/j.jwpe.2020.101680>
- Inamuddin, 2019. Xanthan gum/titanium dioxide nanocomposite for photocatalytic degradation of methyl orange dye. *International Journal of Biological Macromolecules* 121, 1046–1053. <https://doi.org/10.1016/j.ijbiomac.2018.10.064>
- Jawad, A.H., Rashid, R.A., Mahmud, R.M.A., Ishak, M.A.M., Kasim, N.N., Ismail, K., 2016. Adsorption of methylene blue onto coconut (Cocos nucifera) leaf: optimization, isotherm and kinetic studies. *Desalination and Water Treatment* 57, 8839–8853. <https://doi.org/10.1080/19443994.2015.1026282>
- Jeon, I.-Y., Chang, D.W., Kumar, N.A., Baek, J.-B., Jeon, I.-Y., Chang, D.W., Kumar, N.A., Baek, J.-B., 2011. Functionalization of Carbon Nanotubes, in: *Carbon Nanotubes - Polymer Nanocomposites*. IntechOpen. <https://doi.org/10.5772/18396>
- Jong, F.D., Reinhoudt, D.N., 1980. Stability and Reactivity of Crown-Ether Complexes, in: *Advances in Physical Organic Chemistry*. Elsevier, pp. 279–433. [https://doi.org/10.1016/S0065-3160\(08\)60130-6](https://doi.org/10.1016/S0065-3160(08)60130-6)
- Jorio, A., Saito, R., 2021. Raman spectroscopy for carbon nanotube applications. *Journal of Applied Physics* 129, 021102. <https://doi.org/10.1063/5.0030809>
- Jun, L.Y., Mubarak, N.M., Yee, M.J., Yon, L.S., Bing, C.H., Khalid, M., Abdullah, E.C., 2018. An overview of functionalised carbon nanomaterial for organic pollutant removal. *Journal of Industrial and Engineering Chemistry* 67, 175–186. <https://doi.org/10.1016/j.jiec.2018.06.028>
- Jung, C., Son, A., Her, N., Zoh, K.-D., Cho, J., Yoon, Y., 2015. Removal of endocrine disrupting compounds, pharmaceuticals, and personal care products in water using carbon nanotubes: A review. *Journal of Industrial and Engineering Chemistry* 27, 1–11. <https://doi.org/10.1016/j.jiec.2014.12.035>
- Juzsakova, T., Redey, A., Cuong, L.P., Kovacs, Z., Frater, T., Csavdari, A., Raduly, I., Lauer, J., Nemeth, J., Sebestyén, V., 2018. Determination of the rare earth metals in the red mud for possible utilization. *Environ. Eng. Manag. J.* 17, 2001–2009. <https://doi.org/10.30638/eemj.2018.199>
- Juzsakova, T., Varga, B., Pap, T., 2023. Ritkaföldfémek kinyerése és másodlagos nyersanyagok előállítása a vörösiszap komplex hasznosítása keretében (GINOP-2.2.1-15-2017-00106). Pannon Egyetem, Veszprém.
- Khan, Idrees, Saeed, K., Zekker, I., Zhang, B., Hendi, A.H., Ahmad, A., Ahmad, S., Zada, N., Ahmad, H., Shah, L.A., Shah, T., Khan, Ibrahim, 2022. Review on Methylene Blue: Its Properties, Uses, Toxicity and Photodegradation. *Water* 14, 242. <https://doi.org/10.3390/w14020242>
- Khandelia, T., Patel, B.K., 2022. Chapter 11 - Carbon nanotube-based oil-water separation, in: Das, P., Manna, S., Pandey, J.K. (Eds.), *Advances in Oil-Water Separation*. Elsevier, pp. 195–206. <https://doi.org/10.1016/B978-0-323-89978-9.00019-7>

- Kharlamova, M.V., Eder, D., 2020. Carbon Nanotubes, in: *Synthesis and Applications of Nanocarbons*. John Wiley & Sons, Ltd, pp. 107–147. <https://doi.org/10.1002/9781119429418.ch4>
- Kohl, C.A., Gomes, L.P., 2018. Physical and chemical characterization and recycling potential of desktop computer waste, without screen. *Journal of Cleaner Production* 184, 1041–1051. <https://doi.org/10.1016/j.jclepro.2018.02.221>
- Kostikova, G.V., Krasnova, O.G., Tsvadze, A.Yu., Zhilov, V.I., 2018. Scandium Extraction with Benzo-15-crown-5 from Neutral Nitrate–Trichloroacetate Solutions. *Russ. J. Inorg. Chem.* 63, 555–560. <https://doi.org/10.1134/S0036023618040125>
- Kotagiri, N., Kim, J.-W., 2014. Stealth nanotubes: strategies of shielding carbon nanotubes to evade opsonization and improve biodistribution. *Int J Nanomedicine* 9 Suppl 1, 85–105. <https://doi.org/10.2147/IJN.S51854>
- Kumar, P., Sengupta, A., Deb, A.K.S., Ali, Sk.M., 2017. Poly(amidoamine) Dendrimer Functionalized Carbon Nanotube for Efficient Sorption of Trivalent f-Elements: A Comparison Between 1st And 2nd Generation. *ChemistrySelect* 2, 975–985. <https://doi.org/10.1002/slct.201601550>
- Kumari, P., Alam, M., Siddiqi, W.A., 2019. Usage of nanoparticles as adsorbents for waste water treatment: An emerging trend. *Sustainable Materials and Technologies* 22, e00128. <https://doi.org/10.1016/j.susmat.2019.e00128>
- Lakatos, Tamás, Miskei, Mihály, Solymár Károly, Tancsa, András, 1978. Timföldgyári melléktermékek hanzsnosításának technológiája, 9. Magyar Tudományos Akadémia, Veszprém.
- Lakshmanan, V.I., Vijayan, S., 2018. A Review on Application of Crown Ethers in Separation of Rare Earths and Precious Metals, in: Davis, B.R., Moats, M.S., Wang, S., Gregurek, D., Kapusta, J., Battle, T.P., Schlesinger, M.E., Alvear Flores, G.R., Jak, E., Goodall, G., Free, M.L., Asselin, E., Chagnes, A., Dreisinger, D., Jeffrey, M., Lee, J., Miller, G., Petersen, J., Ciminelli, V.S.T., Xu, Q., Molnar, R., Adams, J., Liu, W., Verbaan, N., Goode, J., London, I.M., Azimi, G., Forstner, A., Kappes, R., Bhambhani, T. (Eds.), *Extraction 2018, The Minerals, Metals & Materials Series*. Springer International Publishing, Cham, pp. 1913–1930. https://doi.org/10.1007/978-3-319-95022-8_159
- Lehman, J.H., Terrones, M., Mansfield, E., Hurst, K.E., Meunier, V., 2011. Evaluating the characteristics of multiwall carbon nanotubes. *Carbon* 49, 2581–2602. <https://doi.org/10.1016/j.carbon.2011.03.028>
- Lei, Y., Huang, Q., Dou, J., Huang, H., Yang, G., Deng, F., Liu, M., Li, X., Zhang, X., Wei, Y., 2021. Fast adsorptive removal of cationic organic dye by anionic group functionalized carbon nanotubes with high efficiency. *Colloid and Interface Science Communications* 40, 100328. <https://doi.org/10.1016/j.colcom.2020.100328>
- Leite, E.S., Santana, S.R., Hünenberger, P.H., Freitas, L.C.G., Longo, R.L., 2007. On the relative stabilities of the alkali cations 222 cryptates in the gas phase and in water-methanol solution. *J Mol Model* 13, 1017–1025. <https://doi.org/10.1007/s00894-007-0213-8>
- Li, F., Wang, Y., Wang, D., Wei, F., 2004. Characterization of single-wall carbon nanotubes by N₂ adsorption. *Carbon* 42, 2375–2383. <https://doi.org/10.1016/j.carbon.2004.02.025>
- Li, H., Wei, C., Zhang, D., Pan, B., 2019. Adsorption of bisphenol A on dispersed carbon nanotubes: Role of different dispersing agents. *Science of The Total Environment* 655, 807–813. <https://doi.org/10.1016/j.scitotenv.2018.11.310>
- Li, M., Bian, C., Yang, G., Qiang, X., 2019. Facile fabrication of water-based and non-fluorinated superhydrophobic sponge for efficient separation of immiscible oil/water mixture and water-in-oil emulsion. *Chemical Engineering Journal* 368, 350–358. <https://doi.org/10.1016/j.cej.2019.02.176>
- Lide, D.R., Baysinger, G., Chemistry, S., Berger, L.I., Goldberg, R.N., Kehiaian, H.V., 2008. *CRC Handbook of Chemistry and Physics*.
- Lin, J., Wang, L., 2009. Comparison between linear and non-linear forms of pseudo-first-order and pseudo-second-order adsorption kinetic models for the removal of methylene blue by activated carbon. *Front. Environ. Sci. Eng. China* 3, 320–324. <https://doi.org/10.1007/s11783-009-0030-7>
- Lin, M., Fu, Z.Y., Tan, H.R., Tan, J.P.Y., Ng, S.C., Teo, E., 2012. Hydrothermal Synthesis of CeO₂ Nanocrystals: Ostwald Ripening or Oriented Attachment? *Crystal Growth & Design* 12, 3296–3303. <https://doi.org/10.1021/cg300421x>
- Lu, C., Su, F., Hu, S., 2008. Surface modification of carbon nanotubes for enhancing BTEX adsorption from aqueous solutions. *Applied Surface Science* 254, 7035–7041. <https://doi.org/10.1016/j.apsusc.2008.05.282>

- Luo, H., Dai, S., Bonnesen, P.V., 2004. Solvent Extraction of Sr²⁺ and Cs⁺ Based on Room-Temperature Ionic Liquids Containing Monoaza-Substituted Crown Ethers. *Anal. Chem.* 76, 2773–2779. <https://doi.org/10.1021/ac035473d>
- Mallakpour, S., Behranvand, V., Mallakpour, F., 2021. Adsorptive performance of alginate/carbon nanotube-carbon dot-magnesium fluorohydroxyapatite hydrogel for methylene blue-contaminated water. *Journal of Environmental Chemical Engineering* 9, 105170. <https://doi.org/10.1016/j.jece.2021.105170>
- Mallakpour, S., Tabesh, F., 2021. Green and plant-based adsorbent from tragacanth gum and carboxyl-functionalized carbon nanotube hydrogel bionanocomposite for the super removal of methylene blue dye. *International Journal of Biological Macromolecules* 166, 722–729. <https://doi.org/10.1016/j.ijbiomac.2020.10.229>
- Manuel Aguilar Sanjuán, Cortina, J.L. (Eds.), 2008. Solvent extraction and liquid membranes: fundamentals and applications in new materials. CRC Press, Boca Raton.
- Marcus, Y., 2004. Metal Ion Complexing by Cryptand 222 in Solutions. A Thermodynamic Approach. *Reviews in Analytical Chemistry* 23. <https://doi.org/10.1515/REVAC.2004.23.4.269>
- Margoni, M.M., Mathuri, S., Ramamurthi, K., Babu, R.R., Sethuraman, K., 2017. Sprayed vanadium pentoxide thin films: Influence of substrate temperature and role of HNO₃ on the structural, optical, morphological and electrical properties. *Applied Surface Science, Asian Consortium on Computational Materials Science - Theme Meeting on “First Principles Analysis & Experiment: Role in Energy Research”* 418, 280–290. <https://doi.org/10.1016/j.apsusc.2017.02.039>
- Mikeli, E., Marinos, D., Toli, A., Pilichou, A., Balomenos, E., Panias, D., 2022. Use of Ion-Exchange Resins to Adsorb Scandium from Titanium Industry’s Chloride Acidic Solution at Ambient Temperature. *Metals* 12, 864. <https://doi.org/10.3390/met12050864>
- Molchanova, T.V., Akimova, I.D., Tatarnikov, A.V., 2019. Ion-Exchange Methods of Scandium Recovery from the Ores of the Tomtor Deposit. *Russ. Metall.* 2019, 674–679. <https://doi.org/10.1134/S0036029519070103>
- MSZ, 2009. Water Quality Hungarian Standard. Part 7: Determination of Extractable Petroleum Hydrocarbon Content in a Boiling Point Range from 160°C to 520°C by Gas Chromatographic Method, (2009).
- Murphy, H., Papakonstantinou, P., Okpalugo, T.I.T., 2006. Raman study of multiwalled carbon nanotubes functionalized with oxygen groups. *Journal of Vacuum Science & Technology B: Microelectronics and Nanometer Structures Processing, Measurement, and Phenomena* 24, 715–720. <https://doi.org/10.1116/1.2180257>
- Narayanan, R.P., Ma, L.-C., Kazantzis, N.K., Emmert, M.H., 2018. Cost Analysis as a Tool for the Development of Sc Recovery Processes from Bauxite Residue (Red Mud). *ACS Sustainable Chem. Eng.* 6, 5333–5341. <https://doi.org/10.1021/acssuschemeng.8b00107>
- Nawab, A., Yang, X., Honaker, R., 2022. Parametric study and speciation analysis of rare earth precipitation using oxalic acid in a chloride solution system. *Minerals Engineering* 176, 107352. <https://doi.org/10.1016/j.mineng.2021.107352>
- Neikov, O.D., Naboychenko, S.S., Murashova, I.B., 2019. Production of Rare Metal Powders, in: *Handbook of Non-Ferrous Metal Powders*. Elsevier, pp. 757–829. <https://doi.org/10.1016/B978-0-08-100543-9.00024-5>
- Notthoff, C., Winterer, M., Beckel, A., Geller, M., Heindl, J., 2013. Spatial high resolution energy dispersive X-ray spectroscopy on thin lamellas. *Ultramicroscopy* 129, 30–35. <https://doi.org/10.1016/j.ultramic.2013.02.008>
- Oh, W.-C., Zhang, F.-J., Chen, M.-L., 2010. Characterization and photodegradation characteristics of organic dye for Pt–titania combined multi-walled carbon nanotube composite catalysts. *Journal of Industrial and Engineering Chemistry* 16, 321–326. <https://doi.org/10.1016/j.jiec.2010.01.032>
- Okiel, K., El-Sayed, M., El-Kady, M.Y., 2011. Treatment of oil–water emulsions by adsorption onto activated carbon, bentonite and deposited carbon. *Egyptian Journal of Petroleum* 20, 9–15. <https://doi.org/10.1016/j.ejpe.2011.06.002>
- Olivera A.C., Dantas Neto A.A., Moura M.C.P.A., Castro Dantas T.N., 2023. Use of surfactant-modified adsorbents in the removal of microplastics from wastewater, *Journal of Environmental Chemical Engineering*, 11(5), 1108227, <https://doi.org/10.1016/j.jece.2023.110827>

- Oliveira, M.G., Spaolonzi, M.P., Duarte, E.D.V., Costa, H.P.S., da Silva, M.G.C., Vieira, M.G.A., 2023. Adsorption kinetics of ciprofloxacin and ofloxacin by green-modified carbon nanotubes. *Environmental Research* 233, 116503. <https://doi.org/10.1016/j.envres.2023.116503>
- Osswald, S., Havel, M., Gogotsi, Y., 2007. Monitoring oxidation of multiwalled carbon nanotubes by Raman spectroscopy. *Journal of Raman Spectroscopy* 38, 728–736. <https://doi.org/10.1002/jrs.1686>
- Ovejero, G., Sotelo, J.L., Romero, M.D., Rodríguez, A., Ocaña, M.A., Rodríguez, G., García, J., 2006. Multiwalled Carbon Nanotubes for Liquid-Phase Oxidation. Functionalization, Characterization, and Catalytic Activity. *Ind. Eng. Chem. Res.* 45, 2206–2212. <https://doi.org/10.1021/ie051079p>
- Pan, B., Xing, B., 2008a. Adsorption Mechanisms of Organic Chemicals on Carbon Nanotubes. *Environ. Sci. Technol.* 42, 9005–9013. <https://doi.org/10.1021/es801777n>
- Pan, B., Xing, B., 2008b. Adsorption Mechanisms of Organic Chemicals on Carbon Nanotubes. *Environ. Sci. Technol.* 42, 9005–9013. <https://doi.org/10.1021/es801777n>
- Peng, X., Luan, Z., Ding, J., Di, Z., Li, Y., Tian, B., 2005. Ceria nanoparticles supported on carbon nanotubes for the removal of arsenate from water. *Materials Letters* 59, 399–403. <https://doi.org/10.1016/j.matlet.2004.05.090>
- Petrenko, T.I., Gaidamaka, S.N., Serguchev, Yu.A., 1988. Complexation of crown ethers and heteroanalogs of 18-crown-6 with alkali and alkaline earth metal cations in dichloroethane. *Theor Exp Chem* 24, 184–190. <https://doi.org/10.1007/BF00531193>
- Pourzamani, H., Hajizadeh, Y., Fadaei, S., 2015. Efficiency enhancement of multi-walled carbon nanotubes by ozone for benzene removal from aqueous solution. *International Journal of Environmental Health Engineering* 4, 29. <https://doi.org/10.4103/2277-9183.163972>
- Puech, P., Kandara, M., Paredes, G., Moulin, L., Weiss-Hortala, E., Kundu, A., Ratel-Ramond, N., Plewa, J.-M., Pellenq, R., Monthieux, M., 2019. Analyzing the Raman Spectra of Graphenic Carbon Materials from Kerogens to Nanotubes: What Type of Information Can Be Extracted from Defect Bands? *C* 5, 69. <https://doi.org/10.3390/c5040069>
- Qu, S., Huang, F., Yu, S., Chen, G., Kong, J., 2008. Magnetic removal of dyes from aqueous solution using multi-walled carbon nanotubes filled with Fe₂O₃ particles. *Journal of Hazardous Materials* 160, 643–647. <https://doi.org/10.1016/j.jhazmat.2008.03.037>
- Rakkesh, R.A., Durgalakshmi, D., Balakumar, S., 2015. Nanostructuring of a GNS-V₂O₅-TiO₂ core-shell photocatalyst for water remediation applications under sun-light irradiation. *RSC Adv.* 5, 18633–18641. <https://doi.org/10.1039/C5RA00180C>
- Ramamurthy, S.S., Chen, Y., Kalyan, M.K., Rao, G.N., Chelli, J., Mitra, S., 2011. Carbon Nanotube-Zirconium Dioxide Hybrid for Defluoridation of Water. *Journal of Nanoscience and Nanotechnology* 11, 3552–3559. <https://doi.org/10.1166/jnn.2011.3806>
- Ramasamy, D.L., Puhakka, V., Repo, E., Sillanpää, M., 2018. Selective separation of scandium from iron, aluminium and gold rich wastewater using various amino and non-amino functionalized silica gels – A comparative study. *Journal of Cleaner Production* 170, 890–901. <https://doi.org/10.1016/j.jclepro.2017.09.199>
- Rebelo, S.L.H., Guedes, A., Szeftczyk, M.E., Pereira, A.M., Araújo, J.P., Freire, C., 2016. Progress in the Raman spectra analysis of covalently functionalized multiwalled carbon nanotubes: unraveling disorder in graphitic materials. *Phys. Chem. Chem. Phys.* 18, 12784–12796. <https://doi.org/10.1039/C5CP06519D>
- Redd, J.T., Izatt, R.M., Bradshaw, J.S., 2003. Organic Macrocycles, in: *Encyclopedia of Physical Science and Technology*. Elsevier, pp. 517–528. <https://doi.org/10.1016/B0-12-227410-5/00543-3>
- Ren, X., Chen, C., Nagatsu, M., Wang, X., 2011. Carbon nanotubes as adsorbents in environmental pollution management: A review. *Chemical Engineering Journal, Environmental Nanotechnology* 170, 395–410. <https://doi.org/10.1016/j.cej.2010.08.045>
- Riaz, A., Lipiński, W., Lowe, A., 2021. Cyclic oxygen exchange capacity of Ce-doped V₂O₅ materials for syngas production via high-temperature thermochemical-looping reforming of methane. *RSC Adv.* 11, 23095–23104. <https://doi.org/10.1039/D1RA02234B>
- Rounaghi, G.H., Mohajeri, M., Tarahomi, S., Rahmani, R., 2011. Study of Complex Formation of Dibenzo-18-Crown-6 with Ce³⁺, Y³⁺, UO₂²⁺ and Sr²⁺ Cations in Acetonitrile–Dioxane Binary Solvent Mixtures. *J Solution Chem* 40, 377–389. <https://doi.org/10.1007/s10953-011-9651-0>
- Saad, M.E.K., Mnasri, N., Mhamdi, M., Chafik, T., Elaloui, E., Moussaoui, Y., 2015. Removal of methylene blue onto mineral matrices. *Desalination and Water Treatment* 56, 2773–2780. <https://doi.org/10.1080/19443994.2015.1012338>

- Sajid, M., 2022. Nanomaterials: types, properties, recent advances, and toxicity concerns. *Current Opinion in Environmental Science & Health* 25, 100319. <https://doi.org/10.1016/j.coesh.2021.100319>
- Sajid, M., Asif, M., Baig, N., Kabeer, M., Ihsanullah, I., Mohammad, A.W., 2022. Carbon nanotubes-based adsorbents: Properties, functionalization, interaction mechanisms, and applications in water purification. *Journal of Water Process Engineering* 47, 102815. <https://doi.org/10.1016/j.jwpe.2022.102815>
- Saleh, T.A., 2022. Chapter 9 - Hybrid materials and their impact on industrial and environmental applications, in: Saleh, T.A. (Ed.), *Polymer Hybrid Materials and Nanocomposites*, *Plastics Design Library*. William Andrew Publishing, pp. 285–309. <https://doi.org/10.1016/B978-0-12-813294-4.00010-8>
- Salman, A.D., Juzsakova, T., Jalhoom, M.G., Abdullah, T.A., Le, P.-C., Viktor, S., Domokos, E., Nguyen, X.C., La, D.D., Nadda, A.K., Nguyen, D.D., 2022. A selective hydrometallurgical method for scandium recovery from a real red mud leachate: A comparative study. *Environmental Pollution* 308, 119596. <https://doi.org/10.1016/j.envpol.2022.119596>
- Salman, A.D., Juzsakova, T., Jalhoom, M.G., Le Phuoc, C., Mohsen, S., Adnan Abdullah, T., Zsirka, B., Cretescu, I., Domokos, E., Stan, C.D., 2020. Novel Hybrid Nanoparticles: Synthesis, Functionalization, Characterization, and Their Application in the Uptake of Scandium (III) Ions from Aqueous Media. *Materials* 13, 5727. <https://doi.org/10.3390/ma13245727>
- Salman, A.D., Juzsakova, T., Rédey, Á., Le, P.-C., Nguyen, X.C., Domokos, E., Abdullah, T.A., Vagvolgyi, V., Chang, S.W., Nguyen, D.D., 2021. Enhancing the Recovery of Rare Earth Elements from Red Mud. *Chemical Engineering & Technology* 44, 1768–1774. <https://doi.org/10.1002/ceat.202100223>
- Samy, T.M., Imura, H., Suzuki, N., 1988. Solvent extraction of lanthanoid/III/ with 18-crown-6 from aqueous trichloroacetate solutions to 1,2-dichloroethane. *Journal of Radioanalytical and Nuclear Chemistry Letters* 126, 153–163. <https://doi.org/10.1007/BF02162434>
- Saravanan, R., Gupta, V.K., Mosquera, E., Gracia, F., 2014. Preparation and characterization of V₂O₅/ZnO nanocomposite system for photocatalytic application. *Journal of Molecular Liquids* 198, 409–412. <https://doi.org/10.1016/j.molliq.2014.07.030>
- Saravanan, R., Joicy, S., Gupta, V.K., Narayanan, V., Stephen, A., 2013. Visible light induced degradation of methylene blue using CeO₂/V₂O₅ and CeO₂/CuO catalysts. *Materials Science and Engineering: C* 33, 4725–4731. <https://doi.org/10.1016/j.msec.2013.07.034>
- Sarkar, B., Mandal, S., Tsang, Y.F., Kumar, P., Kim, K.-H., Ok, Y.S., 2018. Designer carbon nanotubes for contaminant removal in water and wastewater: A critical review. *Science of The Total Environment* 612, 561–581. <https://doi.org/10.1016/j.scitotenv.2017.08.132>
- Schilling, C., Hofmann, A., Hess, C., Ganduglia-Pirovano, M.V., 2017. Raman Spectra of Polycrystalline CeO₂: A Density Functional Theory Study. *J. Phys. Chem. C* 121, 20834–20849. <https://doi.org/10.1021/acs.jpcc.7b06643>
- SCY, 2023. Welcome to Scandium International Mining Corp. [WWW Document]. Scandium International Mining Corp. URL <https://scandiummining.com/products/scandium-markets-and-uses-1/> (accessed 5.17.23).
- Selen, V., Güler, Ö., Özer, D., Evin, E., 2016. Synthesized multi-walled carbon nanotubes as a potential adsorbent for the removal of methylene blue dye: kinetics, isotherms, and thermodynamics. *Desalination and Water Treatment* 57, 8826–8838. <https://doi.org/10.1080/19443994.2015.1025851>
- Sengupta, A., Gupta, N.K., 2017. MWCNTs based sorbents for nuclear waste management: A review. *Journal of Environmental Chemical Engineering* 5, 5099–5114. <https://doi.org/10.1016/j.jece.2017.09.054>
- Sengupta, A., Singha Deb, A.K., Kumar, P., Dasgupta, K., Ali, Sk.M., 2017. Amidoamine functionalized task specific carbon nanotube for efficient sorption of penta and hexavalent neptunium: Experimental and theoretical investigations. *Journal of Environmental Chemical Engineering* 5, 3058–3064. <https://doi.org/10.1016/j.jece.2017.05.055>
- Sezer, N., Koç, M., 2019. Oxidative acid treatment of carbon nanotubes. *Surfaces and Interfaces* 14, 1–8. <https://doi.org/10.1016/j.surfin.2018.11.001>
- Shah, K.A., Tali, B.A., 2016. Synthesis of carbon nanotubes by catalytic chemical vapour deposition: A review on carbon sources, catalysts and substrates. *Materials Science in Semiconductor Processing* 41, 67–82. <https://doi.org/10.1016/j.mssp.2015.08.013>

- Shvets, P., Dikaya, O., Maksimova, K., Goikhman, A., 2019. A review of Raman spectroscopy of vanadium oxides. *Journal of Raman Spectroscopy* 50, 1226–1244. <https://doi.org/10.1002/jrs.5616>
- Siddiqui, S.I., Rathi, G., Chaudhry, S.A., 2018. Acid washed black cumin seed powder preparation for adsorption of methylene blue dye from aqueous solution: Thermodynamic, kinetic and isotherm studies. *Journal of Molecular Liquids* 264, 275–284. <https://doi.org/10.1016/j.molliq.2018.05.065>
- Silva, R.G., Morais, C.A., Oliveira, É.D., 2019. Selective precipitation of rare earth from non-purified and purified sulfate liquors using sodium sulfate and disodium hydrogen phosphate. *Minerals Engineering* 134, 402–416. <https://doi.org/10.1016/j.mineng.2019.02.028>
- Simonin, J.-P., 2016. On the comparison of pseudo-first order and pseudo-second order rate laws in the modeling of adsorption kinetics. *Chemical Engineering Journal* 300, 254–263. <https://doi.org/10.1016/j.cej.2016.04.079>
- Sing, K.S.W., 1985. Reporting physisorption data for gas/solid systems with special reference to the determination of surface area and porosity (Recommendations 1984). *Pure and Applied Chemistry* 57, 603–619. <https://doi.org/10.1351/pac198557040603>
- Sohail, M.I., Waris, A.A., Ayub, M.A., Usman, M., Zia ur Rehman, M., Sabir, M., Faiz, T., 2019. Chapter One - Environmental application of nanomaterials: A promise to sustainable future, in: Verma, S.K., Das, A.K. (Eds.), *Comprehensive Analytical Chemistry, Engineered Nanomaterials and Phytonanotechnology: Challenges for Plant Sustainability*. Elsevier, pp. 1–54. <https://doi.org/10.1016/bs.coac.2019.10.002>
- Song, G., Li, A., Shi, Y., Li, W., Wang, H., Wang, C., Li, R., Ding, G., 2021. Sorptive removal of methylene blue from water by magnetic multi-walled carbon nanotube composites. *Environ Sci Pollut Res* 28, 41268–41282. <https://doi.org/10.1007/s11356-021-13543-z>
- Strauss, 2016. The recovery of rare earth oxides from waste fluorescent lamps - ProQuest [WWW Document]. URL <https://www.proquest.com/openview/69fb641c50d7c165598920de40395814/1?cbl=18750&pq-origsite=gscholar&parentSessionId=EmpSEuon5bhXc3ePF1uJQRRRYpAkQ4jIFxF%2F0qL%2FyBw%3D> (accessed 2.10.24).
- Su, F., Lu, C., Johnston, K.R., Hu, S., 2010. CHAPTER 5 - Kinetics, Thermodynamics, and Regeneration of BTEX Adsorption in Aqueous Solutions via NaOCl-Oxidized Carbon Nanotubes, in: Fan, M., Huang, C.-P., Bland, A.E., Wang, Z., Slimane, R., Wright, I. (Eds.), *Environanotechnology*. Elsevier, Amsterdam, pp. 71–97. <https://doi.org/10.1016/B978-0-08-054820-3.00005-8>
- Syrigiannis, Z., Melchionna, M., Prato, M., 2021. Covalent Carbon Nanotube Functionalization, in: Kobayashi, S., Müllen, K. (Eds.), *Encyclopedia of Polymeric Nanomaterials*. Springer, Berlin, Heidelberg, pp. 1–8. https://doi.org/10.1007/978-3-642-36199-9_363-1
- Szépölggyi, János, Kótai, László, 2012. Az ajkai vöröszap ömlés. Második rész. A vöröszap hasznosítási és feldolgozási lehetőségei. *Magyar Kémikusok Lapja* 67, 362–368.
- Tamin, A., Alaoui-Belghiti, A., Laasri, S., Touhtouh, S., Belhora, F., Louzazni, M., Hajjaji, A., 2022. V2O5/CeO2 catalysts for catalytic oxidation of hydrogen sulfide to sulfur and water at low temperature. *Materials Today: Proceedings, 4th International Conference on Advanced Materials for Photonics, Sensing and Energy Conversion Energy Applications* 66, 244–248. <https://doi.org/10.1016/j.matpr.2022.04.758>
- Trovarelli, A., 1996. Catalytic Properties of Ceria and CeO2-Containing Materials. *Catalysis Reviews* 38, 439–520. <https://doi.org/10.1080/01614949608006464>
- Tunkasiri, T., Opasnipat, V., Chantramee, B., Batanasathein, B., Juzhavat, S., Asnachinda, P., 1992. Characterization of ferric oxide obtained from upgrading of iron ores 18, 105–119.
- Umadevi, D., Sastry, G.N., 2014. Saturated vs. unsaturated hydrocarbon interactions with carbon nanostructures. *Front. Chem.* 2. <https://doi.org/10.3389/fchem.2014.00075>
- Vaisman, L., Wagner, H.D., Marom, G., 2006. The role of surfactants in dispersion of carbon nanotubes. *Advances in Colloid and Interface Science, In Honor of Professor Nissim Garti's 60th Birthday* 128–130, 37–46. <https://doi.org/10.1016/j.cis.2006.11.007>
- Valcárcel, M., Cárdenas, S., Simonet, B.M., Moliner-Martínez, Y., Lucena, R., 2008. Carbon nanostructures as sorbent materials in analytical processes. *TrAC Trends in Analytical Chemistry* 27, 34–43. <https://doi.org/10.1016/j.trac.2007.10.012>
- Valentim, B., Abagiú, A.T., Angheliescu, L., Flores, D., French, D., Gonçalves, P., Guedes, A., Popescu, L.G., Predeanu, G., Ribeiro, J., Santos, A.C., Slăvescu, V., Ward, C.R., 2019. Assessment of

- bottom ash landfilled at Ceplea Valley (Romania) as a source of rare earth elements. *International Journal of Coal Geology* 201, 109–126. <https://doi.org/10.1016/j.coal.2018.11.019>
- Venkata Ramana, D.K., Yu, J.S., Seshaiiah, K., 2013. Silver nanoparticles deposited multiwalled carbon nanotubes for removal of Cu(II) and Cd(II) from water: Surface, kinetic, equilibrium, and thermal adsorption properties. *Chemical Engineering Journal* 223, 806–815. <https://doi.org/10.1016/j.cej.2013.03.001>
- Vita, A., 2020. Catalytic Applications of CeO₂-Based Materials. *Catalysts* 10, 576. <https://doi.org/10.3390/catal10050576>
- Wachs, I.E., 2013. Catalysis science of supported vanadium oxide catalysts. *Dalton Trans.* 42, 11762–11769. <https://doi.org/10.1039/C3DT50692D>
- Wani, H.A., Shaikh, V.R., More, D.H., Patil, K.J., 2023. Studies of monomer–dimer equilibria of methylene blue as a probe to investigate the solute–solvent and hydrophobic interactions in aqueous solutions of polyethylene glycols at 298 K. *Chemical Physics Impact* 7, 100288. <https://doi.org/10.1016/j.chphi.2023.100288>
- Wasewar, K.L., Singh, S., Kansal, S.K., 2020. Chapter 13 - Process intensification of treatment of inorganic water pollutants, in: Devi, P., Singh, P., Kansal, S.K. (Eds.), *Inorganic Pollutants in Water*. Elsevier, pp. 245–271. <https://doi.org/10.1016/B978-0-12-818965-8.00013-5>
- Wu, C.-H., 2007. Adsorption of reactive dye onto carbon nanotubes: Equilibrium, kinetics and thermodynamics. *Journal of Hazardous Materials* 144, 93–100. <https://doi.org/10.1016/j.jhazmat.2006.09.083>
- Wu, N.-C., Shi, E.-W., Zheng, Y.-Q., Li, W.-J., 2002. Effect of pH of Medium on Hydrothermal Synthesis of Nanocrystalline Cerium(IV) Oxide Powders. *Journal of the American Ceramic Society* 85, 2462–2468. <https://doi.org/10.1111/j.1151-2916.2002.tb00481.x>
- Xia, Y., Yao, Q., Zhang, W., Zhang, Y., Zhao, M., 2019. Comparative adsorption of methylene blue by magnetic baker's yeast and EDTAD-modified magnetic baker's yeast: Equilibrium and kinetic study. *Arabian Journal of Chemistry* 12, 2448–2456. <https://doi.org/10.1016/j.arabjc.2015.03.010>
- Xu, J., Lv, X., Li, J., Li, Y., Shen, L., Zhou, H., Xu, X., 2012. Simultaneous adsorption and dechlorination of 2,4-dichlorophenol by Pd/Fe nanoparticles with multi-walled carbon nanotube support. *Journal of Hazardous Materials* 225–226, 36–45. <https://doi.org/10.1016/j.jhazmat.2012.04.061>
- Yang, S.-T., Chen, S., Chang, Y., Cao, A., Liu, Y., Wang, H., 2011. Removal of methylene blue from aqueous solution by graphene oxide. *Journal of Colloid and Interface Science* 359, 24–29. <https://doi.org/10.1016/j.jcis.2011.02.064>
- Yang, X.H., Fu, H.T., An, X.Z., Jiang, X.C., Yu, A.B., 2016. Synthesis of V₂O₅@TiO₂ core–shell hybrid composites for sunlight degradation of methylene blue. *RSC Adv.* 6, 34103–34109. <https://doi.org/10.1039/C6RA03376H>
- Yin, S., Hasegawa, T., 2023. Morphology Control of Transition Metal Oxides by Liquid-Phase Process and Their Material Development. *KONA* 40, 94–108. <https://doi.org/10.14356/kona.2023015>
- Yu, Y., Du, F.-P., Yu, J.C., Zhuang, Y.-Y., Wong, P.-K., 2004. One-dimensional shape-controlled preparation of porous Cu₂O nano-whiskers by using CTAB as a template. *Journal of Solid State Chemistry* 177, 4640–4647. <https://doi.org/10.1016/j.jssc.2004.10.025>
- Yudaev, P.A., Kolpinskaya, N.A., Chistyakov, E.M., 2021. Organophosphorous extractants for metals. *Hydrometallurgy* 201, 105558. <https://doi.org/10.1016/j.hydromet.2021.105558>
- Yurekli, K., Mitchell, C.A., Krishnamoorti, R., 2004. Small-Angle Neutron Scattering from Surfactant-Assisted Aqueous Dispersions of Carbon Nanotubes. *J. Am. Chem. Soc.* 126, 9902–9903. <https://doi.org/10.1021/ja047451u>
- Yusa, H., Watanuki, T., 2005. X-ray diffraction of multiwalled carbon nanotube under high pressure: Structural durability on static compression. *Carbon* 43, 519–523. <https://doi.org/10.1016/j.carbon.2004.10.011>
- Zaleski, C.M. (Ed.), 2022. *Advances in Metallacrown Chemistry*. Springer International Publishing, Cham. <https://doi.org/10.1007/978-3-031-08576-5>
- Zelege, M.A., Kuo, D.-H., 2019a. Synthesis and application of V₂O₅-CeO₂ nanocomposite catalyst for enhanced degradation of methylene blue under visible light illumination. *Chemosphere* 235, 935–944. <https://doi.org/10.1016/j.chemosphere.2019.06.230>
- Zelege, M.A., Kuo, D.-H., 2019b. Synthesis and application of V₂O₅-CeO₂ nanocomposite catalyst for enhanced degradation of methylene blue under visible light illumination. *Chemosphere* 235, 935–944. <https://doi.org/10.1016/j.chemosphere.2019.06.230>

- Zhang, N., Li, H.-X., Liu, X.-M., 2016. Recovery of scandium from bauxite residue—red mud: a review. *Rare Met.* 35, 887–900. <https://doi.org/10.1007/s12598-016-0805-5>
- Zhang, W., Yu, S., Zhang, S., Zhou, J., Ning, S., Wang, X., Wei, Y., 2019. Separation of scandium from the other rare earth elements with a novel macro-porous silica-polymer based adsorbent HDEHP/SiO₂-P. *Hydrometallurgy* 185, 117–124. <https://doi.org/10.1016/j.hydromet.2019.01.012>
- Zou, D., Deng, Y., Chen, J., Li, D., 2022. A review on solvent extraction of scandium. *Journal of Rare Earths* 40, 1499–1508. <https://doi.org/10.1016/j.jre.2021.12.009>

SUPPLEMENTARY PART

Table S1. Effect of varying concentrations, mg/L, of macrocyclic compounds on Sc extraction efficiency, E%.

(Sc initial concentration $C_i = 25$ mg/L, pH of aqueous solution 2 and C_f is final Sc final concentration).

MC mol/L	cryptand 222		12-crown-4 ether		15-crown-5 ether		DC18-crown-6 ether	
	C_f	E%	C_f	E%	C_f	E%	C_f	E%
0.001	21.70	13.20	23.15	7.40	23.15	7.40	24.96	0.159
0.002	21.44	14.23	22.32	10.71	22.46	10.15	24.65	1.38
0.004	20.72	17.14	21.74	13.04	22.12	11.50	22.7	9.09
0.006	3.70	85.18	18.25	27.00	18.94	24.24	22.04	11.81
0.008	0.18	99.25	12.50	50.00	12.95	48.18	21.51	13.94
0.010	0.02	99.91	10.16	59.34	11.79	52.83	21.44	14.23

Table S2. Effects of pH of macrocyclic extractant solution on Sc^{3+} extraction.

pH of aqueous solution	cryptand 222		12-crown-4 ether		15-crown-5 ether		DC-18-crown-6 ether	
	C_i	C_f	C_i	C_f	C_i	C_f	C_i	C_f
1	25	8.74	25	12.26	25	14.62	25	21.39
2	25	1.19	25	10.17	25	11.79	25	21.10
3	25	0.12	25	5.53	25	6.83	25	18.73
4	25	0.09	25	0.27	25	1.30	25	18.65
5	25	0.31	25	0.21	25	1.02	25	18.55
1	50	47.35	50	49.51	50	49.51	-	-
2	50	17.13	50	23.70	50	24.40	-	-
3	50	0.03	50	1.21	50	1.12	-	-
4	50	0.31	50	0.98	50	0.88	-	-
5	50	0.94	50	0.90	50	0.80	-	-
1	75	65.74	75	70.10	75	73.53	-	-
2	75	33.34	75	35.89	75	36.75	-	-
3	75	0.13	75	1.07	75	2.12	-	-
4	75	4.36	75	1.20	75	1.34	-	-
5	75	0.58	75	0.80	75	1.03	-	-
1	100	66.27	100	72.47	100	80.65	-	-
2	100	60.98	100	65.79	100	66.67	-	-
3	100	0.04	100	1.76	100	1.62	-	-
4	100	3.01	100	1.54	100	1.42	-	-
5	100	0.31	100	1.31	100	1.21	-	-

Table S3. Spectral analysis data from the deconvolution of D- and G-bands and the calculated ratios.

Ratio changes compared to the MWCNTs sample are displayed in brackets.

Sample	Center	FWHM	Area	Intensity	I _D /I _G	I _G /I _D	A _D /A _G	A _G /A _D
MWCNTs	1284	71.130	0.04722	0.001782	1.48	0.48	1.59	0.96
	1289	36.760	0.05887					
	1598	36.995	0.06684	0.001207				
	2561	71.375	0.10150	0.000862				
MWCNTs ox.	1289	43.178	0.06766	0.001419	1.44 (-0.04)	0.61 (0.06)	1.48 (-0.11)	1.03 (0.08)
	1289	59.332	0.03089					
	1599	44.993	0.06651	0.000988				
	2567	76.308	0.10176	0.000862				
Ce/MWCNTs	1289	67.900	0.06237	0.002172	1.60 (0.12)	0.37 (-0.18)	1.76 (0.17)	0.41 (-0.55)
	1289	40.887	0.07774					
	1599	47.349	0.07962	0.001361				
	2567	59.131	0.05748	0.000794				
V/MWCNTs	1289	73.096	0.04876	0.001454	1.40 (-0.08)	0.43 (-0.11)	1.40 (-0.18)	0.48 (-0.48)
	1289	55.547	0.07993					
	1600	57.770	0.09178	0.001041				
	2561	67.739	0.06200	0.000632				
V:Ce/ MWCNTs	1289	64.762	0.06845	0.002304	1.78 (0.31)	0.38 (-0.17)	2.42 (0.84)	0.45 (-0.51)
	1289	42.833	0.09338					
	1598	45.096	0.06680	0.001291				
	2566	60.566	0.07237	0.000868				

Table S4. Mass loss data from the thermoanalytical measurements

Sample	T start (°C)	T end (°C)	Mass loss step	Total mass loss	Residual mass	Estimated Ce-/V-oxide content (m/m%)
MWCNTs	21	190	0.15 mg (2.5 %)	5.28 mg (89.6 %)	0.614 mg (10.4 %)	n/a
	190	440	0.05 mg (0.8 %)			
	440	750	5.08 mg (86.2 %)			
	750	1016	0 mg (0 %)			
MWCNTs ox.	21	155	1.43 mg (20.1 %)	7.02 mg (98.5 %)	0.108 mg (1.5 %)	n/a
	155	366	1.32 mg (18.5 %)			
	366	500	0.32 mg (4.5 %)			
	500	730	3.84 mg (53.9 %)			
	730	1016	0.11 mg (1.5 %)			
Ce/MWCNTs	22	190	0.35 mg (5.1 %)	6.04 mg (86.6 %)	0.938 mg (13.4 %)	CeO ₂ : 11.9%
	190	360	0.33 mg (4.7 %)			
	360	485	0.49 mg (7 %)			
	485	700	4.86 mg (69.6 %)			
	700	1015	0.01 mg (0.2 %)			
V/MWCNTs	22	190	0.58 mg (8.4 %)	6.6 mg (94.8 %)	0.364 mg (5.2 %)	V ₂ O ₅ : 3.7%
	190	330	0.4 mg (5.7 %)			
	330	418	0.88 mg (12.6 %)			
	418	590	4.59 mg (65.8 %)			
	590	700	0.15 mg (2.1 %)			
	700	1015	0.01 mg (0.2 %)			
V:Ce/MWCNTs	21	190	0.52 mg (7.4 %)	6.21 mg (90.0 %)	0.694 mg (10.0 %)	CeO ₂ +V ₂ O ₅ : 8.5%
	190	316	0.25 mg (3.6 %)			
	316	422	1.02 mg (14.6 %)			
	422	545	3.42 mg (49.1 %)			
	545	700	1.01 mg (14.6 %)			
	700	1016	0.06 mg (0.8 %)			

Acknowledgement

The candidate wishes to express her thanks to her former PhD students *Ms. Noor Abduallah Al-Jammal, Mr. Thamer Adnan Abdullah and Mr. Ali Dawood Salman* (who had already defended her/his Ph.D dissertation), for their scientific cooperation, outstanding support and help.

Moreover, the candidate expresses her gratitude to associate professor *Dr. Kristófné Dr. Makó Éva* and the researcher *Dr. Balázs Zsirka* for their help in analytical investigations as well as to all colleagues of Sustainability Solutions Research Laboratory for their constant assistance.

The candidate would like to offer special thanks and sincere gratitude to *Prof. Dr. Rédey Ákos, D.Sc.*, who, although no longer with us, for his continuous support in the past, encouragement and motivation for accomplishment of this work.

Additionally, the candidate would like to thank *Prof. Dr. Kristóf János, D.Sc.* for his invaluable advices, scientific consultations and direction to prepare DSc dissertation and theses.

Fundings

This work was funded by GINOP-2.3.2-15-2016-00016 project: “Water resources protection, development of modular, mobile water treatment systems and wastewater treatment technologies at the University of Pannonia to promote the dynamic growth of Hungary's export performance” and GINOP-2.2.1-15-2017-00106 project “Complex utilization of red mud: Recovery of rare earth metals from red mud”.